Multibody Dynamic Analysis of the Lift-Off Operation

A Time Domain Approach

Shaofeng Wang

Master of Science Thesis

TU Delft Delft University of Technology

MAMMOET

Multibody Dynamic Analysis of the Lift-Off Operation

A Time Domain Approach

Master of Science Thesis

For the degree of Master of Science in Offshore and Dredging Engineering at Delft University of Technology

Shaofeng Wang

June 05, 2015

Faculty of Mechanical, Maritime and Materials Engineering · Delft University of Technology

The work in this thesis was supported by Mammoet Global Engineering B.V. Their cooperation is hereby gratefully acknowledged.

DELFT UNIVERSITY OF TECHNOLOGY
DEPARTMENT OF
OFFSHORE AND DREDGING ENGINEERING

The undersigned hereby certify that they have read and recommend to the Faculty of Mechanical, Maritime and Materials Engineering for acceptance a thesis entitled

MULTIBODY DYNAMIC ANALYSIS OF THE LIFT-OFF OPERATION

by

SHAOFENG WANG

in partial fulfillment of the requirements for the degree of

MASTER OF SCIENCE

OFFSHORE AND DREDGING ENGINEERING

Dated: June 05, 2015

Chairman of Graduation Committee: ______________________
Prof. Dr. A.V. Metrikine

Company Supervisor: ______________________
Ir. H. Jansen

University Supervisor: ______________________
Ir. A. Tsouvalas

University Supervisor: ______________________
Dr. E. Lourens

University Supervisor: ______________________
Dr. Ir. K.N. van Dalen

Abstract

In the coming decades, the offshore decommissioning industry is becoming a quickly growing market, especially at the North Sea, where most offshore platforms have operated for more than twenty years. There is little room for the mistake in the offshore decommissioning operation, therefore the motion response analysis is essential to avoid the risks.

It is common practice to use frequency domain analysis to simulate the dynamic behavior of floating structures in waves for linear system. However, offshore operations generally involve various nonlinearities such as nonlinear mooring system, wave-induced impacts during lift-off operation, and viscous forces. The frequency domain analysis is not capable of dealing with these nonlinearities, so the time domain analysis is pursued in this study. The Cummins equation provides an attractive way of analyzing the dynamics response of offshore structures in time domain, in which a convolution term is introduced to describe the fluid memory effect.

Neither the frequency domain analysis, nor the time domain convolution integral is convenient for time domain simulation. To facilitate the efficiency of time domain simulation, a state space model is introduced to replace the convolution term leading to a constant parameter time domain model. At the same time, the physical properties of the convolution term can be enforced into the state space model using convex optimization. The proposed time domain approach has been validated by comparing with the frequency domain analysis results for a linear system in the regular and irregular wave conditions.

The topside removal concept proposed by Mammoet consists of a twin barges, in order to eliminate the problem caused by the moment-induced by the topside, as well as wave-induced motion, two linkages are incorporated into this concept. The time domain analysis proves that the purpose of these linkages are achieved that the relative sway and roll are successfully restricted. Finally, different load transfer stages are studied to obtain the dynamic response and its interaction forces between the topside and barges.

Acknowledgements

I owe the successful completion of this thesis to several people involved in the whole process.

Firstly, I would like to express my sincere gratefulness to Henk Jansen, my daily supervisor at Mammoet, for giving me the precious opportunity to work on this challenging topic, guiding me with his vast knowledge and providing me with encouragement and inspiration.

I also want to thank all my committee members at TU Delft. Especially, I wanna give my thanks to Apostolos Tsouvalas for helping me with the academic guide throughout my thesis and giving me useful comments on the report and presentation. And, the sincere gratefulness goes to Professor Metrikine for his valuable advice, guidance and assessment.

Finally, I would like to thank my family for being always supportive.

Delft, The Netherlands
June 05, 2015

Shaofeng Wang

Contents

List of Figures

List of Tables

Nomenclature

BIBO	Bounded Input Bounded Output
BVP	Boundary Value Problem
COG	Center of Gravity
DAE	Differential Algebraic Equations
DTFT	Discrete Time Fourier Transform
EoM	Equation of Motion
FPSO	Floating Production Storage and Offloading
FRF	Frequency Response Function
GBS	Gravity Based Structure
IFT	Inverse Fourier Transform
LMI	Linear Matrix Inequality
LTI	Linear Time Invariant
MIMO	Multi Input Multi Output
ODE	Ordinary Differential Equations
RAO	Response Amplitude Operator
SISO	Single Input Single Output
SSM	State-Space Model
SVD	Singular Value Decomposition

Chapter 1

Introduction

1.1 Background

It is hard to find precise statistics on how many platforms of offshore oil and gas installation exist due to the rapid change of the offshore industry. Parente et al. points out that the number of world petroleum installations currently surpasses 7500 units and these installations are located in the continental shelves of 53 countries worldwide, of which 40 produce offshore oil and gas in significant quantities. The regional distribution of these structures among the different regions can be seen in Fig 1.1 (Parente et al., 2006).

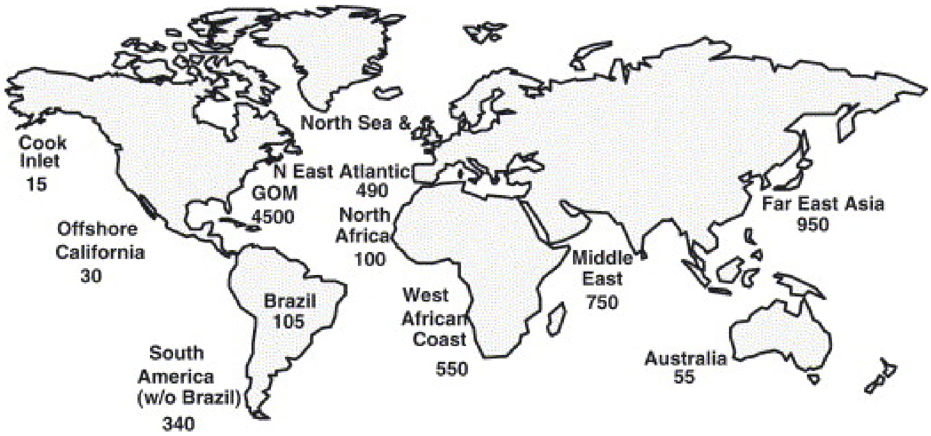

Figure 1.1: *Global Distribution of Offshore Platforms* (Parente et al., 2006)

The North Sea has an aging asset base, with the first field having commenced production in 1967. The average age of North Sea installation is 25 years and the United Kingdom Continental Shelf has the oldest average asset base, whilst Denmark owns the youngest assets. There are currently 245 assets over 30 years old across the North Sea (Scottish Enterprise, 2014). At least since the controversy over the attempted disposal at sea of the Brent Spar structure, the decommissioning of North Sea offshore oil and gas installations has been a matter of intense policy concern. Therefore, it is likely that an increasing number of North Sea structures need to be decommissioned in the coming years (Ekins et al., 2006).

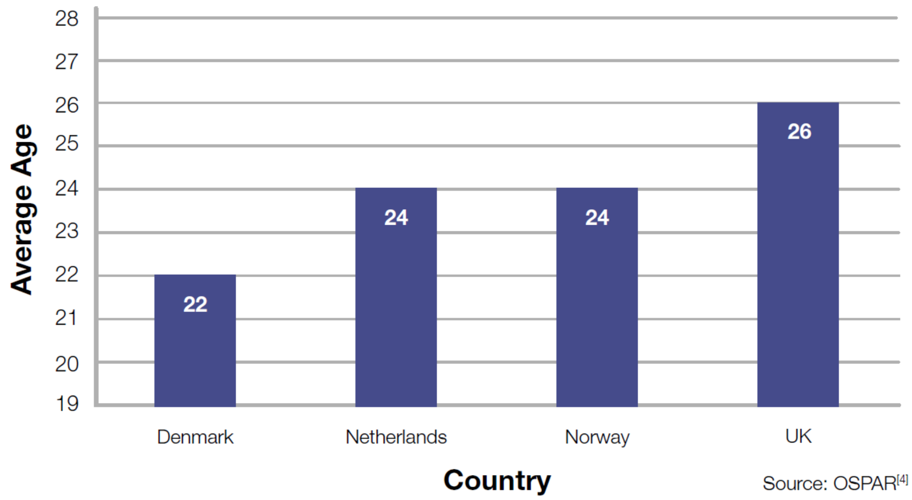

Figure 1.2: *Average Age of the North Sea Installations*

The offshore platforms have a great variety resulting from a particular set of conditions: ranging from fixed structures in 30m of shallow water to floating production storage and offloading (FPSO) in 2000m of deep water. The majority of the platforms located in the North Sea and the North East Atlantic, around two thirds, stands in less than 75m of water or weighing less than 4000 tonnes, so they are referred to as small structures. Over the next 10–20 years, an average of 15–25 installations are expected to be abandoned annually in Europe (Osmundsen and Tveteras, 2003), which will be a significant market for the offshore industry.

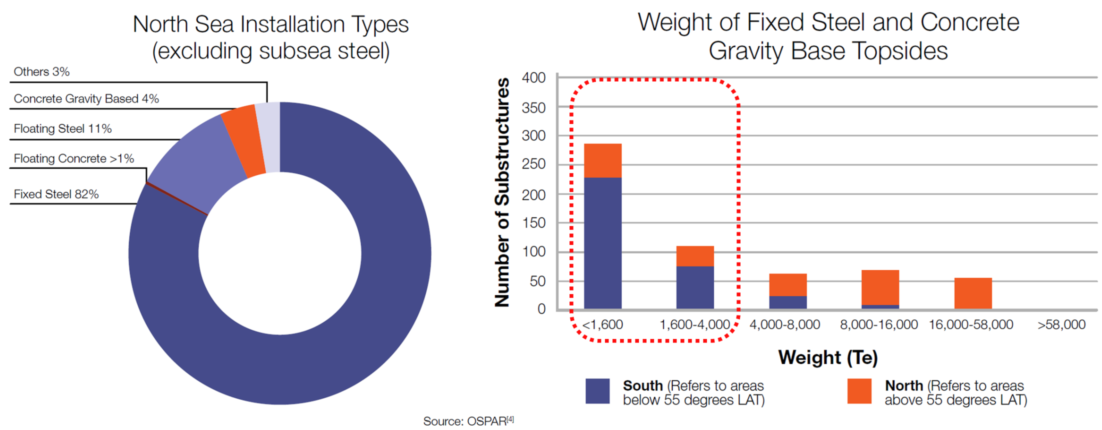

Figure 1.3: *North Sea Installation Types and the Topside's Weight*

A typical fixed platform consists of the topsides, which contain the drilling, processing, utilities and accommodation facilities, and the supporting substructure like jacket or concrete gravity base structure (GBS). The topsides themselves can weigh up to 40000 tonnes. Steel jackets can weigh up to 40000 tonnes and are fixed to the seabed by steel piles. Concrete gravity base structures are even heavier, for example, Troll on the Norwegian continental shelf weighs 700,000 tonnes, and sits on the seabed, stabilized by their own weight and penetration of the skirt into the seabed. In the absence of storing facilities, only the topsides of the platform are in contact with hydrocarbons and may contain limited amounts of potentially hazardous substances, whereas the substructure or jacket is generally clean steel or concrete (Osmundsen and Tveteras, 2003).

1.2 Topside Decommissioning Approaches

This thesis focuses on the topsides removal on the fixed substructures, for example jacket or GBS. The topsides modules are removed and returned to shore for reuse, recycling or disposal.

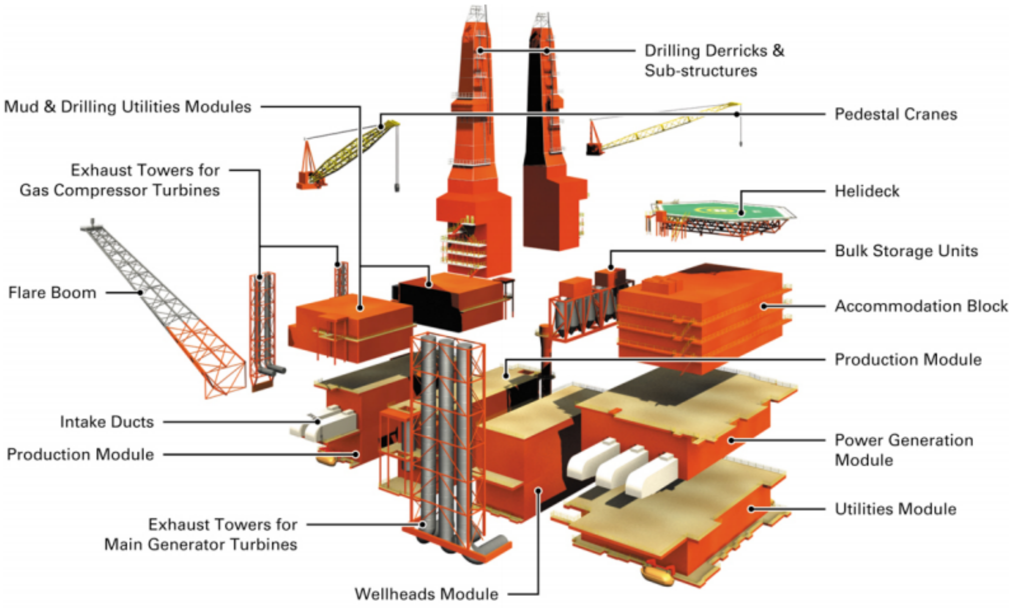

Figure 1.4: *Main Components of the Topsides (North West Hutton)*

The basic options for topsides decommissioning can be divided into two types: partial removal in which the topsides are dismantled into small pieces and total removal in which the topsides keep integrated. Normally, the conventional methods considered within the topsides decommissioning are outlined:

- Offshore Deconstruction (Piece-Small Removal)
  The Offshore Deconstruction of topsides modules is a proven method of dismantling topsides structures. Each module and its components are cut into small manageable pieces, using hydraulic shears and other cutting techniques. These pieces are removed using the platform cranes or temporary lifting devices and transported to shore on supply boats or transport barges. The process usually involves a small number of highly skilled operators working over a relatively long period of time. Overall topsides structural integrity is dependent on the integrity of individual modules, so a progressive dismantling program would have to be planned carefully to ensure overall structural integrity and safety of personnel. Therefore, some topsides modules are more conducive to this type of dismantling (BP, 2011).

- Reverse Installation
  This method requires the modules and other components that comprise the topsides to be separated and lifted from the platform using a heavy lift vessel (HLV) or semi-submersible crane vessel (SSCV) and is in essence a reverse of the original installation procedure. A large number of marine vessels would be required to be in attendance including tugs, cargo barges, anchor handling boats and offshore construction vessels.

- Single Lift Removal
  The term “single lift” applies to those options in which a vessel is used to lift off the topsides with only a minimum requirement for offshore deconstruction. Several designs have been proposed for purpose-built single lift decommissioning vessels that would be capable of removing topsides or steel jackets in one piece and transporting them to shore.

Figure 1.5: *Topsides Removal Approaches (Above: Reverse Installation; Below: Single Lift Removal)*

1.3 Motivation and Objective

As one of the strongest players in the heavy lifting and transport industry, *Mammoet* is involved in the transport, installation and removal of heavy structures in offshore environments. In order to take full advantage of the offshore decommissioning opportunity, an innovative topsides removal concept is proposed by *Mammoet Global Engineering B.V* using the twin barges lift off system. The similar concept for float over installation has been successfully executed by *Technip* as the world's first open sea catamaran float over topside installation on the deep water Kikeh Spar. The main operations are shown diagrammatically in the following figure.

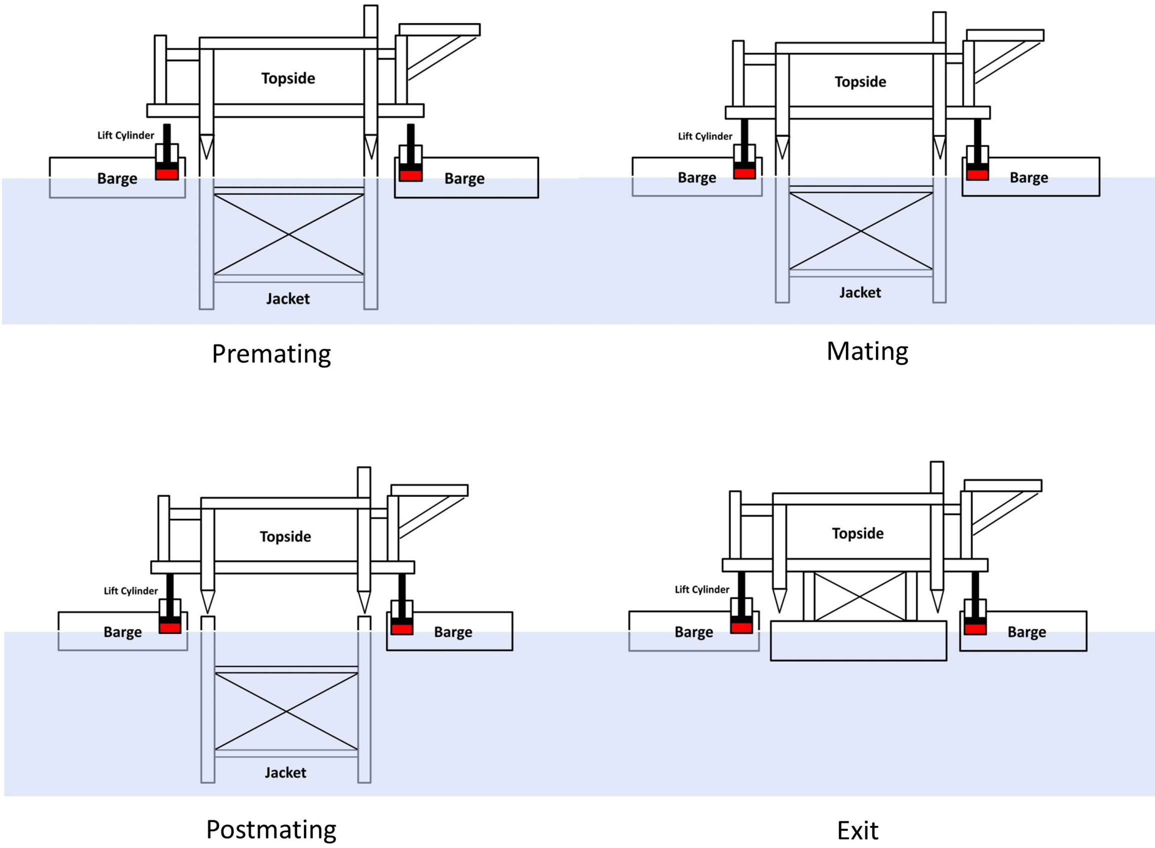

Figure 1.6: *Operation Procedure for Twin Barges Lift Off System*

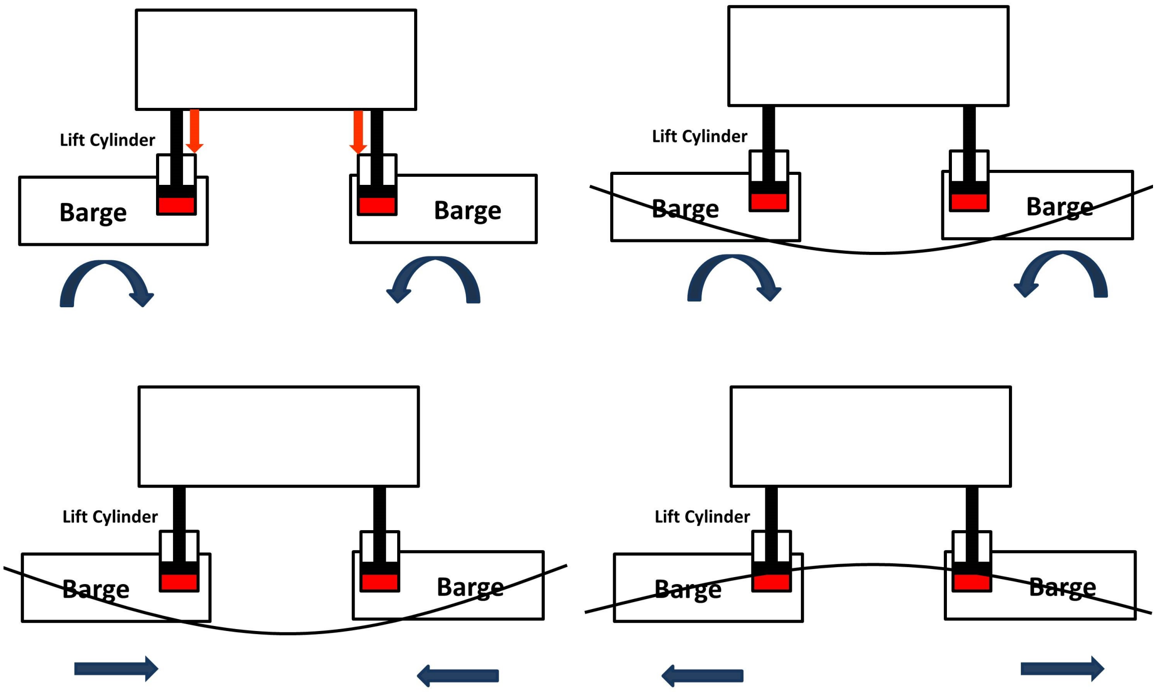

Figure 1.7: *Challenges of Free Floating Twin Barges Lift Off System*

However, the moment induced by the topside would result in excessive relative roll, which possibly causes undesirable mistake in the operations. Besides, the twin barges system will be faced with other challenges same with the semi-submersible vessel, especially under the beam wave situation.

In order to eliminate the threat from the excessive relative sway and roll, two rigid bars are hinged used as the linkages to connect the twin barges. To sum up, the innovative concept developed by Mammoet Global Engineering is designed for the topside removal on the jacket, which consists of two connected standard barges in a catamaran configuration with each hull either side of the jacket. The lift is executed by means of the lift system using winches and steel booms transmitting the weight of the deck to the barges as shown in the sketches below.

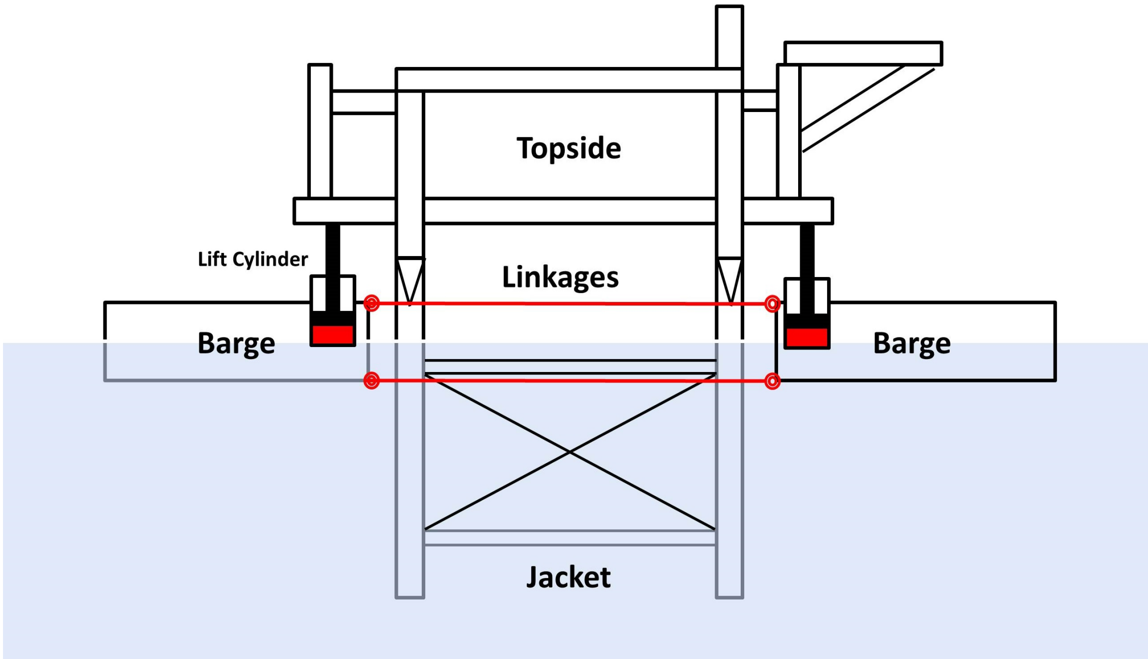

Figure 1.8: *Configuration of the Optimized Twin Barges Lift Off System*

In the offshore decommissioning operations, dealing with the wave-induced motions is one of the critical engineering challenges. Operations are often one-time-only and there is little room for making mistakes, which do not only result in financial consequences, but may also result in human casualties. It is common practice to use frequency domain analysis to simulate the dynamic behavior of floating structures in waves, which is easier and widely used in the preliminary engineering stages. However, although the frequency domain analysis is very convenient for steady state response of linear system, it cannot take into account various non-linearity associated with the offshore operations, such as a nonlinear mooring system, wave-induced impacts during decommissioning, and viscous forces. Moreover, the modern control techniques are usually formulated in the time domain.

The time domain analysis is more comprehensive than frequency domain analysis on dealing with the nonlinear system, in which the *Cummins equation* plays a significantly important role.

$$[M_{RB} + A_{inf}]\,\ddot{\xi}(t) + \int_0^t K\,(t-\tau)\,\dot{\xi}\,(\tau)\,d\tau + G\xi(t) = \tau_w(t) \tag{1.3.1}$$

In the time domain analysis, two important aspects should be paid special attention. The first one is the establishment of the equations of motion (EoM) which can model the multibody system with different types of linkages, sometimes including non-linear system. Usually the equations of motion are derived from the Lagrange method or Kane's method, both of them have been implemented into the *sympy.mechanics*, one core package of *Python,* which is immensely useful for the computer-aided simulation.

The second one is the forces acting on the system, in which the *hydrodynamic forces* plays the most important role. The problem of analyzing *hydrodynamic forces* can be split up in three parts. The *incoming wave* problem, the *scattering wave* problem and the *radiation wave* problem. Firstly, an incoming wave can be considered as a deformation of the water surface that introduces a pressure difference around the hull which results in a net force in a certain direction. Secondly, there is part of that incoming wave that changes direction when it hits the vessel, the forces due to this phenomenon are captured by the scattering problem. Finally, as the vessel oscillates around its equilibrium position, it causes motion of the water. As a result, waves are created that radiate away from the vessel to produce a radiation problem (Janssen et al., 2014).

Janssen et al. (2014) has worked out the radiation problem to provide an attractive way of replacing the time-consuming convolution term in *Cummins equation* with a state space model. Incorporating his work, the goal of this thesis is to develop a *python* toolbox which is capable of analyzing the dynamic behavior of the twin barges lift off system in time domain with a high efficiency and accuracy. To reach the goal, a number of objectives are established, which are stated below.

Objectives:

1. Derive the governing equations for multibody system with linkage constraints, as well considering the interaction from the topsides;
2. Validate the system identification method proposed by Janssen et al. (2014) with high accuracy and efficiency;
3. Apply the system identification method to complicated twin barges situation and verify its reliability;
4. Simulate the dynamic behavior for the twin barges system at different stages using the time domain approach which combines the governing equations with the system identification method.

1.4 Organization

In general, this thesis is organized by 3 main components: Fundamentals of Multibody Dynamics (Chapter 2, 3, 4), System Identification of the Fluid Memory Effect (Chapter 5, 6) and Case Studies (Chapter 7, 8, 9).

Part I: Fundamentals of Multibody Dynamics. This part presents the introduction to multibody dynamics. Chapter 2 defines the ship seakeeping model, focusing on the reference frame and coordinate system definition. A short introduction is given to the frequency domain approach and the time domain approach for dynamic response analysis. Chapter 3 introduces the multibody dynamics and investigates the Lagrange Method and Kane's Method, both of them are widely used in this area. Then, the non-holonomic and holonomic constraints are deliberated in the multibody system. Finally, a *Python* toolbox *PyDy* is introduced in Chapter 4, which plays an important role in the computer-based multibody dynamics.

Part II: System Identification of the Fluid Memory Effect. This part presents the strategy of identifying the fluid memory effect in a state space model using the hydrodynamic data from the software WAMIT. Chapter 5 shows how the frequency-domain added mass and damping values relate to the frequency- and time-domain description of the radiation forces. Subsequently, the properties of the fluid memory effect are listed together with a short notion on their derivations. Chapter 6 gives the concept of subspace system identification, in which the system properties are enforced by the convex optimization constraints. This chapter presents the theory behind the methods and some additional ways to obtain the right model structure. It is shown how these techniques can be combined to arrive at a system identification strategy for the identification of fluid memory effect.

Part III: Case Studies. In this part, different cases are studied to investigate the feasibility of the time domain approach. Chapter 7 is studied to validate the reliability of the time domain approach by comparing it with the frequency domain approach for a linear seakeeping model. Chapter 8 discusses the advantages of twin barges system using bar linkages and simulates its dynamic behavior in different scenarios to ensure the feasibility. Chapter 9 studies the load transfer model in two stages, 0% load transfer stage and 100% load transfer stage, which are corresponding to the first and the last stage for lift off operation. The dynamic behavior is simulated and the interaction forces are given.

Finally, Conclusions and Recommendations are given in the end of thesis, which summary the work in the thesis and gives the successors some advice for future study.

Part I

Fundamentals of Multibody Dynamics

Chapter 2

Ship Seakeeping Model

Seakeeping theory studies the motion of vessels in waves. The motion of a ship in a seaway is the response to sea loads, which are forces and moments that arise due to changes in pressure over the surface of the hull. For the free floating ship, if the sea state is not extreme, the motion responses can be considered within a linear framework. This allows one to apply the principle of superposition to study ship motion: the motion due to an irregular sea can be described as the superposition of the responses to many regular waves (Perez, 2006).

The linear seakeeping theory of ship motion is based on three essential assumptions:

- The sea surface elevation is assumed to be a realization of the Gaussian stochastic process with zero mean. Thus, the process is entirely described by its power spectral density—the sea spectrum.

- The wave-excitation loads and ship motion response are assumed to be linear.

- The ship keeps a steady course and moves at a constant average speed including the case of zero speed.

Within the study of ship seakeeping model, it can be divided into two parts:

- Kinematics
  Kinematics describes geometrical aspects of motion without considering mass and forces: reference frames, variables and transformations.

- Kinetics
  Kinetics describes the effects of forces on the motion.

2.1 Kinematics of Ship Motion

2.1.1 Reference Frames

The ship can move in six degrees of freedom in a seaway. Thus, to describe its motion, three coordinates are needed to define translations (*surge, sway, heave*) and three more coordinates needed to define the orientation (*roll, pitch, yaw*). Normally, two types of reference frames are widely used: *body-fixed frame* and *hydrodynamic frame*.

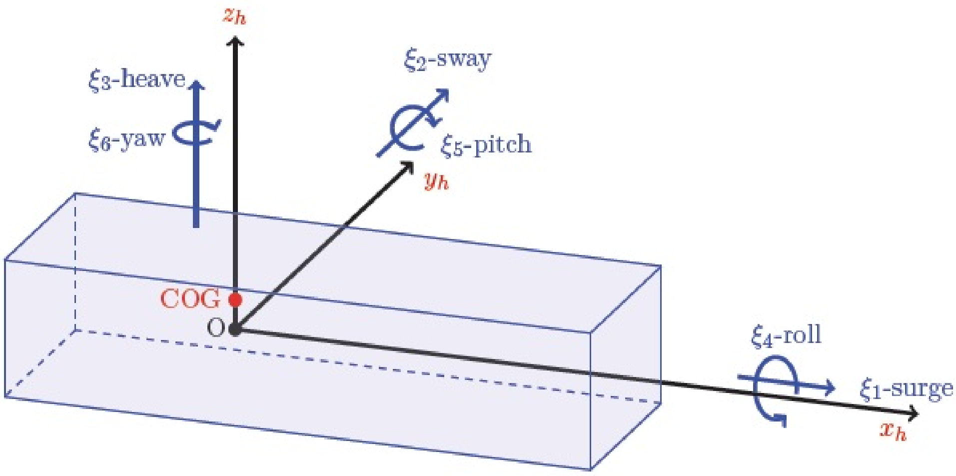

Figure 2.1: *Hydrodynamic Frame and Conventions for Oscillatory Motions*

- *Body-fixed frame* (b-frame; forward-starboard-down). The b-frame (o_b, x_b, y_b, z_b) is fixed to the hull. The positive x_b-axis points towards the bow, the positive y_b-axis points towards starboard and the positive z_b-axis points downwards. For marine vehicles, the axes of this frame are chosen to coincide with the principal axes of inertia; this determines the position of the origin of the frame, o_b, normally corresponds to the center of gravity (COG).
- *Hydrodynamic frame* (h-frame; forward-starboard-down). The h-frame (o_h, x_h, y_h, z_h) is not fixed to the hull, it moves at the average speed of the vessel following its path. The x_h-y_h plane coincides with the mean water free surface. The positive x_h-axis points forward and it is aligned with the low-frequency yaw angle ψ_1 . The positive y_h-axis points towards starboard, and the positive z_h-axis points upwards. The origin o_h is determined such that the z_h-axis passes through the time-average position of the center of gravity. This frame is usually considered when the vessel travels at a constant average speed (which also includes the case of zero speed); and therefore, the wave-induced motion makes the vessel oscillate with respect to the h-frame. This frame is also considered as *inertial frame* (Perez, 2006).

In seakeeping theory, the motion of the ship is commonly described using the h-frame, which is fixed with respect to the equilibrium of motion. The seakeeping coordinates defined in the h-frame will be denoted by:

$$\xi = [\xi_1,\xi_2,\xi_3,\xi_4,\xi_5,\xi_6]^T \tag{2.1.1}$$

in which, ξ_i $(i = 1, 2, 3)$ represents *surge, sway, heave* displacement respectively, whereas the angular coordinates ξ_i $(i = 4, 5, 6)$ are the *roll, pitch and yaw* angle.

2.1.2 Transformation between the b- and h- frame

Taking ϕ, θ, ψ as *roll, pitch and yaw*, the transformation between the b- and h- frame is the result of three consecutive rotations about the principal axes:

$$R_b^h(\Theta_{hb}) \triangleq R_{z,\psi}R_{y,\theta}R_{x,\phi} \tag{2.1.2}$$

with

$$\begin{aligned} R_{x,\phi} &\triangleq \begin{bmatrix} 1 & 0 & 0 \\ 0 & c\phi & -s\phi \\ 0 & s\phi & c\phi \end{bmatrix} \\ R_{y,\theta} &\triangleq \begin{bmatrix} c\theta & 0 & s\theta \\ 0 & 1 & 0 \\ -s\theta & 0 & c\theta \end{bmatrix} \\ R_{z,\psi} &\triangleq \begin{bmatrix} c\psi & -s\psi & 0 \\ s\psi & c\psi & 0 \\ 0 & 0 & 1 \end{bmatrix} \end{aligned} \tag{2.1.3}$$

here, $s \equiv \sin(\cdot)$ and $c \equiv \cos(\cdot)$.

Finally, the $R_b^h(\Theta_{hb})$ is given by:

$$R_b^h(\Theta_{hb}) \triangleq \begin{bmatrix} c\psi c\theta & -s\psi c\phi + c\psi s\theta s\phi & s\psi s\phi + c\psi c\phi s\theta \\ s\psi c\theta & c\psi c\phi + s\phi s\theta s\psi & -c\psi s\phi + s\psi c\phi s\theta \\ -s\theta & c\theta s\phi & c\theta c\phi \end{bmatrix} \tag{2.1.4}$$

Normally, the *roll, pitch, yaw* angles are assumed to be small (for instance $< 0.1\,rad$), which results in $\sin(\xi) = \xi$, $\cos(\xi) = 1$, ignoring the 2nd or higher-order terms ξ^n the transform matrix can be linearized into:

$$R_b^h(\Theta_{hb}) \triangleq \begin{bmatrix} 1 & -\psi & \theta \\ \psi & 1 & -\phi \\ -\theta & \phi & 1 \end{bmatrix} \tag{2.1.5}$$

2.2 Kinetics of Ship Motion

2.2.1 Equations of Motion

The seakeeping theory is based on using the hydrodynamic frame, h-frame to describe the motion of the fluid and the ship. Due to the h-frame is inertial, the vector equation of motion in this frame is:

$$M_{RB}^h \ddot{\xi} = \tau_{hyd}^h \tag{2.2.1}$$

Here, only the hydrodynamic forces are considered at first. The other forces, for instance wind forces, can be easily incorporated into the equations of motion.

The matrix M_{RB}^h is the generalized rigid-body mass matrix (mass and inertia) with respect to the h-frame:

$$\begin{aligned} M_{RB}^h &\triangleq \begin{bmatrix} mI_{3\times3} & -mS(r_g^h) \\ mS(r_g^h) & I^h \end{bmatrix} \\ &= \begin{bmatrix} m & 0 & 0 & 0 & mz_g^h & -my_g^h \\ 0 & m & 0 & -mz_g^h & 0 & mx_g^h \\ 0 & 0 & m & my_g^h & -mx_g^h & 0 \\ 0 & -mz_g^h & my_g^h & I_{xx}^h & -I_{xy}^h & -I_{xz}^h \\ mz_g^h & 0 & -mx_g^h & -I_{yx}^h & I_{yy}^h & -I_{yz}^h \\ -my_g^h & mx_g^h & 0 & -I_{zx}^h & -I_{zy}^h & I_{zz}^h \end{bmatrix} \end{aligned} \tag{2.2.2}$$

The mass of the ship m can be calculated as the product of the water density and the displacement volume V, $m = \rho V$. The coordinates of the center of gravity with respect to the h-frame are given by the vector $r_g^h = [x_g^h,\ y_g^h,\ z_g^h]^T$, and $S(\cdot)$ is the skew-symmetric matrix defined as:

$$S(r_g^h) = -S^T(r_g^h) \triangleq \begin{bmatrix} 0 & z_g^h & -y_g^h \\ -z_g^h & 0 & x_g^h \\ y_g^h & -x_g^h & 0 \end{bmatrix} \tag{2.2.3}$$

where the moments and products of inertia can be calculated using the displaced volume as follows:

$$\begin{aligned} I_{xx} &= \int_V [(y^h)^2 + (x^h)^2]\rho dV & I_{xy} = I_{yx} &= \int_V [y^h x^h]\rho dV \\ I_{yy} &= \int_V [(z^h)^2 + (x^h)^2]\rho dV & I_{xz} = I_{zx} &= \int_V [x^h z^h]\rho dV \\ I_{zz} &= \int_V [(y^h)^2 + (z^h)^2]\rho dV & I_{yz} = I_{zy} &= \int_V [y^h z^h]\rho dV \end{aligned} \tag{2.2.4}$$

The τ_{hyd}^h are the generalized hydrodynamic forces (including moments) for the six degrees of freedom expressed in the h-frame. Here, for the first-order motion analysis, the total hydrodynamic forces are assumed to be the linear superposition of the following components:

$$\tau_{hyd} = \tau_w + \tau_r + \tau_{hs} \tag{2.2.5}$$

- First-order wave excitation forces (τ_w). These forces are the zero mean oscillatory forces caused by the waves, which are separated into two components. The first component gives the, so-called, *Froude-Kriloff forces*, which are forces due to the incident waves under the assumption that the hull is restrained from moving and that the presence of the hull does not disturb the flow field. The second effect is a correction to account for the modification of the flow field due to the hull; otherwise there would be water mass transfer through the hull. This second component gives the so-called *diffraction forces.*

- Radiation forces (τ_r). These forces appear as a consequence of the change in the momentum of the fluid and the waves generated due to the motion of the hull. These forces are proportional to the accelerations of and velocities the ship. Due to this, the radiation forces are separated into the so-called *added-mass forces* (forces proportional to accelerations) and *potential-damping forces* (forces proportional to velocities).

- Hydrostatic forces (τ_{hs}). These are restoring forces due to gravity and buoyancy that tend to preserve the equilibrium of the ship. The hydrostatic forces and moments are proportional to the displacements ξ. Thus, the linearized forces and moments can be expressed as:

$$\tau_{hs} = G^h \xi \tag{2.2.6}$$

The only non-zero linear restoring coefficients are:

$$\begin{aligned} G^h_{33} &= \rho g A_{wp} \\ G^h_{35} &= G^h_{53} = \rho g \iint_{A_{wp}} x^h ds \\ G^h_{44} &= \rho g V GM_t \\ G^h_{55} &= \rho g V GM_l \end{aligned} \tag{2.2.7}$$

where A_{wp} is the water-plane area, V is the displacement volume, and GM_t and GM_l are the transverse and longitudinal metacentric heights.

All the first-order hydrodynamic forces can be solved by in-house software WAMIT in frequency domain, which depends on the potential theory.

2.2.2 Overview of Ship Motion

The kinetics of ship motion is the study of the forces acting on the ship and the motion they produce. Here, only the *first-order wave-induced force/motion* is studied, which is commonly modeled as a time series disturbance obtained by combining the wave spectrum with the vessel *Force Response Amplitude Operator* (Force RAO) or the *Motion Response Amplitude Operator* (Motion RAO), which are transfer function that map the wave elevation or wave slope into force or motion.

- ***Frequency Domain (Motion Superposition)***

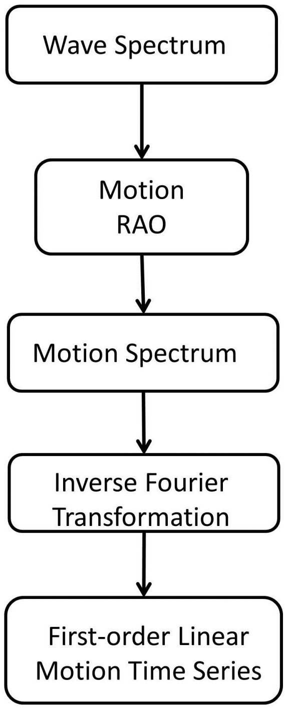

Figure 2.2: *Seakeeping Model with Motion Superposition (Frequency Domain)*

The first approach is to adopt the motion RAO and wave spectrum to obtain the motion spectrum, the procedure is presented in the Figure: 2.2.

The radiation forces are proportional to the accelerations and velocities of the ship motion. The vector of radiation forces can be expressed in the frequency domain as follows:

$$\tau_r = -A(\omega)\ddot{\xi} - B(\omega)\dot{\xi} \tag{2.2.8}$$

where A is the added mass and B damping.

All the terms in the equation can be expressed as complex notation based on the Fourier transformation pair:

$$\overline{f}(\omega) = \int_{-\infty}^{\infty} f(t)e^{-i\omega t}dt$$

$$f(t) = \frac{1}{2\pi}\int_{-\infty}^{\infty} \overline{f}(\omega)e^{i\omega t}d\omega \tag{2.2.9}$$

By substituting the wave-excitation, radiation and hydrostatic forces using the complex notation, we obtain the frequency-domain equations of motion:

$$(-\omega^2[M_{RB} + A(\omega)] + i\omega B(\omega) + G)\tilde{\xi}e^{i\omega t} = \tilde{\tau}_w e^{i\omega t}$$

$$\tilde{\xi} = (-\omega^2[M_{RB} + A(\omega)] + i\omega B(\omega) + G)^{-1}\tilde{\tau}_w \tag{2.2.10}$$

Having the motion $\tilde{\xi}(\omega)$ at hand, it is easy to obtain the time-series response using inverse Fourier transformation with motion superposition.

- ***Time Domain (Force Superposition)***

The alternative approach consists of using a model with force superposition rather than motion superposition, as illustrated in Figure: 2.3. In this model, the Force RAO are combined with the sea spectrum to give the wave-excitation forces.

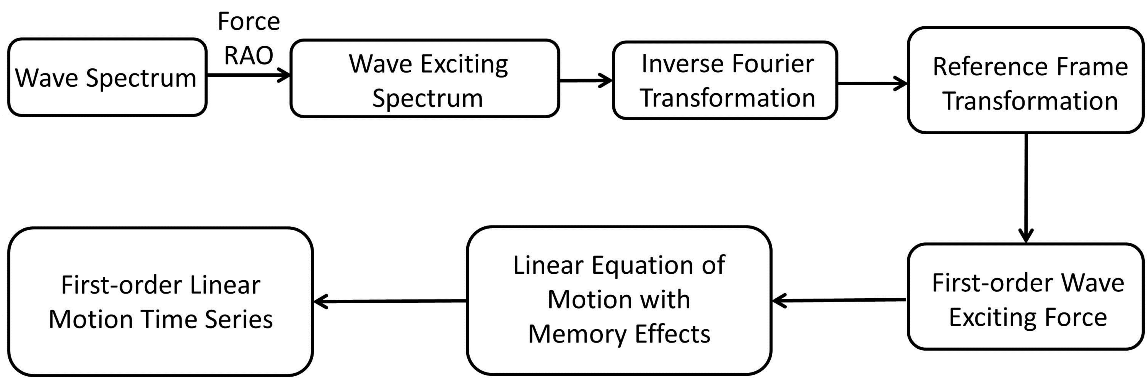

Figure 2.3: *Seakeeping Model with Force Superposition (Time Domain)*

Cummins (1962) considered the behavior of the fluid and the ship in the time domain. He made the assumption of linearity, and considered impulses in the components of motion. This resulted in a boundary value problem in which the potential was separated into two parts; one valid during the duration of the impulses and the other valid after the impulses extinguished. By expressing the pressure as a function of these potentials and integrating it over the wet surface of the vessel, he obtained a vector integro-differential equation, which is known as the *Cummins equation* (Amirouche, 2007):

$$[M_{RB} + A_{inf}]\,\ddot{\xi} + \int_0^t K\,(t-\tau)\,\dot{\xi}\,(\tau)\,d\tau + G\xi = \tau_w(t) \tag{2.2.11}$$

The matrix A_{inf} is the added mass at the infinity frequency, which keeps constant and depends only on the ship geometry. The entries of the matrix $K(t-\tau)$, in the convolution integral, are retardation functions of time, which depend on the forward speed and geometry of the vessel; this functions are the impulse response functions of the velocities. The *Cummins equation* reveals the structure of the true equations of motion of a ship and is valid for any bounded excitation τ_w.

The frequency domain analysis has been widely used in the offshore industry for a linear seakeeping system. However, marine operations generally involve nonlinear properties such as nonlinear mooring system, nonlinear impact forces and viscous forces. Due to arise of these nonlinear properties, the nonlinear dynamic system cannot be evaluated by the conventional frequency domain approach. Therefore, the time domain approach using *Cummins equation* provides an attractive way to deal with the non-linearity and gains more popularity in the offshore industry.

Chapter 3

Governing Equations for Multibody System

The formulation of the governing equations of motion (EoM) in multibody system can be obtained by a number of methods (Amirouche, 2007). Essentially all methods for obtaining equations of motion lead to equivalent results. However, the ease of use of the various methods differs; some are more suited than others for multibody dynamics in specific case.

The Newton-Euler method is comprehensive in a complete solution for all the forces and kinematic variables obtained, but it is inefficient since all internal forces are made explicit. Force and moment balance applied for each body takes in consideration every interactive and constraint force. Therefore, the method is inefficient only when a few of the forces need to be solved for and when the constraints are limited.

Lagrange's Equations provides a method for disregarding all interactive and constraint forces that do not perform work, which is therefore widely used to construct the EoM for multibody system.

Kane's method offers the advantages of both of the Newton-Euler and Lagrange methods. With the use of generalized forces the need for examining interactive and constraint forces between bodies is eliminated. Moreover, since Kane's method does not employ the use of energy functions, differentiation is not necessary. The differentiation required to compute velocities and accelerations can be obtained through the use of algorithms based on vector products. Kane's method provides the elegant means to develop the dynamics equations for multibody system that led itself to automated numerical computation (Unknown, 2009). Kane's first paper on his method appeared in 1961 but did not carry his name. In the 1970s, Huston et al. and Likins et al. used the equations in a number of applications and referred to them as the Lagrange form of D'Alembert's principle. This never conceptualized, and now these equations are best known as *Kane's equations* or *Kane's method*.

3.1 Kane's Method

Generally speaking, Kane's equations for a system S of N bodies modeled by n generalized coordinates X_l in an inertial reference frame R is given by

$$F_l + F_l^* = 0 \;\; (l = 1, ..., n) \tag{3.1.1}$$

where F_l and F_l^* denote the generalized active and inertia forces respectively.

3.1.1 Generalized Active Force

Take a multibody system where all bodies are interconnected by free joints, and allow each rigid body to have six degrees of freedom as depicted in Figure 3.1.

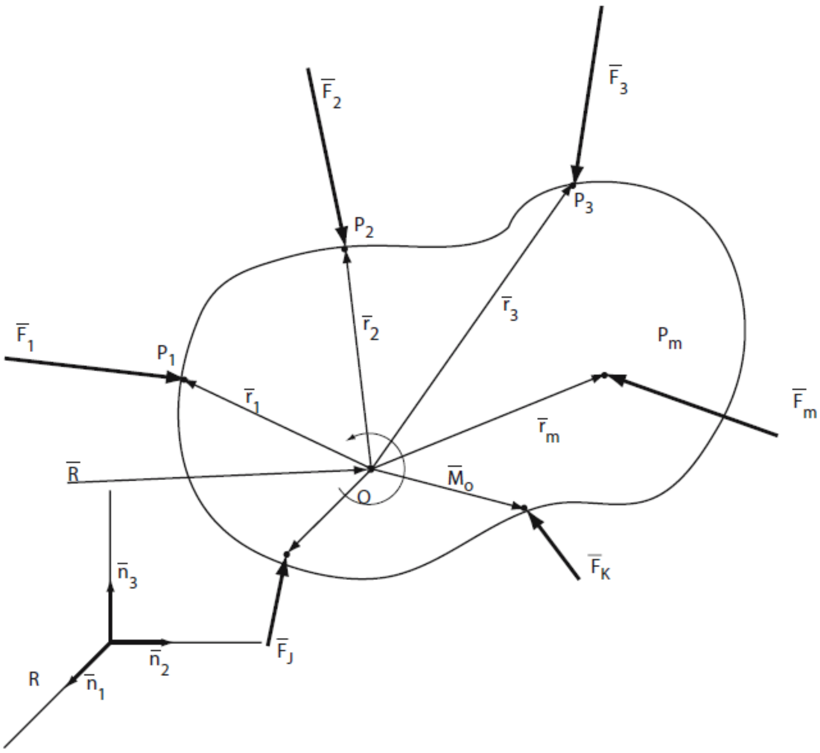

Figure 3.1: *Forces acting on a Rigid Body* (*F.Amironche*, 2007)

Let body k be subject to external forces $\overrightarrow{F}$ $(i = 1, ..., s)$ applied at points of application P_1through P_s, here s is the amount of all forces acting on this body.

The equivalent force system of the forces acting on body k can be replaced by a resultant force $\overrightarrow{F_R}$ acting at a point O (normally, O is the center of gravity) and a couple torque $\overrightarrow{T}$. The generalized active forces are defined as

$$F = \overrightarrow{F_R} \cdot \frac{\partial \overrightarrow{v_k}}{\partial \dot{x}_l} + \overrightarrow{T} \cdot \frac{\partial \overrightarrow{\omega_k}}{\partial \dot{x}_l} \tag{3.1.2}$$

x_l $(l = 1, ..., n)$ are the generalized coordinates that describe the relative orientation and translation between bodies. $\overrightarrow{v_k}$ and $\overrightarrow{\omega_k}$ are the mass center velocity and angular velocity of body k in the inertial reference frame R.

3.1.2 Generalized Inertia Force

The second law of motion can also be expressed in terms of the rate of change of the linear momentum,

$$\overrightarrow{F} = \frac{d\overrightarrow{P}}{dt} = \frac{d}{dt}(m\overrightarrow{v}) \tag{3.1.3}$$

$\overrightarrow{P}$ denotes the linear momentum defined as the product of the mass m times the velocity $\overrightarrow{v}$ of the particle in the inertia reference frame R.

It can be also written as

$$\overrightarrow{F} + \overrightarrow{F^*} = 0 \tag{3.1.4}$$

where

$$\overrightarrow{F^*} = -\frac{d}{dt}(m\overrightarrow{v}) \tag{3.1.5}$$

where $\overrightarrow{F^*}$ is known as the inertia force.

The total contribution to the generalized inertia forces in the presence of translational and rotational motion is defined as

$$F_l^* = \overrightarrow{F^*} \cdot \frac{\partial \overrightarrow{v}}{\partial \dot{x}_l} + \overrightarrow{T^*} \cdot \frac{\partial \overrightarrow{\omega}}{\partial \dot{x}_l} \tag{3.1.6}$$

in which, $\overrightarrow{v}$ and $\overrightarrow{\omega}$ represent the velocity and angular velocity of body k in the inertial reference frame R.

3.2 Derivation of Kane's Equation

The Kane's method is an approach based on vector variational principles (Baruh, 2000).

Using the D'Alembert principle, for any body k, force equilibrium is obtained as:

$$\overrightarrow{F_k} + \overrightarrow{F_k^*} + \overrightarrow{F_k^c} = 0 \tag{3.2.1}$$

Where $\overrightarrow{F_k^*} = -m_k \overrightarrow{a_k}$ is the inertia force of body k, $\overrightarrow{F_k^c}$ is the constraint forces and $\overrightarrow{F_k}$ is the active force.

3.2.1 Principle of Virtual Work

Based on the virtual work theory, denoting the first variation (hold time fixed, vary position) of the body by $\delta \overrightarrow{r_i}$. So, the virtual work is then defined as:

$$\delta W = \sum_{i=1}^{N} \overrightarrow{F} \cdot \delta \overrightarrow{r_i} \tag{3.2.2}$$

Where $\overrightarrow{F_i}$ is the resultant force acting on the i^{th} particle and $\overrightarrow{r_i}$ is the position vector of the particle in R. Here, it should be noted that $\delta \overrightarrow{r_i}$ are virtual or imaginary in the sense that they are assumed to occur without the passage of time and do not necessarily conform to the constraints. In addition, a virtual displacement conforms to the instantaneous constraints; that is, any moving constraints are assumed to be stopped during the virtual displacement (Amirouche, 2007).

Now extending the concept of virtual work to our multibody system considering only the work due to the forces on the system we obtain:

$$\delta W = \left(\overrightarrow{F_k} + \overrightarrow{F_k^*} + \overrightarrow{F_k^c} \right) \cdot \delta \overrightarrow{r_k} = 0 \tag{3.2.3}$$

Many constraints that are commonly encountered are known as *workless constraints*, so the contribution of the constraint force is

$$\overrightarrow{F_k^c} \cdot \delta \overrightarrow{r_k} = 0 \tag{3.2.4}$$

Which will simplify the original virtual work equation into

$$\delta W = \left(\overrightarrow{F_k} + \overrightarrow{F_k^*} \right) \cdot \delta \overrightarrow{r_k} = 0 \tag{3.2.5}$$

or[1]

$$\delta W = \left(\overrightarrow{F_k} + \overrightarrow{F_k^*} \right) \cdot \frac{\partial \overrightarrow{r_k}}{\partial q_r} \delta q_r = 0 \tag{3.2.6}$$

In which, the position vector can be written as a function of the generalized coordinates and time

$$\overrightarrow{r_k} = \overrightarrow{r_k}(q_r, t)$$

Differentiation of the above equation results in

[1] $r_k = r_k\,(q_r, t)$

$$\begin{aligned}\dot{\overrightarrow{r_t}} &= \frac{\partial \overrightarrow{r_k}}{\partial q_r}\frac{dq_r}{dt} + \frac{\partial \overrightarrow{r_k}}{\partial t} \\ &= \frac{\partial \overrightarrow{r_k}}{\partial q_r}\dot{q}_r + \frac{\partial \overrightarrow{r_k}}{\partial t}\end{aligned} \tag{3.2.7}$$

Taking the partial derivative of $\dot{r}_k$ with respect to $\dot{q}_r$ yields

$$\frac{\partial \dot{\overrightarrow{r_k}}}{\partial \dot{q}_r} = \frac{\partial \overrightarrow{r_k}}{\partial q_r} \tag{3.2.8}$$

or simply

$$\frac{\partial \overrightarrow{v_k}}{\partial \dot{q}_r} = \frac{\partial \overrightarrow{r_k}}{\partial q_r} \tag{3.2.9}$$

Since the virtual displacement δq_r is arbitrary without violating the constraints we can obtain Eq: 3.2.6as:

$$f_r + f_r^* = 0 \tag{3.2.10}$$

Where f_r and f_r^* are the generalized active and inertia forces respectively and are defined as follows:

$$f_r = \overrightarrow{F_k} \cdot \frac{\partial \overrightarrow{v_k}}{\partial \dot{q}_r} \tag{3.2.11}$$

and

$$f_r^* = \overrightarrow{F_k^*} \cdot \frac{\partial \overrightarrow{v_k}}{\partial \dot{q}_r} \tag{3.2.12}$$

In a similar way, the moments can be written using virtual work as:

$$M_r + M_r^* = 0 \tag{3.2.13}$$

In which, M_r and M_r^* are the generalized active and inertia moments respectively and can be showed as:

$$M_r = \overrightarrow{T_k} \cdot \frac{\partial \overrightarrow{\omega_k}}{\partial \dot{q}_r} \tag{3.2.14}$$

and

$$M_r^* = -\left(\overrightarrow{\alpha_k} \cdot I + \overrightarrow{\omega_k} \times I \cdot \overrightarrow{\omega_k}\right) \cdot \frac{\partial \overrightarrow{\omega_k}}{\partial \dot{q}_r} \tag{3.2.15}$$

where α_k is the angular acceleration of body k in R, and I is the inertia dyadic of k relative to the mass center G_k.

These equations form the foundation for the *Kane's equation*:

$$F_r + F_r^* = 0 \tag{3.2.16}$$

where

$$F_r = f_r + M_r \tag{3.2.17}$$

$$F_r^* = f_r^* + M_r^* \tag{3.2.18}$$

3.2.2 General Procedure

The general procedure of applying the Kane's method to derive the EoM for multibody system can be divided into 6 steps:

1. Label important points: The important points are defined as all center of mass locations, and locations of applied forces with the exception of conservative constraint forces.
2. Set up generalized coordinates (q_r) and generalized speeds (u_r) and generate expressions for angular velocity and acceleration of all bodies and velocity and acceleration of the import points.
3. Construct a partial velocity table, which donates the relation between the partial velocity of particle in reference coordinate system and the partial speeds.
4. Obtain the generalized active and inertia forces to form $F_r + F_r^* = 0$.
5. Write in a state-space form for the equations of motion:

$$M\dot{u} = f(u) \tag{3.2.19}$$

3.3 Relationship Between Kane's and Lagrange Equation

The equations of motion of a multibody system are unique, therefore irrespective of the method used to derive them, they should be the same. In what follows is a proof that in essence Lagrange method is equivalent to Kane's method.

The standard Lagrange function L is defined as:

$$L = T - V \tag{3.3.1}$$

where T is the total kinetic energy of the system and V is corresponding potential energy. Lagrange equations of motion are then obtained by

$$\frac{d}{dt}\left[\frac{\partial L}{\partial \dot{x}_l}\right] - \frac{\partial L}{\partial x_l} = 0 \tag{3.3.2}$$

Let the generalized active forces be given by $f_l = \frac{\partial V}{\partial x_l}$, so the Lagrange equation becomes

$$\frac{d}{dt}\left[\frac{\partial T}{\partial \dot{x}_l}\right] - \frac{\partial T}{\partial x_l} = f_l \tag{3.3.3}$$

Following from the above equation, the generalized inertia forces are

$$f_l^* = -\frac{d}{dt}\left[\frac{\partial T}{\partial \dot{x}_l}\right] + \frac{\partial T}{\partial x_l} \quad (l = 1, ..., n) \tag{3.3.4}$$

where n denotes the number of degrees of freedom of the system.

On the other side, the generalized inertia forces are also given by Kane's equation as:

$$f_l^* = \overrightarrow{F_k^*} \cdot \frac{\partial \overrightarrow{v_k}}{\partial \dot{x}_l} + \overrightarrow{T_k^*} \cdot \frac{\partial \overrightarrow{\omega_k}}{\partial \dot{x}_l} \tag{3.3.5}$$

where $\overrightarrow{F_k^*}$ is the inertia force and $\overrightarrow{T_k^*}$ the inertia torque of body k. The above equation can be simplified as

$$f_l^* = F_l^* + T_l^* \tag{3.3.6}$$

By definition,

$$\begin{aligned} F_l^* &= \overrightarrow{F_k^*} \cdot \frac{\partial \overrightarrow{v_k}}{\partial \dot{x}_l} \\ &= -[\frac{d}{dt}(m_k \overrightarrow{v_k} \cdot \frac{\partial \overrightarrow{v_k}}{\partial \dot{x}_l}) - m_k \overrightarrow{v_k} \cdot \frac{d}{dt}(\frac{\partial \overrightarrow{v_k}}{\partial \dot{x}_l})] \\ &= -[\frac{d}{dt}\frac{\partial}{\partial \dot{x}_l}(\frac{1}{2} m_k \overrightarrow{v_k} \cdot \overrightarrow{v_k}) - m_k \overrightarrow{v_k} \cdot \frac{d}{dt}(\frac{\partial \overrightarrow{r_k}}{\partial x_l})] \end{aligned} \tag{3.3.7}$$

Note that $\partial \bar{r}_k / \partial x_l$ is equal to $\partial \bar{v}_k / \partial \dot{x}_l$. The above equation can be expressed further to get

$$\begin{aligned} F_l^* &= -[\frac{d}{dt}(\frac{\partial T_f}{\partial \dot{x}_l}) - m_k \overrightarrow{v_k} \frac{\partial \overrightarrow{v_k}}{\partial \dot{x}_l}] \\ &= -[\frac{d}{dt}(\frac{\partial T_f}{\partial \dot{x}_l}) - \frac{\partial}{\partial x_l}(\frac{1}{2} m_k \overrightarrow{v_k} \cdot \overrightarrow{v_k})] \end{aligned} \tag{3.3.8}$$

so

$$F_l^* = -[\frac{d}{dt}(\frac{\partial T_f}{\partial \dot{x}_l}) - \frac{\partial T_f}{\partial x_l}] \tag{3.3.9}$$

where T_f is the kinetic energy due to the inertia forces only. Similarly, for the generalized inertia torque,

$$\begin{aligned} T_l^* &= -[\overrightarrow{M_k^*} \cdot \frac{\partial \overrightarrow{\omega_k}}{\partial \dot{x}_l}] \\ &= -[\frac{d}{dt}(\overrightarrow{\omega_k} \cdot I \cdot \frac{\partial \overrightarrow{\omega_k}}{\partial \dot{x}_l}) - \overrightarrow{\omega_k} \cdot I \cdot \frac{d}{dt} \cdot \frac{\partial \overrightarrow{\omega_k}}{\partial \dot{x}_l}] \end{aligned} \tag{3.3.10}$$

where

$$\frac{d}{dt}(\frac{\partial \overrightarrow{\omega_k}}{\partial \dot{x}_l}) = \frac{\partial \overrightarrow{\omega_k}}{\partial x_l} \tag{3.3.11}$$

Substituting the equation into T_l^* to get

$$\begin{aligned} T_l^* &= -[\frac{d}{dt}\frac{\partial}{\partial \dot{x}_l}(\frac{1}{2}\overrightarrow{\omega_k} \cdot I \cdot \overrightarrow{\omega_k}) - \overrightarrow{\omega_k} \cdot I \cdot \frac{\partial \overrightarrow{\omega_k}}{\partial x_l}] \\ &= -[\frac{d}{dt}(\frac{\partial T_m}{\partial \dot{x}_l}) - \frac{\partial T_m}{\partial \dot{x}_l}] \end{aligned} \tag{3.3.12}$$

where T_m is the kinetic energy due to the rotation only.

Thus, the generalized inertia forces obtained from Kane's and Lagrange method are equivalent. Similarly, the generalized active forces from both methods are the same. Hence the equations of motion of system S in the reference frame R can be found through either method.

3.4 Constraints

Constraints in the mechanical system are used to restrict the motion of parts in the system. There are a number of modeling elements that can be used to do this and the constraint may restrict the absolute motion of a body relative to the ground or the relative motion between interconnected parts (Blundell and Harty, 2004). Normally, constraints can be classified into two types: holonomic and non-holonomic constraints.

3.4.1 Holonomic Constraints

If there are some generalized coordinates in the multibody system that depend on some others, these constraints are considered as holonomic constraints. Assuming a multibody system is specified by n generalized coordinates, and furthermore, that there are m independent equations of constraint of the form:

$$f_i(x_1,\ x_2,\ ...,\ x_n, t) = 0 \ \ (i = 1,\ 2,\ ...,\ m) \tag{3.4.1}$$

The constraints that can be expressed in this form are said as holonomic. The holonomic constraints eliminate all dependent coordinates and thus end up with a system of $n - m$ independent coordinates.

3.4.2 Non-Holonomic Constraints

The treatment of constraint equations in which only the generalized coordinates and time are present is well known and fairly straightforward. However, in some systems the constraints are not expressible only in terms of coordinates, but also with coordinate velocities, these non-integrable relations between velocities are considered as non-holonomic constraints, which are in the form of:

$$f_i(x_1,\ \dot{x}_1,\ ...,\ x_n,\ ,\dot{x}_n, t) = 0\ \ (i = 1,\ 2,\ ...,\ m) \tag{3.4.2}$$

In some cases, the holonomic constraints may be differentiated with respect to time yielding the velocity constraints:

$$f(x,\ \dot{x}) := \frac{d}{dt}f(x) = (\frac{d}{dx}f(x))\dot{x} = G(x)\dot{x} \tag{3.4.3}$$

with the constraint matrix $G(x)$. Although this is in the form of non-holonomic constraints, f is not non-holonomic constraints since it obviously can be integrated to yield holonomic constraints.

3.5 Showcase Example

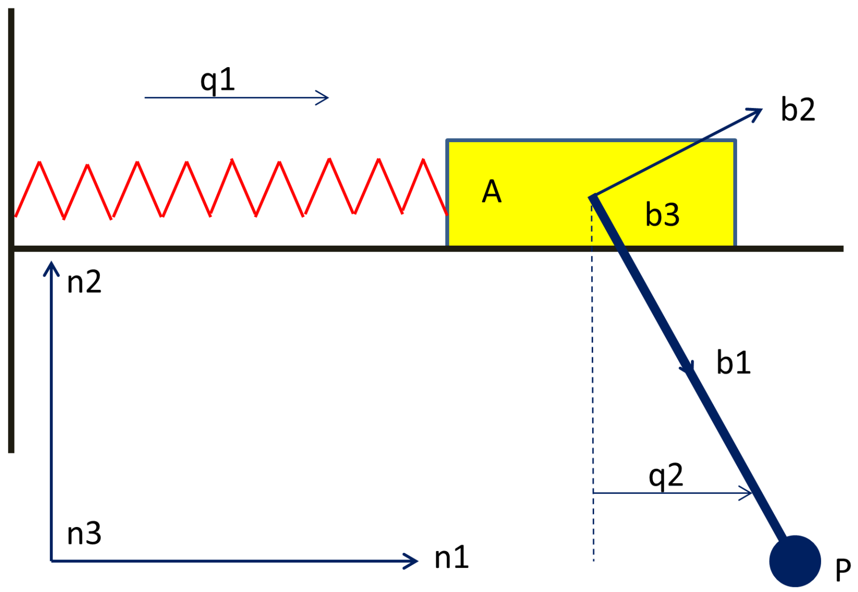

Figure 3.2: ***Pendulum attached on a Moving Body***

Here, an example is studied to prove that the equations from both of Kane's and Lagrange method are the same. The kinematics equation is same for both of Kane and Lagrange. Based on the reference frame n, the transformation matrix between local frame b and n can be easily got as:

$$S = \begin{bmatrix} s2 & c2 & 0 \\ -c2 & s2 & 0 \\ 0 & 0 & 1 \end{bmatrix} \tag{3.5.1}$$

in which, $s2 = \sin q_2$ and $c2 = \cos q_2$.
Then, we can get the mass center velocity and acceleration for body A and P.

$$\overrightarrow{{}^N v^A} = u_1\overrightarrow{n_1} \qquad \overrightarrow{{}^N a^A} = \dot{u}_1\overrightarrow{n_1} \tag{3.5.2}$$

$$\begin{aligned}\overrightarrow{{}^{N}v^{P}} &= \overrightarrow{{}^{N}v^{A}} + \overrightarrow{{}^{A}u^{P}} \\ &= \overrightarrow{{}^{N}v^{A}} + \overrightarrow{{}^{A}\omega^{P}} \times \overrightarrow{\gamma_{PA}} \\ &= u_1\overrightarrow{n_1} + u_2\overrightarrow{n_3} \times l\overrightarrow{b_1} \\ &= u_1\overrightarrow{n_1} + lu_2(\cos q_2\overrightarrow{n_1} + \sin q_2\overrightarrow{n_2}) \\ &= (u_1 + lu_2\cos q_2)\overrightarrow{n_1} + lu_2\sin q_2\overrightarrow{n_2}\end{aligned} \tag{3.5.3}$$

$$\overrightarrow{{}^{N}a^{P}} = (\dot{u}_1 + l\cos q_2\dot{u}_2 + lu_2(-\sin q_2)u_2)\overrightarrow{n_1} + (l\sin q_2\dot{u}_2 + lu_2\cos q_2 u_2)\overrightarrow{n_2} \tag{3.5.4}$$

- **Lagrange Equation**
The kinetic energy is then found as:

$$\begin{aligned}T &= \frac{1}{2}m_A\overrightarrow{v_A}\overrightarrow{v_A} + \frac{1}{2}m_P\overrightarrow{v_P}\overrightarrow{v_P} \\ &= \frac{1}{2}m_A u_1^2 + \frac{1}{2}m_P[(u_1 + lu_2\cos q_2)^2 + (lu_2\sin q_2)^2] \\ &= \frac{1}{2}m_A u_1^2 + \frac{1}{2}m_P u_1^2 + m_P l u_1 u_2\cos q_2 + \frac{1}{2}m_P l^2 u_2^2\end{aligned} \tag{3.5.5}$$

and the potential energy is obtained as:

$$V = -m_P gl\cos q_2 + \frac{1}{2}kq_1^2 \tag{3.5.6}$$

Hence, the Lagrange equation is:

$$L = T - V \tag{3.5.7}$$

then,

$$\begin{aligned}\frac{\partial L}{\partial q_1} &= -kq_1 \\ \frac{\partial L}{\partial q_2} &= -m_P l u_1 u_2\sin q_2 - m_P gl\sin q_2 \\ \frac{\partial L}{\partial u_1} &= m_A u_1 + m_P u_1 + m_P l u_2\cos q_2 \\ \frac{\partial L}{\partial u_2} &= m_P l u_1\cos q_2 + m_P l^2 u_2\end{aligned} \tag{3.5.8}$$

Substituting the above relations into the following equation

$$\frac{d}{dt}(\frac{\partial L}{\partial u}) - \frac{\partial L}{\partial q} = 0 \tag{3.5.9}$$

to get

$$\begin{aligned}m_A\dot{u}_1 + m_P\dot{u}_1 + m_P l\dot{u}_2\cos q_2 - m_P l u_2\sin q_2 u_2 - (-kq_1) &= 0 \\ m_P l\dot{u}_1\cos q_2 - m_P l u_1\sin q_2 u_2 + m_P l^2\dot{u}_2 - (-m_P l u_1 u_2\sin q_2 - m_P gl\sin q_2) &= 0\end{aligned} \tag{3.5.10}$$

which can be presented in the state space model:

$$\begin{bmatrix} m_A + m_P & m_P l\cos q_2 \\ m_P l\cos q_2 & m_P l^2 \end{bmatrix}\begin{bmatrix} \dot{u}_1 \\ \dot{u}_2 \end{bmatrix} = \begin{bmatrix} m_P l u_2^2\sin q_2 - kq_1 \\ -m_P gl\sin q_2 \end{bmatrix} \tag{3.5.11}$$

  - **Kane's Equation**
  The foundation of Kane's method is to construct the equation

$$f + f^* = 0 \tag{3.5.12}$$

in which

$$
\begin{aligned}
f &= \overrightarrow{F} \cdot \frac{\partial \overrightarrow{v_k}}{\partial \dot{q}_r} \\
f^* &= \overrightarrow{F^*} \cdot \frac{\partial \overrightarrow{v_k}}{\partial \dot{q}_r}
\end{aligned}
$$

substituting the kinematic relations into the above equation to obtain

$$
\begin{aligned}
&f_1 = (-kq_1\overrightarrow{n_1} - m_A g\overrightarrow{n_2}) \cdot \overrightarrow{n_1} + (-m_P g\overrightarrow{n_2}) \cdot \overrightarrow{n_1} = -kq_1 \\
&f_2 = (-kq_1\overrightarrow{n_1} - m_A g\overrightarrow{n_2}) \cdot 0 + (-m_P g\overrightarrow{n_2}) \cdot (l\cos q_2\overrightarrow{n_1} + l\sin q_2\overrightarrow{n_2}) = -m_P gl\sin q_2 \\
&f_1^* = (-m_A{}^N a^A) \cdot \overrightarrow{n_1} + (-m_P{}^N a^P) \cdot \overrightarrow{n_1} = -m_A\dot{u}_1 - m_P(\dot{u}_1 + l\cos q_2\dot{u}_2 + lu_2^2(-\sin q_2)) \\
&f_2^* = (-m_A{}^N a^A) \cdot 0 + (-m_P{}^N a^P) \cdot (l\cos q_2\overrightarrow{n_1} + l\sin q_2\overrightarrow{n_2}) \\
&\quad = -m_P(\dot{u}_1 l\cos q_2 + l^2\dot{u}_2)
\end{aligned}
\tag{3.5.13}
$$

Hence, the equations of motion can be obtained as:

$$
\begin{bmatrix} m_A + m_P & m_P l\cos q_2 \\ m_P l\cos q_2 & m_P l^2 \end{bmatrix} \begin{bmatrix} \dot{u}_1 \\ \dot{u}_2 \end{bmatrix} = \begin{bmatrix} m_P l u_2^2 \sin q_2 - kq_1 \\ -m_P gl\sin q_2 \end{bmatrix} \tag{3.5.14}
$$

It is obvious to validate that the equations of motion obtained from both of Kane's and Lagrange method are identical and there is no significant difference on the efficiency of both methods, the Kane's method is used in the following study.

Chapter 4

Computer - Aided Simulation

A *Python* package is introduced in the thesis for the computer-aided simulation, which is called *PyDy*. Generally speaking, *PyDy* is a workflow that utilizes an array of scientific tools written in the *Python* programming language to study multibody dynamics. The core of this tool set is the *Sympy.mechanics* package which generates symbolic equations of motion for complex multibody systems.

The *PyDy* workflow consists of setting up three steps:

1. Physical Model
2. Mathematical Model
3. Numerical Simulation

4.1 Physical Model

The first step of *PyDy* is setting the physical model in a proper coordinate system, which is essential to describe the multibody system correctly. First of all, all parts of the multibody system should be defined in a common coordinate system to set up the mathematical equations uniformly, so a fundamental reference frame should be set, usually, it is fixed. Because of two or more than two bodies in the system, for each body, one body fixed coordinate system should be defined, which is the best way to describe the rotation with respect to its own axis.

After the coordinate system has been set up, the states (displacement and velocity) and forces can be defined as the vector in the corresponding coordinate system.

$$\overrightarrow{x} = mag \cdot \overrightarrow{unit} \tag{4.1.1}$$

The last step is to incorporate the forces and states in the multibody system (particle, body, etc), then the whole physical model can be regarded as finished.

Basically, the physical model can be divided as:

- Reference coordinate system and body-fixed coordinate system (Frame and Original Point)
- System properties definition (Mass, Inertia, Particle or Body)
- States and forces definition (Magnitude and direction)
- Connection of system, states and forces

4.2 Mathematical Model

After the physical model has been built, it should be converted to symbolic mathematical equations. In the *Sympy* package, two existing methods have been programmed to build the symbolic equations, *Kane's Method* and *Lagrange Method*. Basically, both of Kane's and Lagrange method can be used equivalently, which has been proved before.

Kane's method forms two expressions F_r and F_r^*, the generalized inertia force and generalized active force, whose sum is zero. It can deal with a variety of constraints such as holonomic constraints, non-holonomic constraints, kinematic differential equations, dynamic equations and differentiated non-holonomic equations.

The products of *Kane's Method* are a forcing vector and a mass matrix. With a list of state derivatives inserted, we can actually obtain the equations of motion.

$$M \cdot \dot{u} = f\left(u, t\right) \tag{4.2.1}$$

Where u are the state variables, M is the mass matrix and $f(u,t)$ is the force vector.

4.3 Numerical Simulation

In order to simulate the previously built equations, a lot of solvers have been made available on Internet. Even though the *Sympy* itself contains some solvers, but its application is still limited. Here, a more powerful package is being introduced, which is called as *Assimulo*.

Assimulo is a simulation package for solving ordinary differential equations, which was created from a collaboration between the Department of Numerical Analysis and the Department of Automatic Control at Lund University together with the company *Medelon AB*.

It is written in the high-level programming language *Python* and combines a variety of different solvers written in FORTRAN, C and even Python via a common high-level interface. The primary aim of *Assimulo* is not to develop new integration algorithms. The aim is to provide a high-level interface for a wide variety of solvers, both new and old, solvers of industrial standards as well as experimental solvers. The aim is to allow comparison of solvers for a given problem without the need to define the problem in a number of different programming languages to accommodate the different solvers.

Assimulo presents both one-step methods and multi-step methods, which can be used to solve most Ordinary Differential Equation (ODE) and Differential Algebraic Equation (DAE) problems. Because of the complexity of multi-body dynamical analysis, the suitable solver should be chosen from the *Assimulo* library to keep balance between efficiency and accuracy.

4.4 Showcase Example

In order to inspect the reliability of these solvers in *Assimulo,* the very simple case is studied using two approaches to simulate the motion response. Assuming the barge can move only in one direction, it can be simplified as a dash-pot system, which is sketched below.

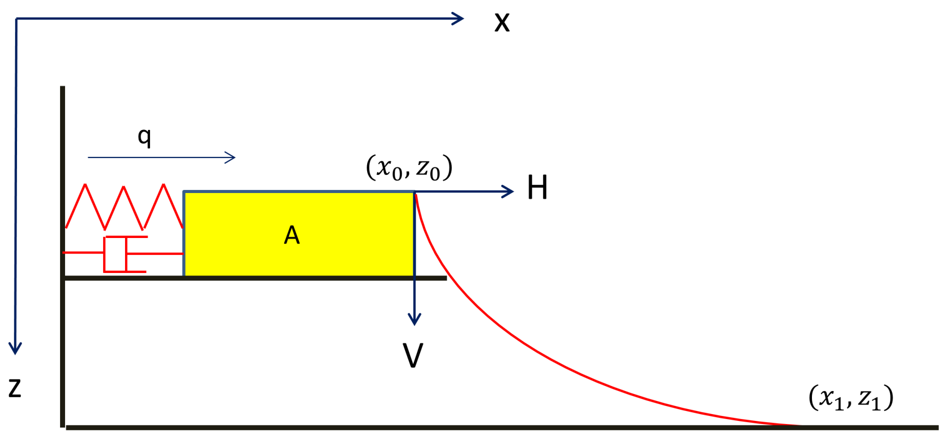

Figure 4.1: *Configuration of One Barge with One Mooring Line*

- **Equation of Motion**
  - Define important points as the center of mass of A.
  - Select generalized coordinate as shown in the figure and generate velocity and acceleration expressions for the import point.

$$
\begin{aligned}
{}^N v^A &= u_1 \vec{x} \\
{}^N a^A &= \dot{u}_1 \vec{x}
\end{aligned}
\tag{4.4.1}
$$

  - Construct a partial velocity table.

u_r	${}^N v_r^A$
$r = 1$	$\vec{x}$

  - $F_r + F_r^* = 0$

$$F_r = (-kq_1 - cu_1 + H)\vec{x} \cdot {}^N v_r^A \qquad F_r^* = (-m\, {}^N a^A) \cdot {}^N v_r^A \tag{4.4.2}$$

so

$$F_1 = -kq_1 - cu_1 + H \qquad F_1^* = -m\dot{u}_1 \tag{4.4.3}$$

  - Assemble $F_r + F_r^* = 0$

$$\begin{bmatrix} 1 & 0 \\ 0 & m \end{bmatrix} \begin{bmatrix} \dot{q}_1 \\ \dot{u}_1 \end{bmatrix} = \begin{bmatrix} u_1 \\ -kq_1 - cu_1 + H \end{bmatrix} \tag{4.4.4}$$

Which obviously meets the common sense of simple dash-pot system.

- **Constraints**

From this figure, it is obvious to notice that the barge can only move in the x direction of the fixed coordinate system, and the fairlead point of mooring line has to move along with the barge. The horizontal force and vertical force from the mooring line, H and V respectively, can be calculated using the following equation (Irvine and Irvine, 1992):

$$L_H = x_1 - x_0 = \frac{HL_0}{EA} + \frac{HL_0}{W} \cdot \left[\sinh^{-1}\left(\frac{V}{H}\right) - \sinh^{-1}\left(\frac{V-W}{H}\right)\right] \tag{4.4.5}$$

$$L_V = z_1 - z_0 = \frac{WL_0}{EA} \cdot \left(\frac{V}{W} - \frac{1}{2}\right) + \frac{HL_0}{W} \cdot \left\{\left[1 + \left(\frac{V}{H}\right)^2\right]^{\frac{1}{2}} - \left[1 + \left(\frac{V-W}{H}\right)^2\right]^{\frac{1}{2}}\right\} \tag{4.4.6}$$

It is significant that these equations show a strong nonlinear implicit properties, in which x_0, $z_{0,}$ $z_1$are fixed, so they can be briefly denoted as:

$$f(x, H, V) = 0 \tag{4.4.7}$$

$$g(H, V) = 0 \tag{4.4.8}$$

Here, if the holonomic constraints are differentiated into a form of velocity constraints, it results in a ODE for the whole system, this approach is considered as ODE approach. Otherwise, the holonomic constraints can be incorporated into the equation of motion without any preprocess, it results in a DAE form, and this one is considered as DAE approach.

The simulation results for ODE and DAE approach are plotted below:

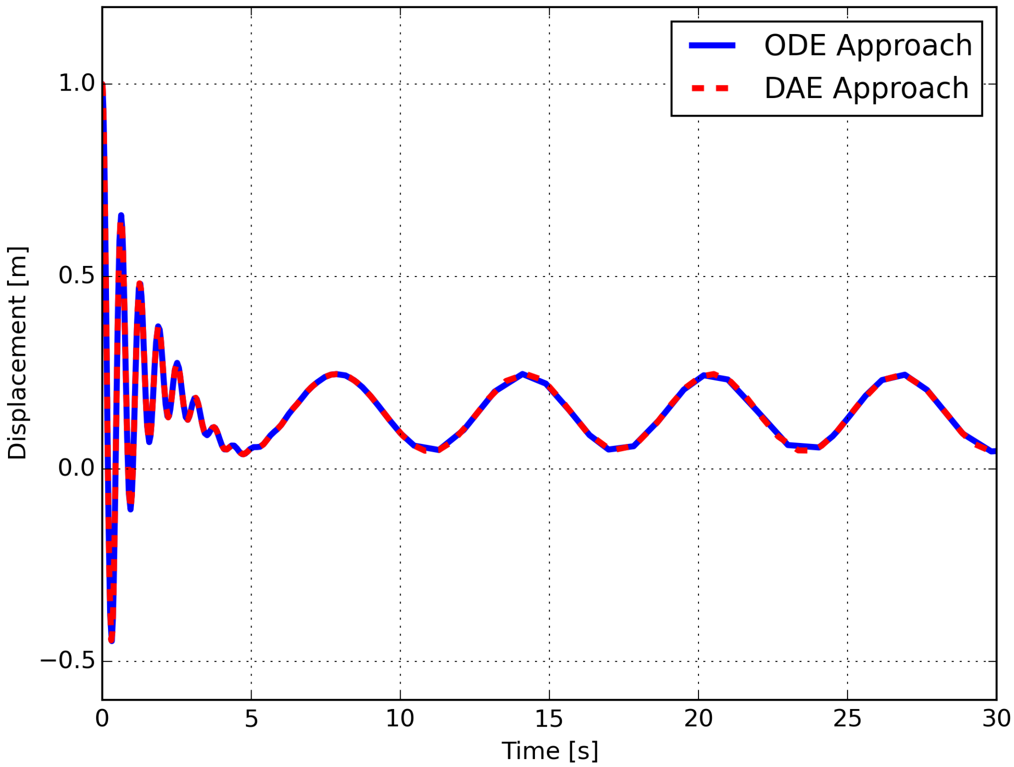

Figure 4.2: *Dynamic Response Comparison* (*ODE and DAE Approach*)

It is obvious to see that the simulation results from both approaches are identical, so the solvers are regarded as reliable. The efficiency difference has been observed in the computer-aided simulation that the DAE approach has a higher efficiency and a shorter computation time.

Part II

System Identification of the Fluid Memory Effect

Chapter 5

Description of the Wave Effect

5.1 Introduction

As the vessel oscillates around its equilibrium point, a certain amount of water moves along with it, which is called added mass. Besides, the motion of the vessel also introduces motion into the nearby water body, which plays the role similar with damping. Hence, the kinetic energy is transferred from the vessel to the water body, which makes the water radiate away from the vessel. In total, the added mass A $[kg]$ and damping B $[Ns/m]$ are used to describe the radiation force.

The challenge with describing the radiation forces is that the added mass and damping values are not constant, but vary with the motion of the vessel (Janssen et al., 2014). One approach to overcome the difficulties is to apply a frequency-domain approach, e.g. by using simplified bilinear and trilinear frequency response functions (Taghipour et al., 2008). More specifically, the values of added mass and damping vary with the frequency ω at which the vessel oscillates. For the oscillatory motion with frequency ω, the complex expression of the radiation forces can be read as:

$$\tau_R(t) = \Re\{[-\omega^2 A(\omega) + j\omega B(\omega)]\tilde{x} \cdot e^{j\omega t}\} \tag{5.1.1}$$

where $A \in \mathbb{R}^{6\times 6}$, $B \in \mathbb{R}^{6\times 6}$ and $x \in \mathbb{R}^6$ for single floating body.

However, the frequency-domain approaches is not a very convenient way for the response simulation and control system design. In the early sixties, a key step for the modeling of the response of marine structures in waves is made by Cummins, which relates the motion of the marine structure to the wave-induced forces within the linear time-invariant framework (Cummins, 1962). The *Cummins equation* has been introduced before.

5.1.1 The Cummins Equation

The forces and responses of floating structures are usually obtained by means of a linear analysis in the frequency domain (Chen et al., 2014). *Cummins* considered the behavior of the fluid and the structure in time domain. The assumptions of linear behavior and impulses in the components of motion result in a boundary value problem (BVP) in which the potential was separated into two parts: one valid during the duration of the impulses and the other valid afterwards. By expressing the pressure as a function of these potentials and integrating it over the wet surface of the vessel, he obtained a vector integro-differential equation, which is know as the *Cummins equation*. It governs the motions of a floating body at zero forward speed in the time domain and can be written as (Cummins, 1962):

$$[M + A]\ddot{x}(t) + \int_0^t K(t-\tau)\dot{x}(\tau)\,d\tau + Cx(t) = f^{ext}(t) \tag{5.1.2}$$

So, the following term represents the radiation force:

$$\tau_{rad} = -A\ddot{x}(t) - \int_0^t K(t-\tau)\dot{x}(\tau)\,d\tau \tag{5.1.3}$$

The convolution term in *Cummins equation* captures the effect that the change in momentum of the fluid at a particular time affects the motion at subsequent time, which is known as the fluid memory effect.

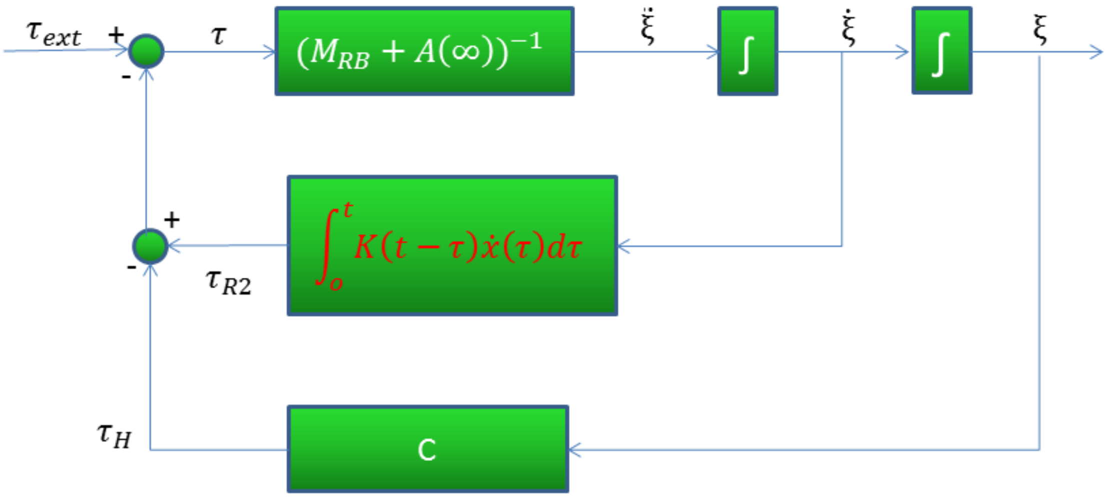

Figure 5.1: *Simulation Diagram with the Convolution Term*

5.1.2 Frequency and Time Domain Relations

Ogilvie considered Cummins equation in the frequency domain by using the Fourier transform and derived the following frequency domain model (Ogilvie, 1964):

$$-\omega^2[M + A(\omega)]X(j\omega) + j\omega B(\omega) X(j\omega) + CX(j\omega) = F^{ext}(j\omega) \tag{5.1.4}$$

where $X(j\omega)$ and $F^{ext}(j\omega)$ are Fourier transforms of $x(t)$ and $f^{ext}(t)$. The hydrodynamic coefficients (added mass $A(\omega)$ and radiation damping $B(\omega)$) and wave excitation force $F^{ext}(j\omega)$ can be readily obtained from 3D hydrodynamic codes such as software WAMIT used in this research.

Let the vessel perform simple harmonic motion with frequency ω, $x(t) = \Re\{\tilde{X}e^{j\omega t}\}$, then Eq: 5.1.3 can be written as:

$$\begin{aligned}
\tau_{rad} &= -A\ddot{x}(t) - \int_0^t K(t-\tau)\dot{x}(\tau)d\tau \\
&= -A\ddot{x}(t) - \int_{-\infty}^t K(t-\tau)\dot{x}(\tau)d\tau \\
&= -A\ddot{x}(t) - \int_0^\infty K(\tau)\dot{x}(t-\tau)d\tau \\
&= -A\Re\{-\omega^2\tilde{X}e^{j\omega t}\} - \int_0^\infty K(\tau)\Re\{j\omega\tilde{X}e^{j\omega t}e^{-j\omega t}\}d\tau \\
&= -A\Re\{-\omega^2\tilde{X}(\cos(\omega t) + j\sin(\omega t))\} \\
&- \int_0^t K(\tau)\Re\{j\omega\tilde{X}(\cos(\omega t) + j\sin(\omega t))(\cos(\omega t) - j\sin(\omega t))\}d\tau \\
&= \omega^2\cos(\omega t)A\tilde{X} - \omega\cos(\omega t)\int_0^\infty K(\tau)\tilde{X}\sin(\omega\tau)d\tau \\
&+ \omega\sin(\omega t)\int_0^\infty K(\tau)\tilde{X}\cos(\omega\tau)d\tau
\end{aligned} \tag{5.1.5}$$

The radiation force in the frequency domain can be written with real-valued $A(\omega)$ and $B(\omega)$:

$$\begin{aligned}\tau_{rad} &= -A(\omega)\ddot{x}\,(t) - B(\omega)\dot{x}(t) \\ &= -A(\omega)\Re\{-\omega^2\tilde{X}e^{j\omega t}\} - B(\omega)\Re\{j\omega\tilde{X}e^{j\omega t}\} \\ &= -A(\omega)\Re\{-\omega^2\tilde{X}(\cos(\omega t) + j\sin(\omega t))\} \\ &- B(\omega)\Re\{j\omega\tilde{X}(\cos(\omega t) + j\sin(\omega t))\} \\ &= \omega^2\cos(\omega t)A(\omega)\tilde{X} + \omega\sin(\omega t)B(\omega)\tilde{X}\end{aligned} \tag{5.1.6}$$

Comparing the parts depending on $\cos(\omega t)$ and $\sin(\omega t)$ in the Eq: 5.1.5 and Eq: 5.1.6, the following relations follow (Unneland, 2007):

$$A\,(\omega) = A - \frac{1}{\omega}\int_0^\infty K\,(t)\sin\,(\omega\tau)\,d\tau \tag{5.1.7}$$

$$B\,(\omega) = \int_0^\infty K\,(t)\cos\,(\omega\tau)\,d\tau \tag{5.1.8}$$

The Fourier cosine transform is the real part of the Fourier transform, which is defined as follows:

$$\begin{aligned}\mathcal{F}_c[x(t)] = \overline{X}_{re}(j\omega) &= \int_0^\infty x(t)\cos(\omega t)dt \\ \mathcal{F}_c^{-1}[\overline{X}_{re}(j\omega)] = x(t) &= \frac{2}{\pi}\int_0^\infty \overline{X}_{re}(j\omega)\cos(\omega t)d\omega\end{aligned} \tag{5.1.9}$$

$\overline{X}_{re}(j\omega)$ is referred as the Fourier cosine transform of $x(t)$.

The Fourier sine transform is the imaginary part of the Fourier transform, which is defined as follows:

$$\begin{aligned}\mathcal{F}_s[x(t)] = \overline{X}_{im}(j\omega) &= \int_0^\infty x(t)\sin(\omega t)dt \\ \mathcal{F}_s^{-1}[\overline{X}_{im}(j\omega)] = x(t) &= \frac{2}{\pi}\int_0^\infty \overline{X}_{im}(j\omega)\sin(\omega t)d\omega\end{aligned} \tag{5.1.10}$$

$\overline{X}_{im}(j\omega)$ is referred as the Fourier sine transform of $x(t)$.

The retardation function $K\,(t)$ can be formulated as follows by taking the Inverse Fourier Cosine or Sine Transform (IFT):

$$K\,(t) = \frac{2}{\pi}\int_0^\infty B\,(\omega)\cos\,(\omega t)\,d\omega \tag{5.1.11}$$

or

$$K\,(t) = -\frac{2}{\pi}\int_0^\infty \omega\,(A\,(\omega) - A\,(\infty))\sin\,(\omega t)\,d\omega \tag{5.1.12}$$

$$A = \lim_{\omega\to\infty} A\,(\omega) = A\,(\infty) \tag{5.1.13}$$

The Eq 5.1.11 is the preferred way to calculate $K\,(t)$ since it converges faster than Eq: 5.1.12. This then provides the way to evaluate the time domain model based on frequency domain results.

From the Fourier transform, for frequency-domain identification, the following relation is used to describe the frequency response:

$$K\,(j\omega) = \int_0^\infty K\,(t)\,e^{-j\omega t}dt = B\,(\omega) + j\omega\,(A\,(\omega) - A\,(\infty)) \tag{5.1.14}$$

since $K\,(j\omega)$ is complex, the frequency response can be plotted separately as a magnitude plot and a phase plot.

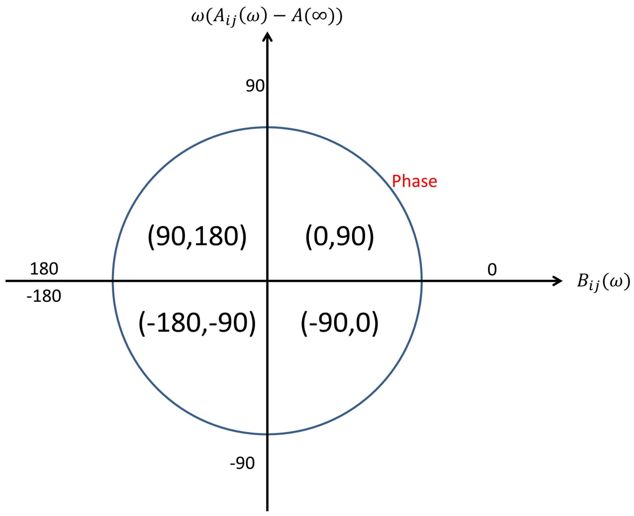

Figure 5.2: *Relation between Phase of $K_{ij}(j\omega)$ and Added Mass and Damping*

5.1.3 Non-Parametric Model Identification

Hydrodynamic codes based on potential theories (2D and 3D) are nowadays readily available for the computation of the frequency-dependent added mass, $A(\omega)$, and potential damping, $B(\omega)$. These data can be computed for a reduced set of frequencies of interest; and therefore, they provide means to determine nonparametric models of the convolution terms via application of retardation equations and frequency response equations. These codes, however, have their inherent limitations due to theoretical and implementation issues.

In 3D or panel method codes, the size of the panels used to discretize the surface of the hull limit the accuracy of the computations at high frequency. As a rule of thumb, the characteristic size of the panels should be of the order of 1/8 of the wave length corresponding to the larger frequency used in the computations (Faltinsen, 1990). This limits the upper frequency since smaller panels increase the number of computations significantly and result in numerical problems. 3D codes often solve for the particular cases of infinite and zero frequency, which result from particular boundary conditions on the free-surface that ensure no waves are generated.

For slender vessels, codes based on strip theory (2D) can be used. Slenderness results in the velocity field being nearly constant along the longitudinal direction. This characteristic allows reducing the 3D problem to a 2D problem (Newman, 1977). These codes have a limit on the lower frequency which is due to an assumption made on the free surface condition that results in a simplification of the boundary-value problem (Salvesen et al., 1970). The two-dimensional hydrodynamic problem associated with each section or strip of the hull can be solved, for example, using conformal mapping or panel methods. If the 2D code uses panel methods to compute the hydrodynamic parameters associated with each strip, then the same limitations for high frequencies discussed for the 3D codes hold. Strip theory codes do not compute the zero and infinite frequency cases (Pérez and Fossen, 2008).

5.2 Parametric Model Identification

5.2.1 Convolution Replacement

The convolution term in the *Cummins equation* describes a casual linear time-invariant system. This model is, however, cumbersome for numerical simulation and not well suited for the design and analysis of motion control systems (Kristiansen et al., 2005). In addition, it may be very time-consuming to directly evaluate the convolutions depending on the simulation time length, time step and degrees of freedom of the considered problems.

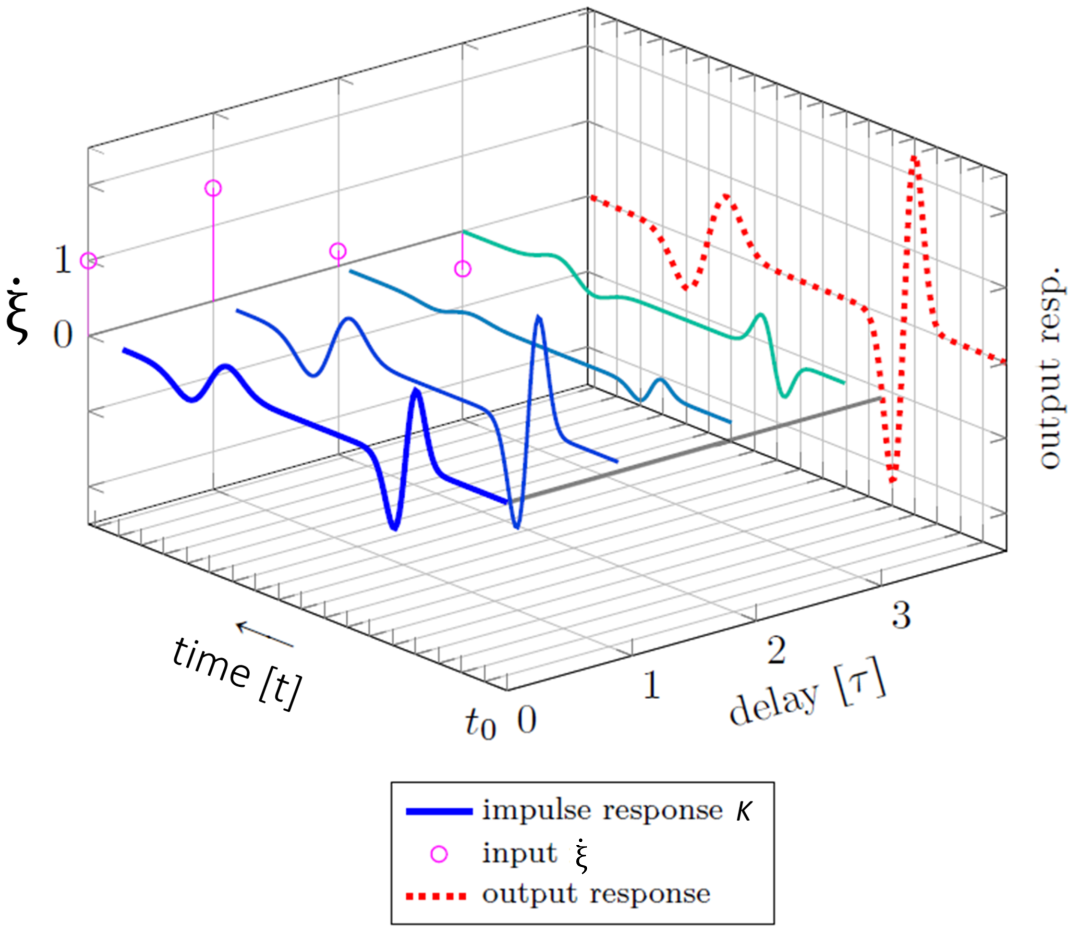

Figure 5.3: *Visualization of the Linear Time Invariant System*

For these reasons, significant efforts have been dedicated to finding the alternative representation of the convolution terms in the *Cummins equation.* These alternative representations can be broadly grouped into the following types (Taghipour et al., 2008):

- Replacement of the frequency-dependent added mass and damping by constant coefficients to form the constant coefficient method (CCM):

$$\left[M + \tilde{A}\right] \ddot{x}\left(t\right) + \tilde{B}\dot{x}\left(t\right) + Cx\left(t\right) = f^{ext}\left(t\right) \tag{5.2.1}$$

- Replacement of the convolution term by a state-space formulation:

$$\left[M + A\left(\infty\right)\right] \ddot{x}\left(t\right) + f^{R}\left(t\right) + Cx\left(t\right) = f^{ext}\left(t\right)$$

$$\dot{z}(t) = A'z\left(t\right) + B'\dot{x}\left(t\right) \tag{5.2.2}$$

$$f^{R}\left(t\right) = C'z\left(t\right) + D'\dot{x}\left(t\right)$$

- Replacement of the force-to-motion response by a state-space model:

$$\dot{z}(t) = A'z\left(t\right) + B'f^{ext}\left(t\right)$$

$$y\left(t\right) = C'z\left(t\right) + D'f^{ext}\left(t\right) \tag{5.2.3}$$

$$with \;\; y = \left[x, \dot{x}\right]^{T}$$

The first approach is a low-order approximation as defined by the size of the associated state vector. This form is the simplest possible approach in which the frequency-dependent added mass and damping values are directly replaced by constant matrices. The accuracy of the method depends on how frequency sensitive the added mass and damping are for the specific problem. Such an approximation would normally be based on radiation quantities corresponding to the modal or the zero-crossing frequency of the sea wave spectrum. Such a simple method leads to relatively large errors in modeling the system transient response due to a single frequency excitation or system steady-state response due to multiple frequency excitation. Therefore, this method will not be pursued in this thesis. The other two methods are higher order approximations (Taghipour et al., 2008).

The convolution term can be approximated by a state-space model (SSM) since they are equivalent in describing a linear time invariant (LTI) system. Besides, the state-space model is convenient for the analysis of multiple-input and multiple-output (MIMO) systems and well suited for the design and analysis of motion control tools (Chen et al., 2014). In general, the state-space model has provided an attractive alternative for simulation due to the simple form of its solution. In our research, the second approach Eq: 5.2.2 is adopted to replace the convolution term because it is easy to incorporate into the state-space equations of motion produced by Kane's method.

5.2.2 State-Space Model (SSM)

As mentioned before, the convolution term in *Cummins equation* can be formulated in the state-space model as follows:

$$f^R(t) = \int_0^t K(t-\tau)\,\dot{x}(\tau)\,d\tau \Longrightarrow \begin{cases} \dot{z}(t) = A'z(t) + B'\dot{x}(t) \\ f^R(t) = C'z(t) + D'\dot{x}(t) \end{cases} \tag{5.2.4}$$

where $z(t)$ is the state vector summarizing all the past information of the system, A', B', C', D' are continuous-time state-space matrices. If the Cummins convolution term is replaced by the state-space model, the simulation diagram can be depicted as follows:

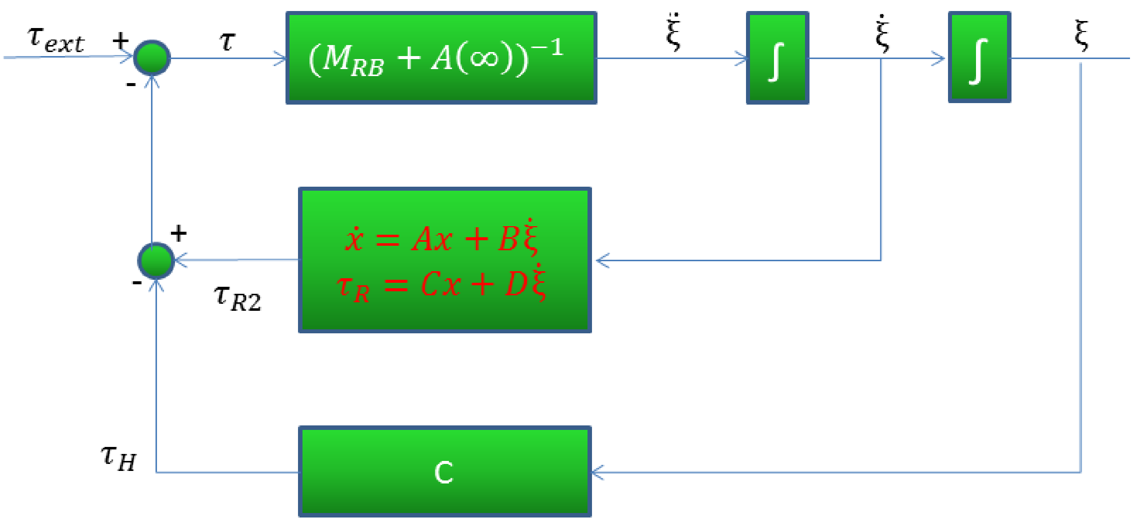

Figure 5.4: *Simulation Diagram with a State Space Model*

After the convolution term is formulated in the state-space model, the transfer function can be derived as:

$$K(s) = C'(sI - A')^{-1}B' + D' \tag{5.2.5}$$

in which s denotes the complex frequency $s = j\omega$. It is also expressed as follows in system identification.

$$K(s) = \frac{P(s)}{Q(s)} = \frac{p_m s^m + p_{m-1}s^{m-1} + \cdots + p_1 s + p_0}{s^n + q_{n-1}s^{n-1} + \cdots + q_1 s + q_0} \tag{5.2.6}$$

The roots of the numerator polynomial $P(s)$ are the zeros of the system and the roots of the denominator are the poles. The order of the system is the degree of the denominator polynomial (after canceling common factors between numerator and denominator): $n = \deg(Q)$, and the relative degree of the system is the difference $\deg(Q) - \deg(P) = n - m$. The relative degree has implications on the initial value of the impulse response, which are of importance (Taghipour et al., 2008).

The unknown parametric matrices of the SSM is obtained using system identification. Generally, every identification method consists of selecting a series of data, choosing a model structure (model type and order) and a fitting criterion. The objective of system identification is to obtain the lowest order model possible that is able to produce the behavior of the system for the desired purpose while maintaining stability of the resulting model (Taghipour et al., 2008).

The general idea is to replace the convolution terms by alternative models based on the following types of data:

- Complex hydrodynamic coefficients: $\bar{A}(j\omega)$ and $\bar{B}(j\omega)$ for added mass and damping respectively.

- The retardation functions $K(t)$ and its frequency response $K(j\omega)$.

- The force-to-motion Frequency Response Function (FRF): $H^{FM}(j\omega)$.

Depending upon which type of data is used, the identification method can be divided into two main groups:

- Frequency-Domain Identification

- Time-Domain Identification

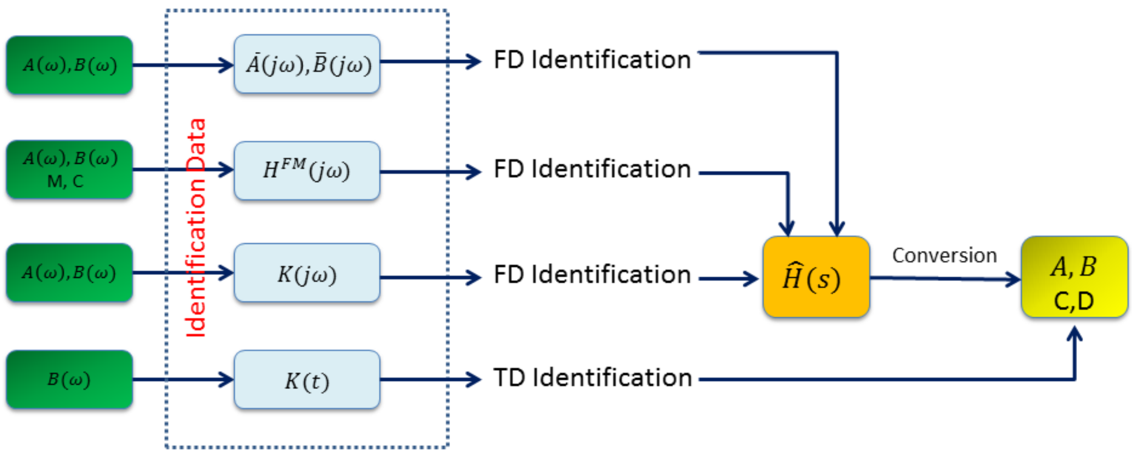

Figure 5.5: *Identification Approaches for the System Identification (R. Taghipour 2008)*

An import aspect of any identification problem is the amount of a prior knowledge available about the dynamic system under study and how this information is used. In general, using a prior information to set constraints on the model structure and parameters leads to better estimators (Agüero, 2005). Because these prior information can be easily defined in the retardation functions and their implications on the parametric models, so the third path in the Fig: 5.5 is adopted in the system identification for my research.

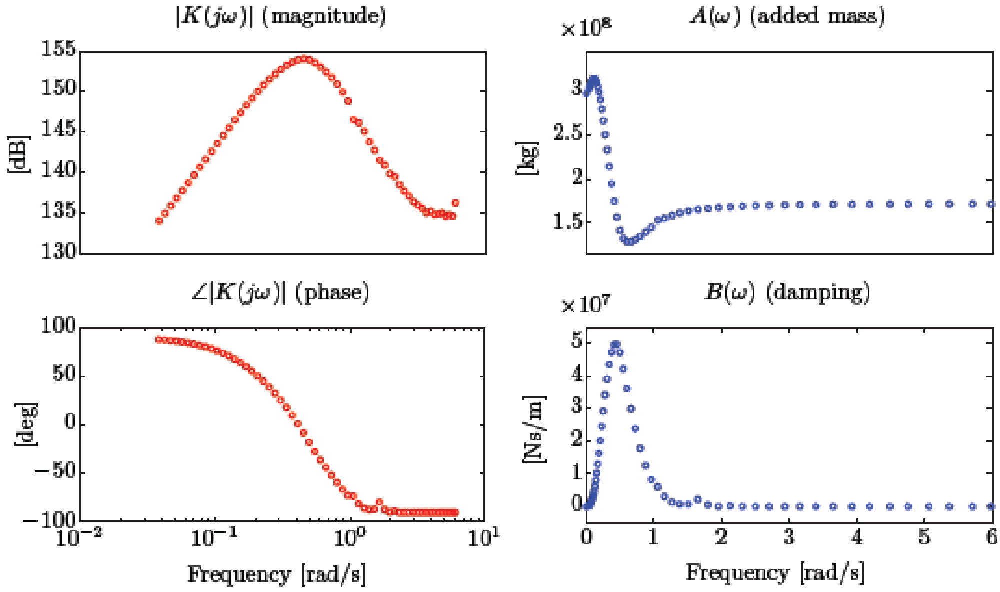

Figure 5.6: *The Identification Data from Added Mass and Damping*

5.2.3 Properties of the Fluid Memory Effect

These properties of convolution term in *Cummins equation* which can be used as the prior information in the system identification have been summarized by Perez and Fossen (2008), which can be listed in the following Table 5.1.

Property	Implication on Parametric Models $K_{ik}(s) = P_{ik}(s)/Q_{ik}(s)$
$\lim_{\omega\to 0} K(j\omega) = 0$	There are zeros at $s = 0$
$\lim_{\omega\to \infty} K(j\omega) = 0$	Strictly proper
$\lim_{t\to 0} K(t) \neq 0$	Relative degree 1
$\lim_{t\to \infty} K(t) = 0$	BIBO stable
$The\, mapping\, \dot{\xi} \to \mu\, is\, passive$	$K(j\omega)$ is positive real ($\Re[K_{ii}(j\omega] \geq 0$)

Table 5.1: *Properties of the Fluid Memory Effect Perez and Fossen (2008)*

Low-frequency Asymptotic Value

In the limit as $\omega \to 0$, the potential damping $B(\omega)$ tends to be zero since structure cannot generate waves at zero frequency, which is due to the approximating free-surface condition establishes that there cannot be both horizontal and vertical and velocity components in the free surface (Faltinsen, 1993). As a result the real part of $K(j\omega)$ tends to zero. On the other hand, in the limit as $\omega \to 0$, the imaginary part also tends to zero since the difference $A(0) - A(\infty)$ is finite:

$$\begin{aligned} A(0) - A(\infty) &= \lim_{\omega\to 0} \frac{-1}{\omega} \int_0^\infty K(t)\sin(\omega t)\,dt \\ &= \int_0^\infty K(t) \lim_{\omega\to 0} \frac{-1}{\omega} \sin(\omega t)\,dt \\ &= -\int_0^\infty K(t)\,dt \end{aligned} \tag{5.2.7}$$

The low-frequency asymptotic value is

$$\lim_{\omega\to 0} K(j\omega) = 0 \tag{5.2.8}$$

The implication on parametric model is that $K(s) = 0$ when $s \to 0$.

High-frequency Asymptotic Value

The radiation damping $B(\omega)$ tends to zero in the limit $\omega \to \infty$ since the same reason in the limit $\omega \to 0$, so the real part of $K(j\omega)$ is also zero.

The imaginary part also tends to zero, and this follows from the Riemann-Lebesgue Lemma[1]:

$$\lim_{\omega\to\infty} \omega\left[A(0) - A(\infty)\right] = \lim_{\omega\to\infty} - \int_0^\infty K(t)\sin(\omega t)\,dt = 0 \tag{5.2.9}$$

The high-frequency value asymptotic value is

$$\lim_{\omega\to\infty} K(j\omega) = 0 \tag{5.2.10}$$

The implication on the parametric model is that $K(s) = 0$ when $s \to \infty$. Due to $K(s) = \frac{P(s)}{Q(s)}$, so the relative degree must be greater than zero.

Initial-time Value

The initial time value of the retardation function is non-zero and finite:

$$\lim_{t\to 0^+} K(t) = \lim_{t\to 0^+} \frac{2}{\pi} \int_0^\infty B(\omega)\cos(\omega t)\,d\omega \neq 0 \tag{5.2.11}$$

The second equality follows from the application of the Riemann-Lebesgue Lemma and the last inequality is a consequence of energy considerations, which establish that $B_{ii}(\omega) > 0$. For the off-diagonal couplings (which are not uniformly zero due to the symmetry of the hull), the damping can be negative at some frequencies, but the area under the damping curve is generally non-zero. Note that regularity conditions are satisfied for the exchange of limit and integration (Perez and Fossen, 2009).

The initial value of the response function can be computed using the Initial-Value Theorem of the Laplace transform:

$$\lim_{t\to 0^+} K(t) = \lim_{s\to\infty} sK(s) = \lim_{s\to\infty} s\frac{P(s)}{Q(s)} \neq 0 \tag{5.2.12}$$

This limit will be different from zero only if $m = n-1$. That is, $K(0^+) \neq 0$ if and only if the system has relative degree 1 (Taghipour et al., 2008).

In the frequency-domain transfer function SISO fitting, specifying the relative degree is part of the identification process. Otherwise, using other types of identification for MIMO system, knowing the relative degree is of no importance and it is therefore ignored.

Final-time Value

The final time value can be obtained easily based on the Riemann-Lebesgue Lemma :

$$\lim_{t\to\infty} K(t) = \lim_{t\to\infty} \frac{2}{\pi} \int_0^\infty B(\omega)\cos(\omega t)\,d\omega = 0 \tag{5.2.13}$$

This property establishes necessary and sufficient conditions for bounded-input bounded-output (BIBO) stability of the convolution term in the *Cummins equation.*

Indeed, for each term $\int_0^t K_{ik}(t-\tau)\,\dot{x_k}(\tau)\,d\tau$ to be bounded for any bounded excitation function $\dot{x_k}(\tau)$, it is necessary that

$$\int_0^t |K(t)|dt < \infty \tag{5.2.14}$$

which holds provided that Eq: 5.2.13 holds.

[1] If $f(x)$ is integrable on $[a,b]$ then:

$$\begin{aligned} \lim_{t\to\infty} \int_a^b f(x)sin(tx)dx &= 0 \\ \lim_{t\to\infty} \int_a^b f(x)cos(tx)dx &= 0 \end{aligned}$$

Passivity

The radiation forces are passive, which describes an intrinsic characteristic of systems that can store and dissipate energy but not create it. This is a fundamental property which implies that the time averaged energy transport from the body is non-negative (Rogne et al., 2014). For a LTI system, a necessary but insufficient condition for passivity can be translated into the frequency domain as positive realness; that is, the real part of the transfer function is positive for all frequencies, which means that $Re\left\{K\left(j\omega\right)\right\} \geq 0,\ \forall\omega$. In the case of structures with zero-average forward speed, this follows from the fact that $B\left(\omega\right) = B\left(\omega\right)^T \geq 0$, which implies that $B_{ii}\left(\omega\right) > 0$ for all frequencies. But, the non-diagonal terms $K_{ik}\left(s\right),\ i \neq k$ do not necessarily have to be positive real (Perez and Fossen, 2009).

Chapter 6

Subspace System Identification

6.1 Problem Formulation

In practice, information about a system is often characterized in terms of the frequency response of the system at some discrete set of frequencies (McKelvey et al., 1996). These system information can either come from the experiment measurements or from the commercial software. For the experiment measurement, if the excitation of the system is well-designed, e.g. periodic input or stepped-sine, each transfer function measurement is of high quality compiled from a large number of time-domain measurement. Data original from different excitation condition can be easily combined in the frequency domain. Besides, most widely-used hydrodynamic software based on the potential theory can provide information about the system in frequency domain. In our research, the original data of the system in frequency domain is from WAMIT. Both of these methods provide system information in discrete frequency domain, sometimes in a limited range of frequency.

The problem of fitting a real-rational model to a given frequency response has been addressed by many authors in recent decades. The approach used to extract a linear model description from the measured data is called system identification and widely used in the field of system and control. The traditional way is to model a system as a fraction of two polynomials with real coefficients, and a non-linear least-square to fit with the frequency data sought. On the other hand, one particular system identification method is proposed recently, which is called subspace identification method. The method is suitable for both of the time- and frequency-domain data. In practical, subspace-based algorithms deliver state-space models without the need for an explicit parametrization of the model set. Essentially, there is no difference between multi-input multi-output (MIMO) system identification and single-input single-output (SISO) system identification for a subspace-based algorithm. The algorithm also results in estimated models in a state-space model basis, wherein the transfer function is insensitive to small perturbations in the matrix elements, which leads to the ability to identify high-order systems (McKelvey et al., 1996).

6.2 System Definition

The convolution term in *Cummins equation* can be discretized to a stable, MIMO, linear time-invariant (LTI) system for the discrete-time with input-output properties in the following format:

$$y\left[t\right] = \sum_{k=0}^{k=t} K\left(t-k\right)\dot{\xi}\left(k\right) \tag{6.2.1}$$

The system can thus be described by a state-space model

$$\begin{aligned} x\left(t+1\right) &= \bar{A}x\left(t\right) + \bar{B}u\left(t\right) \\ y\left(t\right) &= \bar{C}x\left(t\right) + \bar{D}u\left(t\right) \end{aligned} \tag{6.2.2}$$

in which, $u\left(t\right) \in R^n$ is the input vector, $y\left(t\right) \in R^m$ is the output vector and $x\left(t\right) \in \mathbb{R}^l$ is the state vector. Here, n denotes the order (the number of states), m the number of input and l the number of output.

In the state-space model, the discrete-time system matrix $\bar{A}, \bar{B}, \bar{C}, \bar{D} \in R^{n\times n}, R^{n\times m}, R^{l\times n}, R^{l\times m}$ are different with the continuous-time system matrix A, B, C, D. Classical control theory indicates that, the continuous-time system can be converted to discrete-time system with the appropriate sampling time and vice versa. The goal of the subspace identification is to find the matrices $\left(\bar{A}, \bar{B}, \bar{C}, \bar{D}\right)$ from the input and output data batches.

6.2.1 Data Preprocess

Good data preparation is key to producing valid and reliable models. Like most databases in the real world, the identification data provided by WAMIT is also faced with the commonplace properties of incomplete, noisy and inconsistent. Low quality data will lead to a low quality system model, so the preprocess is of importance to estimate a high quality model.

For the subspace identification, all transfer functions (coupling terms in the transfer matrix) are fitted to the same state space model, thus, the error to be minimized is a sum over all coupling terms and frequencies:

$$\epsilon^2 = \frac{\Sigma_q \Sigma_i \Sigma_k w_q |K^S_{ik}(j\omega_q) - K_{ik}(j\omega_q)|^2}{\Sigma_q \Sigma_i \Sigma_k w_q |K_{ik}(j\omega_q)|^2} \tag{6.2.3}$$

The frequency weights w_q here are chosen to reflect the data importance in the frequency vector, normally, the low-frequency data should gain more weight. The relative weighting of the different coupling terms, which can be reflected by the condition number, is taken care of by a pre-scaling step.

Here, the following power conservative scaling transformation is widely used:

$$\begin{aligned} K^S_{ik}(j\omega) &= \alpha_i \alpha_k K_{ik}(j\omega) \\ K^S(j\omega) &= \alpha^T K(j\omega)\alpha \end{aligned} \tag{6.2.4}$$

with $\alpha = diag(\alpha_1,\ \alpha_2,\ ..,\alpha_n)$. The coupling term weights α_i are chosen such that the mean magnitude of the diagonal elements of the scaled matrix, mean $\alpha_i^2|K_{ii}(j\omega)|$, is unity. This weighting scheme reflects the fact that the degrees of freedom associated with small radiation forces are not necessarily less important and should thus be given a larger weight to compensate. At the same time, insignificant off-diagonal elements are given less weight. It is worth noting that since the scaling transformation is power conservative, K will be passive provided that K^S is still passive. We can therefore use the scaled transfer matrix in the passivity enforcement as well (Rogne et al., 2014).

6.2.2 Data Equation

The first step of subspace identification is constructing the data-equation either in the time-domain or in the frequency-domain, which relates the input-output batches through a extended observability matrix $\mathcal{O}s$ and a lower triangular Toeplitz matrix Γ. Here, we only introduce the data-equation in frequency-domain because the sampled data is in frequency-domain, the data-equation in time-domain is quite similar.

The Discrete-Time-Fourier-Transform (DTFT) of the state sequence $x\left(k\right)$ can be written as:

$$DTFT\left(x\left(k\right)\right) = \bar{X}\left(\bar{\omega}\right) = \sum_{k=-\infty}^{k=\infty} x\left(k\right) e^{j\bar{\omega}k} \tag{6.2.5}$$

where $DTFT\left(x\left(k+r\right)\right) = e^{j\bar{\omega}r}\bar{X}\left(\bar{\omega}\right)$.

Using the DTFT, the state-space model in time-domain Eq: 6.2.2 can be transformed to in the frequency-domain:

$$\begin{aligned} e^{j\bar{\omega}}\bar{X}\left(\bar{\omega}\right) &= \bar{A}\bar{X}\left(\bar{\omega}\right) + \bar{B}\bar{U}\left(\bar{\omega}\right) \\ \bar{Y}\left(\bar{\omega}\right) &= \bar{C}\bar{X}\left(\bar{\omega}\right) + \bar{D}\bar{U}\left(\bar{\omega}\right) \end{aligned} \tag{6.2.6}$$

Rewrite the equation above to obtain that:

$$\begin{bmatrix} \bar{Y}\left(\bar{\omega}\right) \\ e^{j\bar{\omega}}\bar{Y}\left(\bar{\omega}\right) \\ \vdots \\ e^{j\bar{\omega}(s-1)}\bar{Y}\left(\bar{\omega}\right) \end{bmatrix} = \mathcal{O}s\bar{X}\left(\bar{\omega}\right) + \Gamma \begin{bmatrix} \bar{U}\left(\bar{\omega}\right) \\ e^{j\bar{\omega}}\bar{U}\left(\bar{\omega}\right) \\ \vdots \\ e^{j\bar{\omega}(s-1)}\bar{U}\left(\bar{\omega}\right) \end{bmatrix} \tag{6.2.7}$$

which holds for all $\bar{\omega}$.

In which, the extended observability matrix $\mathcal{O}s$ and lower triangular Toeplitz matrix Γ can be extended as:

$$\mathcal{O}s = \begin{bmatrix} \bar{C} \\ \bar{C}\bar{A} \\ \bar{C}\bar{A}^2 \\ \vdots \\ \bar{C}\bar{A}^{s-1} \end{bmatrix} \tag{6.2.8}$$

$$\Gamma = \begin{bmatrix} \bar{D} & 0 & 0 & \cdots & 0 \\ \bar{C}\bar{B} & \bar{D} & 0 & & 0 \\ \bar{C}\bar{A}\bar{B} & \bar{C}\bar{B} & \bar{D} & & 0 \\ \vdots & & \ddots & \ddots & \\ \bar{C}\bar{A}^{S-2}\bar{B} & \bar{C}\bar{A}^{S-3}\bar{B} & \cdots & \bar{C}\bar{B} & \bar{D} \end{bmatrix} \tag{6.2.9}$$

Define the compound state matrix as

$$\bar{X} = \left[\bar{X}\left(\bar{\omega}_1\right) \;\; \bar{X}\left(\bar{\omega}_2\right) \;\; \cdots \;\; \bar{X}\left(\bar{\omega}_M\right)\right] \in \mathbb{C}^{n \times mM} \tag{6.2.10}$$

By recursive use of the Eq: 6.2.7 and Eq: 6.2.10, we obtain the relation:

$$\underbrace{\begin{bmatrix} \bar{Y}_1 & \bar{Y}_2 & \cdots & \bar{Y}_m \\ e^{j\bar{\omega}}\bar{Y}_1 & e^{j\bar{\omega}}\bar{Y}_2 & \cdots & e^{j\bar{\omega}}\bar{Y}_m \\ \vdots & \vdots & \ddots & \vdots \\ e^{j\bar{\omega}(s-1)}\bar{Y}_1 & e^{j\bar{\omega}(s-1)}\bar{Y}_2 & \cdots & e^{j\bar{\omega}(s-1)}\bar{Y}_m \end{bmatrix}}_{\bar{Y} \in \mathbb{C}^{sl \times mM}} =$$
$$\mathcal{O}s\bar{X} + \Gamma \underbrace{\begin{bmatrix} I_m & I_m & \cdots & I_m \\ e^{j\bar{\omega}}I_m & e^{j\bar{\omega}}I_m & \cdots & e^{j\bar{\omega}}I_m \\ \vdots & \vdots & \ddots & \vdots \\ e^{j\bar{\omega}(s-1)}I_m & e^{j\bar{\omega}(s-1)}I_m & \cdots & e^{j\bar{\omega}(s-1)}I_m \end{bmatrix}}_{\bar{U} \in \mathbb{C}^{sm \times mM}} \tag{6.2.11}$$

Here, the input $\bar{U}\left(\bar{\omega}\right)$ is defined as identity. This frequency-domain data-equation can be expressed in a more compact notation:

$$\bar{Y} = \mathcal{O}s\bar{X} + \Gamma\bar{U} \tag{6.2.12}$$

Put the sampled frequency response function $K\left(j\omega_k\right)$ into the $\bar{Y}$, so the discrete-time data-equation has been constructed. Then, the system matrices $\bar{A}$,$\bar{B}$,$\bar{C}$,$\bar{D}$ can be identified by using unconstrained subspace identification or constrained subspace identification techniques.

6.2.3 Bilinear Transformation

The system matrices $\bar{A}$,$\bar{B}$,$\bar{C}$,$\bar{D}$ can be identified in the discrete-time domain, then it can be transformed to A, B, C, D based on the following properties of the bilinear transformation (McKelvey and Moheimani, 2005).

- The McMillan degree is unchanged by the transformation.
- Let the continuous-time frequency response be $Y(\omega)$ and let $\bar{Y}(\bar{\omega})$ denote the discrete-time version. Then for sampling time $T > 0$,

$$Y(\omega) = \bar{Y}(\bar{\omega}), \quad when \quad \omega = {}^{2\tan\left(\frac{\bar{\omega}}{2}\right)}/_{T} \tag{6.2.13}$$

- If $\left(\bar{A}, \bar{B}, \bar{C}, \bar{D}\right)$ is the discrete-time state-space realization for $\bar{Y}(\omega)$, then a continuous-time realization for $Y(\omega)$ is

$$\begin{aligned} A &= \frac{2}{T}\left(I + \bar{A}\right)^{-1}\left(\bar{A} - I\right) \\ B &= \frac{2}{\sqrt{T}}\left(I + \bar{A}\right)^{-1}\bar{B} \\ C &= \frac{2}{\sqrt{T}}\bar{C}\left(I + \bar{A}\right)^{-1} \\ D &= \bar{D} - \bar{C}\left(I + \bar{A}\right)^{-1}\bar{B} \end{aligned} \tag{6.2.14}$$

Using the properties stated above the following technique is used. Assume input-output data samples are given at the continuous-time frequencies ω_k. The necessary steps for the identification of a continuous-time transfer function are:

1. Select an appropriate value of T, the frequency scaling. As a rule of thumb a value of $T = {}^{5}/_{\max(\omega_k)}$ can be used.
2. Associate the given frequency response at frequency ω_k with the discrete-time frequency

$$\bar{\omega}_k = 2\arctan\left({}^{T\omega_k}/_{2}\right) \tag{6.2.15}$$

3. From the frequency response data and frequencies $\bar{\omega}_k$ estimate a discrete-time state-space model.
4. Use the transform relation Eq: 6.2.14 to obtain the final continuous-time state-space realization.

It should be noted that the conversion to the discrete-time domain, and back is exact and hence do not introduce any symmetric errors or approximations (McKelvey and Moheimani, 2005).

6.3 Two Identification Methods

6.3.1 Unconstrained Identification Method

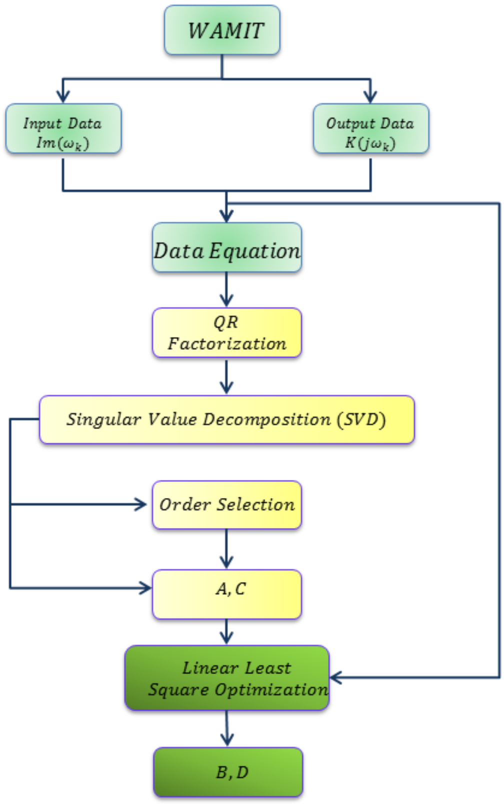

Figure 6.1: *The Unconstrained Identification Method*

Subspace Estimate of A and C

The basic idea of extracting A, C from the data equation is to make an estimation of the extended observability matrix $\mathcal{O}s$, which relies on three steps: A QR-factorization, a singular value decomposition (SVD) and an order selection (Janssen et al., 2014).

- QR-Factorization

Here, the notation $Y^{re} \triangleq [Re\, Y,\ Im\, Y]$is introduced in the following section. Due to the state-space realization (A, B, C, D) has real-valued matrices, the complex matrix expression can equivalently be formulated as

$$Y^{re} = \mathcal{O}X^{re} + \Gamma U^{re} \tag{6.3.1}$$

in which, only the matrices Y^{re} and U^{re} are known.

Let $\Pi^{\perp}$ denote a matrix which projects onto the null space of U^{re} and then multiply this matrix from the right in the above equation. Since $U^{re}\Pi^{\perp} = 0$

$$Y^{re}\Pi^{\perp} = \mathcal{O}X^{re}\Pi^{\perp} \tag{6.3.2}$$

A numerically efficient and stable way to perform this step is using the QR-factorization

$$\left[U^{reT} \;\; Y^{reT}\right] = [Q_1 \;\; Q_2] \begin{bmatrix} R_{11} & R_{12} \\ 0 & R_{22} \end{bmatrix} \tag{6.3.3}$$

and noting that $Y^{re}\Pi^{\perp} = R_{22}^T Q_2^T$.

- SVD and Order Selection

In this step, a basis of the range space of $\mathcal{O}$ is estimated. The singular value decomposition (SVD) is used for this purpose:

$$R_{22}^T = [U_n \;\; U_0] \begin{bmatrix} \Sigma_n & 0 \\ 0 & \Sigma_0 \end{bmatrix} \begin{bmatrix} V_n^T \\ V_0^T \end{bmatrix} \tag{6.3.4}$$

where $[U_n \;\; U_0]$ and $[V_n \;\; V_0]$ are two square orthogonal matrices and $[\Sigma_n \;\; \Sigma_0]$ is diagonal matrices with non-negative singular values sorted such that all diagonal entries in Σ_n are larger than the ones in Σ_0. In addition, the dimensions of Σ_n is selected to be $n \times n$. In our case $rank(R_{22}) = rank(Y^{re}\Pi^{\perp}) \leq rank\,(\mathcal{O}) = n$, i.e., the rank can at most be n. This implies that $\Sigma_0 = 0$. It can be shown that the projection does not decrease the rank any further, so in fact $rank(R_{22}) = n$ and hence all n singular values in Σ_n are positive. Therefore,

$$R_{22}^T = U_n \Sigma_n V_n^T \tag{6.3.5}$$

- Extract A and C

If we set $T = X^{re}\Pi^{\perp} Q_2 V_n \Sigma_n^{-1}$, it is quite straightforward to verify that

$$\hat{\mathcal{O}} = U_n = \mathcal{O}T = \begin{bmatrix} \bar{C}T \\ \bar{C}T(T^{-1}\bar{A}T) \\ \vdots \\ \bar{C}T(T^{-1}\bar{A}T)^{S-1} \end{bmatrix} = \begin{bmatrix} C_T \\ C_T A_T \\ \vdots \\ C_T {A_T}^{S-1} \end{bmatrix} \tag{6.3.6}$$

Here, only the range space of $\mathcal{O}$ has been calculated, which is, however, enough to recover the transfer function in some realization.

Now, the estimates of $\bar{A}$ and $\bar{C}$ are immediate. Firstly C_T is taken as the first l rows of $\hat{\mathcal{O}}$. Secondly, if we define $\bar{\hat{\mathcal{O}}}$ as the matrix obtained from $\hat{\mathcal{O}}$ by removing the top l rows and defining $\underline{\hat{\mathcal{O}}}$ as the matrix obtained by removing the bottom l rows, it is clear that $\underline{\hat{\mathcal{O}}} A_T = \bar{\hat{\mathcal{O}}}$. The linear optimization problem can be formed as:

$$\underset{A_T}{minimize} \quad \left\| \underline{\hat{\mathcal{O}}} A_T - \bar{\hat{\mathcal{O}}} \right\|_F \tag{6.3.7}$$

Then, the state-transition matrix is obtained by

$$A_T = \underline{\hat{\mathcal{O}}}^{+} \bar{\hat{\mathcal{O}}} \tag{6.3.8}$$

where the notation $(.)^{+}$ denotes the pseudo-inverse of a matrix.

With the discrete time estimates at hand, we now proceed by using the bilineaer transform to calculate the continuous time matrices A and C.

Solving for B and D

With the system matrices A and C at hand, the B and D can be estimated using a linear least squares technique. Now, we already have the frequency response $K\,(j\omega)$ available, and the A and C have been calculated. Based on the known information, the classic control theory gives us the relation between a continuous-time state-space model and its frequency response:

$$H\,(j\omega) = C\,(j\omega I - A)^{-1}\,B + D \tag{6.3.9}$$

The error is easily to be defined as:

$$E\,(k) = K\,(j\omega) - H\,(j\omega) \tag{6.3.10}$$

B and D can be found by solving an unconstrained linear optimization problem.

$$\underset{B,D}{minimize} \quad \sum_{k=1}^{M} \left\| K\,(j\omega_k) - C\,(j\omega_k I - A)^{-1}\,B + D \right\|_F \tag{6.3.11}$$

6.3.2 Constrained Identification Method

Even though the unconstrained identification technique is of high efficiency, when looking for a solution that satisfies the properties of the fluid memory effect system, we can no longer rely on such technique. Miller provides a potential method where the eigenvalue constraints are cast into linear matrix inequalities (LMI) such that the problem of finding $\bar{A}$ can be formulated as a convex optimization problem with guaranteed convergence.

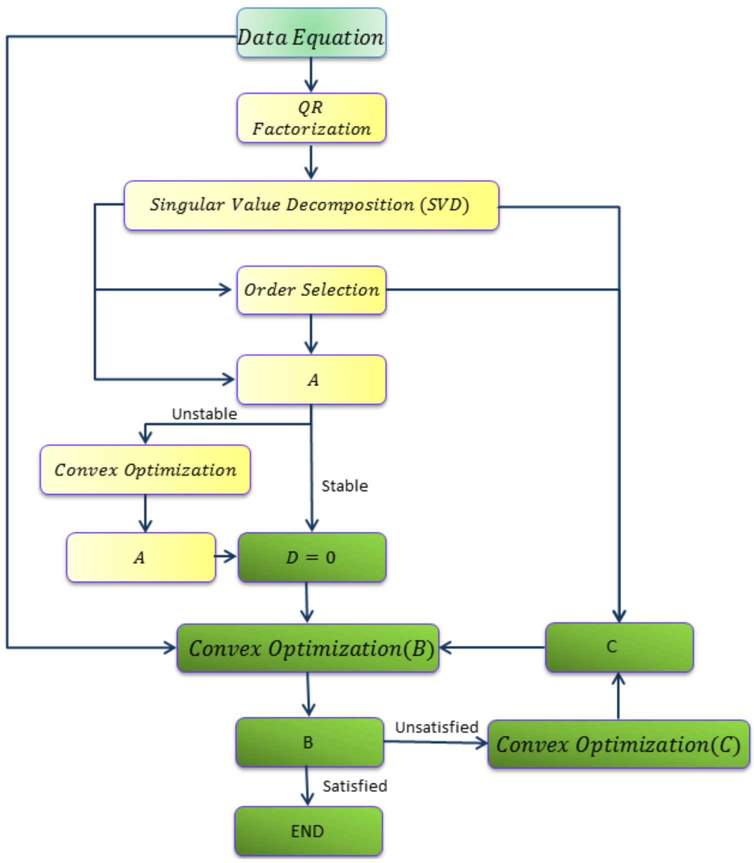

Figure 6.2: *The Constrained Identification Method*

Subspace Estimate of A and C

To develop eigenvalue constraints, the concept of LMI regions needs to be introduced which define convex region of the complex plane as LMIs (Miller and de Callafon, 2013).

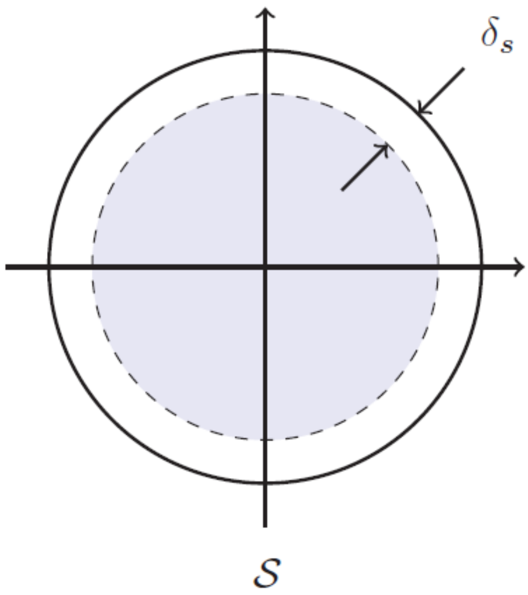

Figure 6.3: *LMI Region in the Complex Plane (Miller and de Callafon, 2013)*

LMI Regions
An LMI region is a convex region D of the complex plane, defined in terms of a symmetric matrix α and a square matrix β, as

$$D = \{z \in \mathbb{C}\colon f_D(z) \geq 0\} \tag{6.3.12}$$

where

$$f_D(z) = \alpha + \beta z + \beta^T \bar{z} \tag{6.3.13}$$

LMI regions generalize standard notions of stability for continuous and discrete time systems, and the function parameters α and β may be used to form Lyapunov-type inequalities (Miller and de Callafon, 2013). We repeat the central theorem of Chilali and Gahinet here for future reference.

Theorem 1. The eigenvalues of a matrix A lie within an LMI region given by Eq: 6.3.12 if and only if there exists a matrix $P \in \mathbb{R}^{n\times n}$ such that

$$P = P^T > 0, M_D\left(\bar{A}, P\right) \geq 0 \tag{6.3.14}$$

in which,

$$M_D\left(\bar{A}, P\right) = \alpha \otimes P + \beta \otimes \left(\bar{A}P\right) + \beta^T \otimes \left(\bar{A}P\right)^T \tag{6.3.15}$$

The intersection of two LMI regions $D1$ and $D2$ is also an LMI region, described by the matrix function

$$f_{D_1 \cap D_2}(z) = \begin{bmatrix} f_{D_1}(z) & 0 \\ 0 & f_{D_2}(z) \end{bmatrix} \tag{6.3.16}$$

- LMI Region Useful for Identification

Stable system estimates are often desirable in the identification problem. Standard subspace methods, however, do not guarantee stability of the identified model. To provide some known degree of stability for the identified model, we may constrain eigenvalues to the disc of radius $1 - \delta_S$ (Miller and de Callafon, 2013).

Fact 1. The set

$$S = \{z \in \mathbb{C}\colon\ |z| \leq 1 - \delta_S, 0 \leq \delta_S \leq 1\} \tag{6.3.17}$$

is equivalent to the LMI region $f_S(z) \geq 0$

$$f_S(z) = \underbrace{(1 - \delta_S)}_{\alpha} I_2 + \underbrace{\begin{bmatrix} 0 & 1 \\ 0 & 0 \end{bmatrix}}_{\beta} z + \begin{bmatrix} 0 & 0 \\ 1 & 0 \end{bmatrix} \bar{z} \tag{6.3.18}$$

This region results in the discrete-time Lyapunov stability condition if $\delta_S = 0$, so

$$P > 0, \quad and \begin{bmatrix} P & \bar{A}P \\ P\bar{A}^T P & P \end{bmatrix} > 0 \tag{6.3.19}$$

- Convex Constrained Optimization

The goal of subspace identification with eigenvalue constraints is to formulate a convex cost function similar to linear optimization problem Eq: 6.3.7 that can be solved subject to constraints of the form above. Here, this linear optimization problem is modified to also contain the product $\bar{A}P$ by adding P as a right-hand weighting matrix, forming the cost function

$$J\left(\bar{A}, P\right) = \left\| \underline{\hat{\mathcal{O}}}\bar{A}P - \bar{\hat{\mathcal{O}}}P \right\|_F \tag{6.3.20}$$

Letting $Q = \bar{A}P$, we form the following convex optimization problem with convex constraints. Given an estimate $\mathcal{O}$ and an LMI region described by parameters α and β,

$$\begin{aligned} &minimize \;\; J(Q,\ P) \\ &subject\ to \;\; M(Q,\ P) \geq 0 \\ &\qquad P = P^T > 0 \end{aligned} \tag{6.3.21}$$

in which

$$\begin{aligned} J(Q, P) &= \left\| \underline{\hat{\mathcal{O}}}Q - \bar{\hat{\mathcal{O}}}P \right\|_F \\ M(Q, P) &= \alpha \otimes P + \beta \otimes (Q) + \beta^T \otimes (Q)^T \end{aligned} \tag{6.3.22}$$

Once Q and P are solved for, we let $\bar{A} = QP^{-1}$. This solution, however, allows for arbitrarily small Q and P, which may introduce errors in the computation of $\bar{A}$. To improve numerical conditioning of the problem, we add the constraint

$$trace(P) = C \tag{6.3.23}$$

where C is some constant. Although any C is valid, we recommend choosing $C = n$ to allow for the possible solution$P = I$ (Miller and de Callafon, 2013).

Before continuing with computing B and D, $\bar{A}$ and $\bar{C}$ are transformed back to continuous-time through the bilinear transform.

Solving for B and D

The A and C have been constrained to guarantee the stability, the additional constraints such that the following properties can be incorporated in the identified model.

1. Strictly Proper
2. Zeros at $s = 0$
3. Passivity

- Strictly Proper and Zeros at $s = 0$

Let's recall the continuous-time state space model:

$$\begin{aligned} \bar{x}(t) &= Ax(t) + Bu(t) \\ y(t) &= Cx(t) + Du(t) \end{aligned} \tag{6.3.24}$$

The transfer function $H(s) = C(sI - A)^{-1} B + D$. A system is strictly proper if $H(j\omega) \rightarrow 0$ as $\omega \rightarrow \infty$, which is corresponding to a zero D matrix.

The problem of enforcing a zero at $s = 0$ in the identification of radiation force models is covered, for transfer function identification, by Perez and Fossen.

Consider the frequency response function (FRF) data $H(j\omega_l)$ with ω_l a set of frequency points at which $K(j\omega_l)$ is known. Integrating in the time domain is equivalent to dividing by $j\omega$ in the frequency domain.

$$H_I(j\omega_l) = \frac{1}{j\omega_l} G(j\omega_l) \tag{6.3.25}$$

Firstly, B can be determined for $D = 0$, which guarantees a strictly proper system. After the identification, the model needs to be augmented with differentiators. Enforcing that a zero in $s = 0$ corresponds to a frequency response at $\omega = 0$ of $H(\omega) = 0$. Substituting $\omega = 0$ to get the following constraint.

$$H(0) = CA^{-1}B + D = 0 \tag{6.3.26}$$

Since $D = 0$, this becomes

$$H(0) = CA^{-1}B = 0 \tag{6.3.27}$$

- Passivity (Positive Real)

By constraining the phase behavior of the diagonal terms to be within $+90$ degrees to -90 degrees, the system the has the passivity property (McKelvey and Moheimani, 2005).

Positive Real Constraint (for computing B)
Given $A \in \mathbb{R}^{n\times n}, B, C^T \in \mathbb{R}^{n\times m}, D \in R^{m\times m}$,
with $\det(j\omega I - A) \neq 0$ and (A, C) observable,
$\Psi(\omega) = D + C(j\omega I - A)^{-1} B$, the following two statements are equivalent:

1. A square transfer function $\Psi(\omega)$ is positive real if for $\omega \in R$

$$\Psi(\omega) + \Psi(\omega)^* \geq 0 \tag{6.3.28}$$

2. There exists $P = P^T \in R^{n\times n}$

$$p_{pr} = \begin{bmatrix} PA^T + AP & B + PC^T \\ B^T + CP & D + D^T \end{bmatrix} \geq 0 \tag{6.3.29}$$

Define an error function as

$$E_k = K(j\omega_k) - \left(D + C(j\omega_k I - A)^{-1} B\right) U(\omega_k) \tag{6.3.30}$$

So, the convex constrained optimization problem is

Given $A \in \mathbb{R}^{n\times n}, C \in \mathbb{R}^{m\times n}, D = 0, K(j\omega_k) \in \mathbb{R}^{m\times n}$ for $k = 1, 2, ..., M$ and weighting matrix $W_k \in \mathbb{R}^{m\times L}$

$$\begin{aligned} &\underset{B,P}{minimize} \quad \sum_{k=1}^{M} \|W_k E_k\|_F \\ &subject\ to \quad p_{pr} \geq 0 \\ &\qquad CA^{-1}B = 0 \end{aligned} \tag{6.3.31}$$

Iteration of B and C

In the previous section, two separate convex optimization problems were presented. Performing two convex optimization problems sequentially does not make the total optimization convex.

The stability property is completely determined by the properties of the A matrix. Hence, having calculated A, changing the values of the other system matrices B, C and D will not affect stability. For the case where C is known and B is to be computed, the appropriate constraints are presented in the previous section. However, to preserve convexity when B is known and C is to be computed, another formulation of the passivity constraint is needed, which is given by McKelvey et al. (1996).

Positive Real Constraints (for computing C)
Given $A \in \mathbb{R}^{n\times n}, B, C^T \in \mathbb{R}^n, D \in R$,
with $\det(j\omega I - A) \neq 0$ and (B, D) controllable,
$\Psi(\omega) = D + C(j\omega I - A)^{-1} B$, the following two statements are equivalent:

1. A square transfer function $\Psi(\omega)$ is positive real if for $\omega \in R$

$$\Psi(\omega) + \Psi(\omega)^* \geq 0 \tag{6.3.32}$$

2. There exists $P = P^T \in R^{n\times n}$

$$p_{pr} = \begin{bmatrix} PA + A^T P & PB + C^T \\ B^T P + C & D + D^T \end{bmatrix} \geq 0 \tag{6.3.33}$$

The convex optimization iteration between B and C can enforce the certain system properties into identification model of high accuracy without sacrificing the other property such as stability.

Part III

Case Studies

Chapter 7

Single Barge Case Study

7.1 Introduction

In order to validate the methodology proposed in this thesis is reliable, the frequency domain and the time domain approaches are compared for a linear system of a moored barge in which the mooring system is assumed as linear. The configuration of barge and its dimensions has been given as following:

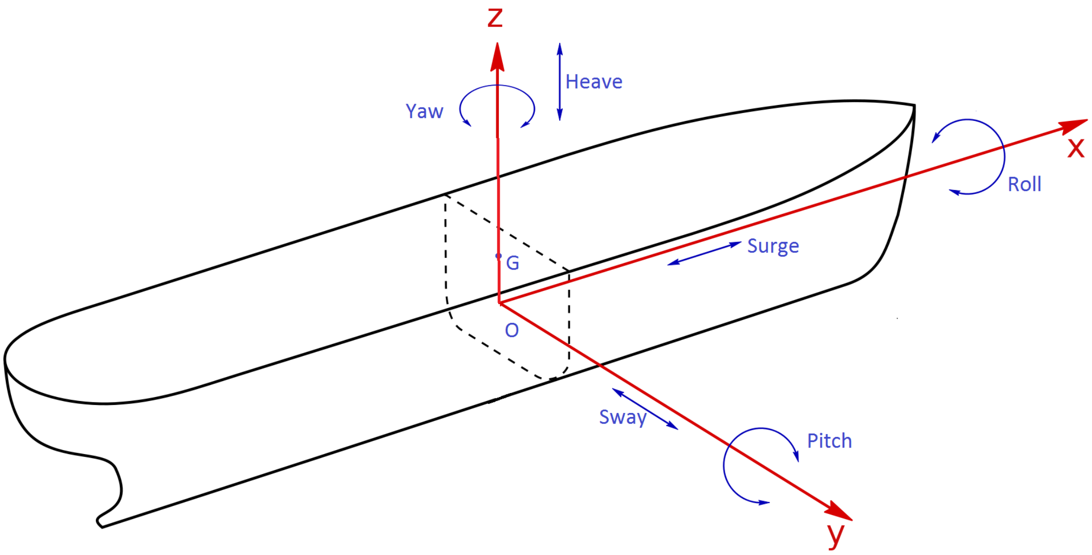

Figure 7.1: *Barge Model with Hydrodynamic Coordinates (Mooring System not shown)*

Ship Dimensions		Mooring Stiffness	
Length [m]	120	K_{surge} [KN/m]	3×10^5
Width [m]	40	K_{sway} [KN/m]	3×10^5
Draft [m]	5	K_{yaw} [KN·m/rad]	1.2×10^7

Table 7.1: *Dimensions of the Barge and its Mooring Stiffness*

7.2 Equations of Motion

Either Lagrange or Kane's method can be applied to form the equation of motion, here, the Kane's method is used following these steps:

- Define important points as the center of mass of the barge G and the point O which is the original point of h-frame.
- Transfer function between b-frame and h-frame. Here, the angle should be quite small, so the rotation matrix can be linearized as:

	$\vec{b_1}$	$\vec{b_2}$	$\vec{b_3}$
$\vec{n_1}$	1	$-\psi$	θ
$\vec{n_2}$	ψ	1	$-\phi$
$\vec{n_3}$	$-\theta$	ϕ	1

Table 7.2: *Transformation Matrix between h-frame and b-frame*

in which, $\phi,\ \theta,\ \psi$ represents the $q_4,\ q_5,\ q_6$ (roll, pitch and yaw) respectively.

- Select generalized coordinate (q_r) and generate speeds (u_r), then generate expressions for angular velocity and acceleration of all bodies and velocity and acceleration of the important points.

$$\begin{aligned}
\overrightarrow{{}^N v^O} &= u_1\overrightarrow{n_1} + u_2\overrightarrow{n_2} + u_3\overrightarrow{n_3} \qquad \overrightarrow{{}^N a^O} = \dot{u}_1\overrightarrow{n_1} + \dot{u}_2\overrightarrow{n_2} + \dot{u}_3\overrightarrow{n_3} \\
\overrightarrow{{}^N v^G} &= \overrightarrow{{}^N v^O} + \overrightarrow{\omega} \times \overrightarrow{\gamma_{GO}} \\
&= u_1\overrightarrow{n_1} + u_2\overrightarrow{n_2} + u_3\overrightarrow{n_3} \\
&+ (u_4\overrightarrow{n_1} + u_5\overrightarrow{n_2} + u_6\overrightarrow{n_3}) \times (x_g\overrightarrow{b_1} + y_g\overrightarrow{b_2} + z_g\overrightarrow{b_3}) \\
&= [u_1 + z_g u_5 - y_g u_6]\overrightarrow{n_1} + [u_2 + x_g u_6 - z_g u_4]\overrightarrow{n_2} + [u_3 + y_g u_4 - x_g u_5]\overrightarrow{n_3}
\end{aligned} \tag{7.2.1}$$

$$\overrightarrow{{}^N a^G} = [\dot{u}_1 + z_g\dot{u}_5 - y_g\dot{u}_6]\overrightarrow{n_1} + [\dot{u}_2 + x_g\dot{u}_6 - z_g\dot{u}_4]\overrightarrow{n_2} + [\dot{u}_3 + y_g\dot{u}_4 - x_g\dot{u}_5]\overrightarrow{n_3}$$

$$\begin{aligned}
\overrightarrow{\omega} &= u_4\overrightarrow{n_1} + u_5\overrightarrow{n_2} + u_6\overrightarrow{n_3} \\
\overrightarrow{\alpha} &= \dot{u}_4\overrightarrow{n_1} + \dot{u}_5\overrightarrow{n_2} + \dot{u}_6\overrightarrow{n_3}
\end{aligned}$$

- Construct the partial velocity table.

u_r	$\overrightarrow{{}^N v_r^G}$	$\overrightarrow{{}^N \omega_r^G}$
$r=1$	$\overrightarrow{n_1}$	0
$r=2$	$\overrightarrow{n_2}$	0
$r=3$	$\overrightarrow{n_3}$	0
$r=4$	$-z_g\overrightarrow{n_2} + y_g\overrightarrow{n_3}$	$\overrightarrow{n_1}$
$r=5$	$z_g\overrightarrow{n_1} - x_g\overrightarrow{n_3}$	$\overrightarrow{n_2}$
$r=6$	$-y_g\overrightarrow{n_1} + x_g\overrightarrow{n_2}$	$\overrightarrow{n_3}$

Table 7.3: *Partial Velocity Table for Single Barge System*

- $f_r + f_r^* = 0$
  The generalized forces can be divided as:

$$f_r = F_r + M_r \qquad f_r^* = F_r^* + M_r^*$$

$$F_r = (F_1\overrightarrow{n_1} + F_2\overrightarrow{n_2} + F_3\overrightarrow{n_3}) \cdot \overrightarrow{{}^N v_r^G} \qquad F_r^* = (-m \cdot \overrightarrow{{}^N a^G}) \cdot \overrightarrow{{}^N v_r^G} \tag{7.2.2}$$

$$M_r = (T_1\overrightarrow{n_1} + T_2\overrightarrow{n_2} + T_3\overrightarrow{n_3}) \cdot \overrightarrow{{}^N\omega_r^G} \qquad M_r^* = -(\overrightarrow{\alpha} \cdot I + \overrightarrow{\omega} \times I \cdot \overrightarrow{\omega}) \cdot \overrightarrow{{}^N\omega_r^G}$$

So,

$$\begin{gathered}
F_1 = F_1 \qquad F_1^* = -m(\dot{u}_1 + z_g\dot{u}_5 - y_g\dot{u}_6) \\
F_2 = F_2 \qquad F_2^* = -m(\dot{u}_2 + x_g\dot{u}_6 - z_g\dot{u}_4) \\
F_3 = F_3 \qquad F_3^* = -m(\dot{u}_3 + y_g\dot{u}_4 - x_g\dot{u}_5) \\
F_4 = -F_2z_g + F_3y_g \qquad F_4^* = m(\dot{u}_2 + x_g\dot{u}_6 - z_g\dot{u}_4)z_g - m(\dot{u}_3 + y_g\dot{u}_4 - x_g\dot{u}_5)y_g \\
F_5 = F_1z_g - F_3x_g \qquad F_5^* = -m(\dot{u}_1 + z_g\dot{u}_5 - y_g\dot{u}_6)z_g + m(\dot{u}_3 + y_g\dot{u}_4 - x_g\dot{u}_5)x_g \\
F_6 = -F_1y_g + F_2x_g \qquad F_6^* = m(\dot{u}_1 + z_g\dot{u}_5 - y_g\dot{u}_6)y_g - m(\dot{u}_2 + x_g\dot{u}_6 - z_g\dot{u}_4)x_g \\
M_1 = M_1^* = M_2 = M_2^* = M_3 = M_3^* = 0 \\
M_4 = T_1 \qquad M_4^* = -I_{xx}\dot{u}_4 \\
M_5 = T_2 \qquad M_5^* = -I_{yy}\dot{u}_5 \\
M_6 = T_3 \qquad M_4^* = -I_{zz}\dot{u}_6
\end{gathered} \tag{7.2.3}$$

- Assemble $F_r + F_r^* = 0$.

$$\begin{bmatrix}
m & 0 & 0 & 0 & mz_g & -my_g \\
0 & m & 0 & -mz_g & 0 & mx_g \\
0 & 0 & m & my_g & -mx_g & 0 \\
0 & -mz_g & my_g & I_{xx} + mz_g^2 + my_g^2 & -mx_gy_g & -mx_gz_g \\
mz_g & 0 & -mx_g & -mx_gy_g & I_{yy} + mz_g^2 + mx_g^2 & -my_gz_g \\
-my_g & mx_g & 0 & -mx_gz_g & -my_gz_g & I_{zz} + my_g^2 + mx_g^2
\end{bmatrix}
\begin{bmatrix} \dot{u}_1 \\ \dot{u}_2 \\ \dot{u}_3 \\ \dot{u}_4 \\ \dot{u}_5 \\ \dot{u}_6 \end{bmatrix}
= \begin{bmatrix} f_1 \\ f_2 \\ f_3 \\ f_4 \\ f_5 \\ f_6 \end{bmatrix} \tag{7.2.4}$$

The equation obtained from Kane's method is identical with the seakeeping model. Here, the f is the hydrodynamics force, which is assumed to be the linear superposition of these components:

$$f = \tau_{exc} + \tau_{rad} + \tau_{stat} \tag{7.2.5}$$

in which,

$$\begin{aligned}
\tau_{rad} &= A_{inf}\dot{u} + \int_0^t K(t-\tau)\,\dot{x}(\tau)\,d\tau \\
\tau_{stat} &= \bar{G}q
\end{aligned} \tag{7.2.6}$$

Then, the equations of motion can be simplified in a concise format:

$$[M + A_{inf}]\,[\dot{u}] = \left[\tau_{exc} + \int_0^t K(t-\tau)\,\dot{x}(\tau)\,d\tau + \bar{G}q\right] \tag{7.2.7}$$

7.3 System Identification of the Fluid Memory Effect

In this section, the fluid memory effect of a flat-bottom barge, which is involved in a old project at Mammoet Solution will be obtained from the frequency dependent added mass matrix $A(\omega)$ and damping matrix $B(\omega)$ computed by WAMIT which is based on 3-D panel method. The added mass and damping coefficients $A(\omega)$, $B(\omega)$ from 0.05 to 10 rad/s and added mass in infinity frequency have been obtained as the original data. The conventional method has been compared with the novel method, constrained frequency domain system identification, to validate that all the system properties will be enforced into the identified state space model successfully.

7.3.1 Data Set

Due to the port/starboard symmetry, there is no coupling between the odd and even numbered DOFs, so the 6-DOF matrix can be split in one longitudinal system containing *surge, heave* and *pitch*, and one lateral system containing *sway, roll* and *yaw.* Doing so, the transfer functions from the identification data has been eliminated and the complexity reduces.

Using $K\left(j\omega\right) = B\left(\omega\right) + j\omega\left(A\left(\omega\right) - A\left(\infty\right)\right)$ to produce the identification data matrix.

$$K = \begin{bmatrix} k_{11} & 0 & k_{13} & 0 & k_{15} & 0 \\ 0 & k_{22} & 0 & k_{24} & 0 & k_{26} \\ k_{31} & 0 & k_{33} & 0 & k_{35} & 0 \\ 0 & k_{42} & 0 & k_{44} & 0 & k_{46} \\ k_{51} & 0 & k_{53} & 0 & k_{55} & 0 \\ 0 & k_{62} & 0 & k_{64} & 0 & k_{66} \end{bmatrix} \tag{7.3.1}$$

$$K_{1,3,5} = \begin{bmatrix} k_{11} & k_{13} & k_{15} \\ k_{31} & k_{33} & k_{35} \\ k_{51} & k_{53} & k_{55} \end{bmatrix} \qquad K_{2,4,6} = \begin{bmatrix} k_{22} & k_{24} & k_{26} \\ k_{42} & k_{44} & k_{46} \\ k_{62} & k_{64} & k_{66} \end{bmatrix} \tag{7.3.2}$$

However, the original identification data directly obtained from added mass and damping is in a large scale such as 10^5 or larger, which will cause the illness problem for the convex optimization due to the absolute error will be too big to be accepted in the convex setting. So, the original identification data should be zoomed out to a proper scale which is suitable for the convex optimization.

7.3.2 Data Scaling

Following the scaling method introduced in the previous chapter, the data can be easily transformed into a proper scale, which can be reflected by its condition number.

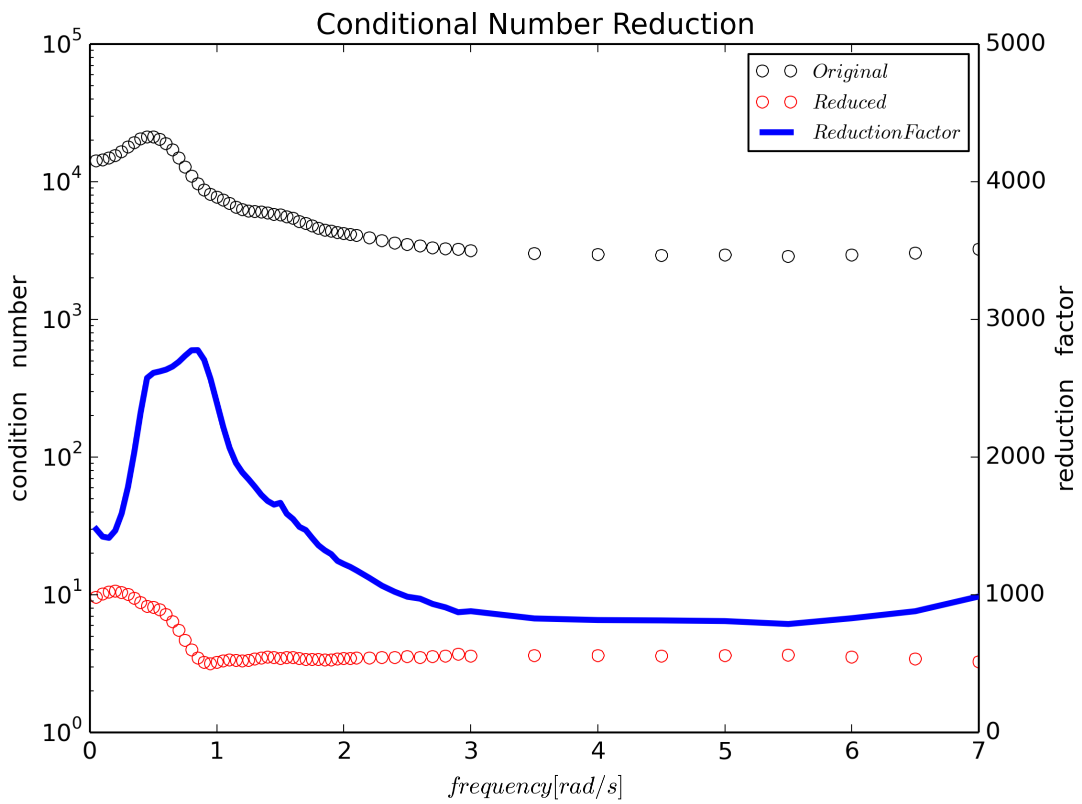

Figure 7.2: *Decreasing Condition Number with Data Scaling (surge, heave, pitch)*

The above figure presents that the condition number has been significantly reduced into 10 or smaller value, which means the system information in the identification matrix can avoid the illness problem in the convex optimization.

7.3.3 Order Selection

The order estimation is key for the identification. In order to keep the balance between the accuracy and efficiency, normally, the singular value below 1% of the maximum should be ignored.

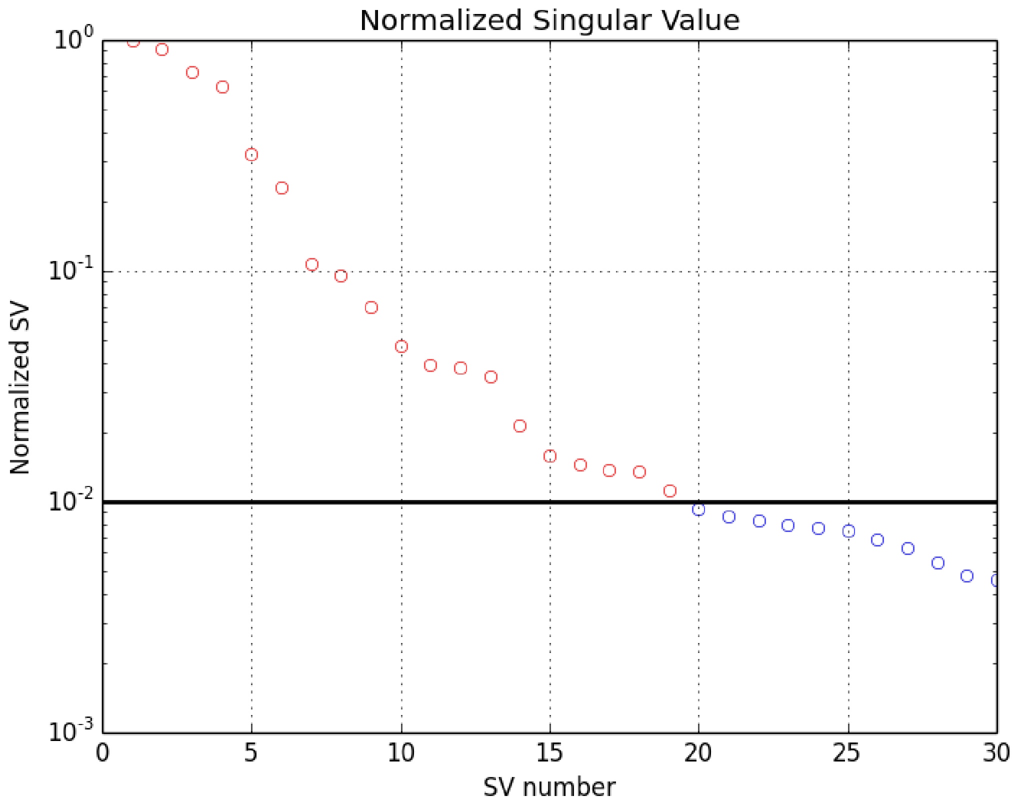

Figure 7.3: *Order selection from Singular Value Distribution*

The above figure shows the distribution of singular values, in which the red ones are the dominating singular values which should be taken into consideration and the blue ones are ignored, therefore, 19 orders are enough to describe this system in a high accuracy.

7.3.4 Results Comparison

Using the same order number to commit the unconstrained identification and constrained identification, the results are listed below.

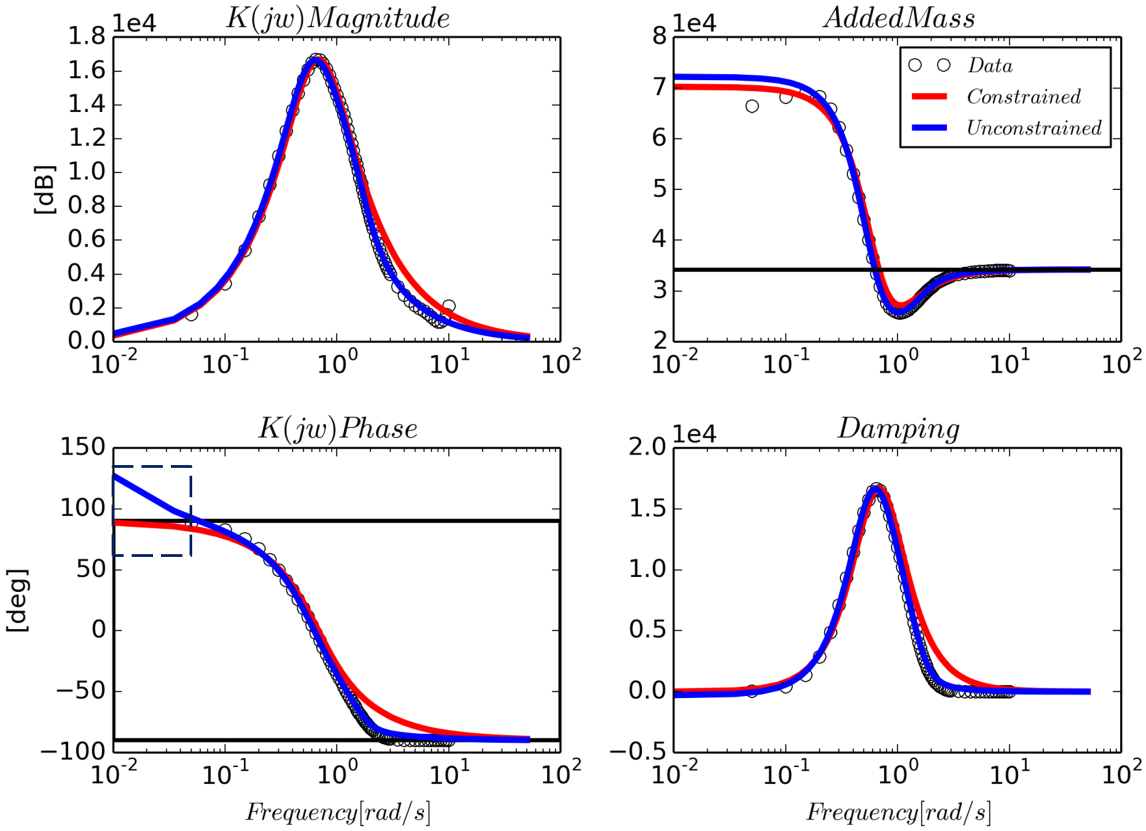

Figure 7.4: *Effect of Constrained Identification Method (heave-heave)*

Here, taking the heave-heave (k_{33}) item as an example. It is obvious to see that both of the unconstrained and constrained identification can provide good fit with the original data, whereas, the unconstrained identification can not guarantee the system is passive because phase of the transfer function is out of range between -90^0 and 90^0 in the low frequencies. In the Appendix A, all the diagonal items in the transfer function matrix has been plotted to prove that the constrained identification can satisfy all the preliminary properties of the wave effect.

Here, the system identified using unconstrained identification method is stable. However, it should be noted that sometimes the unconstrained identification can not give a stable system description, which will cause a totally wrong estimation.

7.3.5 Quality of the Fit

Typically, system identification algorithms are used to construct mathematical models based on measurements from a physical system. Then, the quality of the model can be assessed by comparing the model output to the data of the true system. From such validation experiments, it can be concluded whether a model is accurate enough for its application. With this data, the closest we can approximate reality is as close as we can approximate the software output data.

The quality of the models, however, is not only visible within the range of the identification data, but is also determined by how well the model reflects the prior knowledge. Within the narrow frequency range of the identification data, a measure of quality that we can use, is by measuring the average distance from the model to the identification data. However, this measure of quality does not contain information on the model's behavior outside of the identification data. A visual inspection is then needed to asses how well the model reflects the prior knowledge. To asses the quality of the fit within the identification data, we introduce the quality measure Q which has a value between 0 and 100, representing a bad fit and a perfect fit, respectively (Janssen et al., 2014).

$$Q_{ik} = \max(0, (1 - \frac{\sum_{l=1}^{N} \left\| K(\omega)_{ik} - K(\hat{\omega})_{ik} \right\|_2^2}{\sum_{l=1}^{N} \| K(\omega)_{ik} \|_2^2}) \cdot 100\%) \tag{7.3.3}$$

Based on such criterion, the quality of the fit for the example case can be summarized:

	Item	Quality of Fit		Item	Quality of Fit
(1,1)	surge-surge	99.32%	(2,2)	sway-sway	99.97%
(1,3)	surge-heave	99.64%	(2,4)	sway-roll	99.99%
(1,5)	surge-pitch	99.60%	(2,6)	sway-yaw	97.15%
(3,1)	heave-surge	97.22%	(4,2)	roll-sway	99.97%
(3,3)	heave-heave	99.57	(4,4)	roll-roll	99.93
(3,5)	heave-pitch	97.03%	(4,6)	roll-yaw	97.22%
(5,1)	pitch-surge	99.83%	(6,2)	yaw-sway	97.36%
(5,3)	pitch-heave	98.00%	(6,4)	yaw-roll	96.42%
(5,5)	pitch-pitch	99.81%	(6,6)	yaw-yaw	99.74%

Table 7.4: *Fitting Quality of the Identified State Space Model*

The worst accuracy can reach above 96%, which verifies that the identified model can provide correct description for the system of fluid memory effect.

7.3.6 Impulse Response Function Validation

The identified state space model is identical with the original identification data in the frequency domain, which has been given in the previous section. So, they should also be identical in the time domain.

The identified state-space model describes the linear time-invariant system of fluid memory effect, which also can be converted back to the impulse response function to validate the identified SSM satisfy all of the system properties in time-domain.

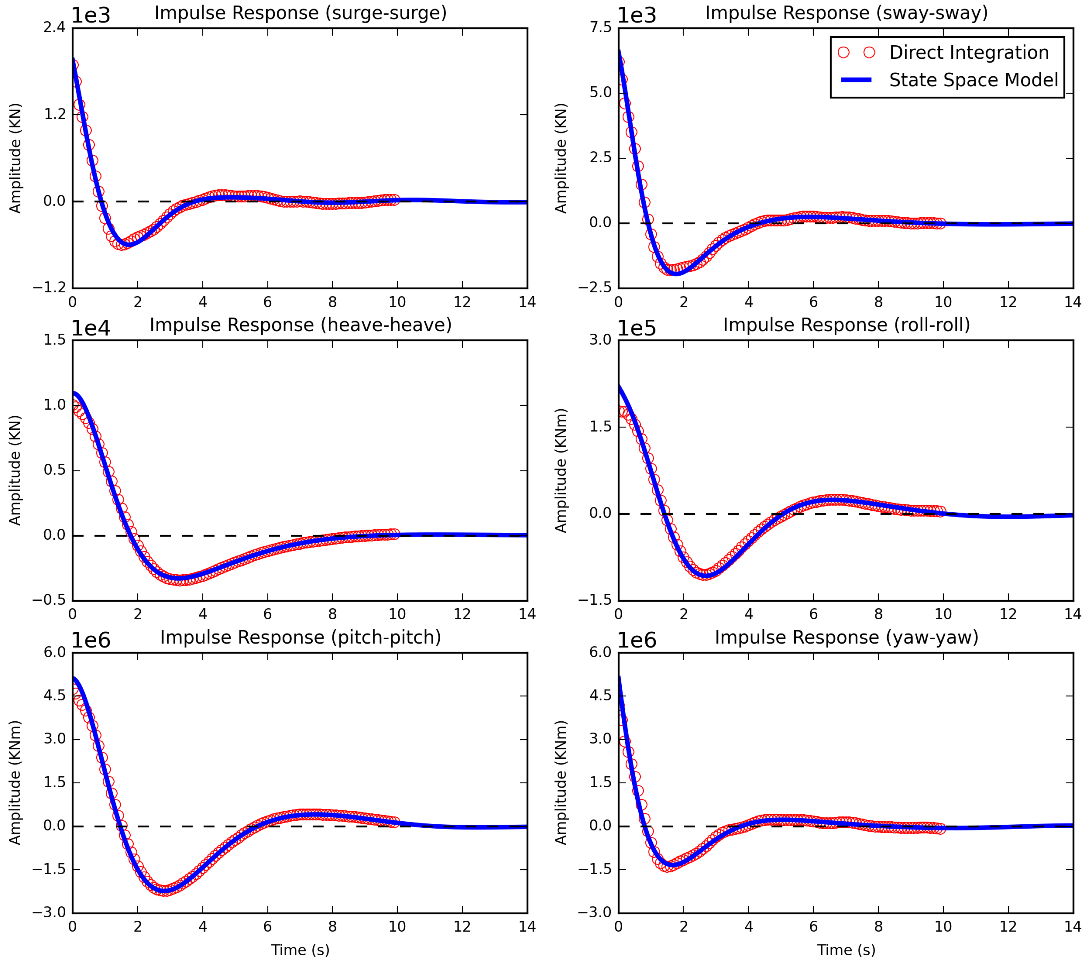

Figure 7.5: *Impulse Response Function Validation*

It is obvious to notice that the impulse functions from identified state space model and direct integration close to each other perfectly. The major deviation happens at the starting time, which results from the incompleteness of the damping data in the high frequency area.

7.4 State-Space Model of EoM

The identified state-space model of fluid memory effect can be incorporated into the equations of motion to obtain a uniform format in state space model:

$$\begin{bmatrix} I_{6\times6} & 0 & 0 \\ 0 & \mathbf{I_{n\times n}} & 0 \\ 0 & 0 & M + A_{inf} \end{bmatrix} \begin{bmatrix} \dot{q} \\ \dot{\mathbf{x}} \\ \dot{u} \end{bmatrix} = \begin{bmatrix} u \\ \bar{\mathbf{A}}\mathbf{x} + \bar{\mathbf{B}}\mathbf{u} \\ \bar{\mathbf{C}}\mathbf{x} + \bar{G}q + \tau_{exc} \end{bmatrix} \tag{7.4.1}$$

where, the emphasized terms are the fluid memory effect and n is the new orders number in the identified state space model of the fluid memory effect.

7.5 Simulation of the Dynamic Response

In order to validate that the response simulation from the EoM with identified state-space fluid memory effect is of high accuracy, three different scenarios are investigated to compare it with frequency domain simulation result.

- Free Decay Scenario

- Regular Wave Scenario
- Irregular Wave Scenario

7.5.1 Free Decay Scenario

In this scenario, it is assumed that the structure is in the calm water without incoming waves. A initial displaced condition in heave and pitch corresponding to $1m$ and -5^o is considered. The objective is to simulate the transient response of the vessel after it is released from this condition.

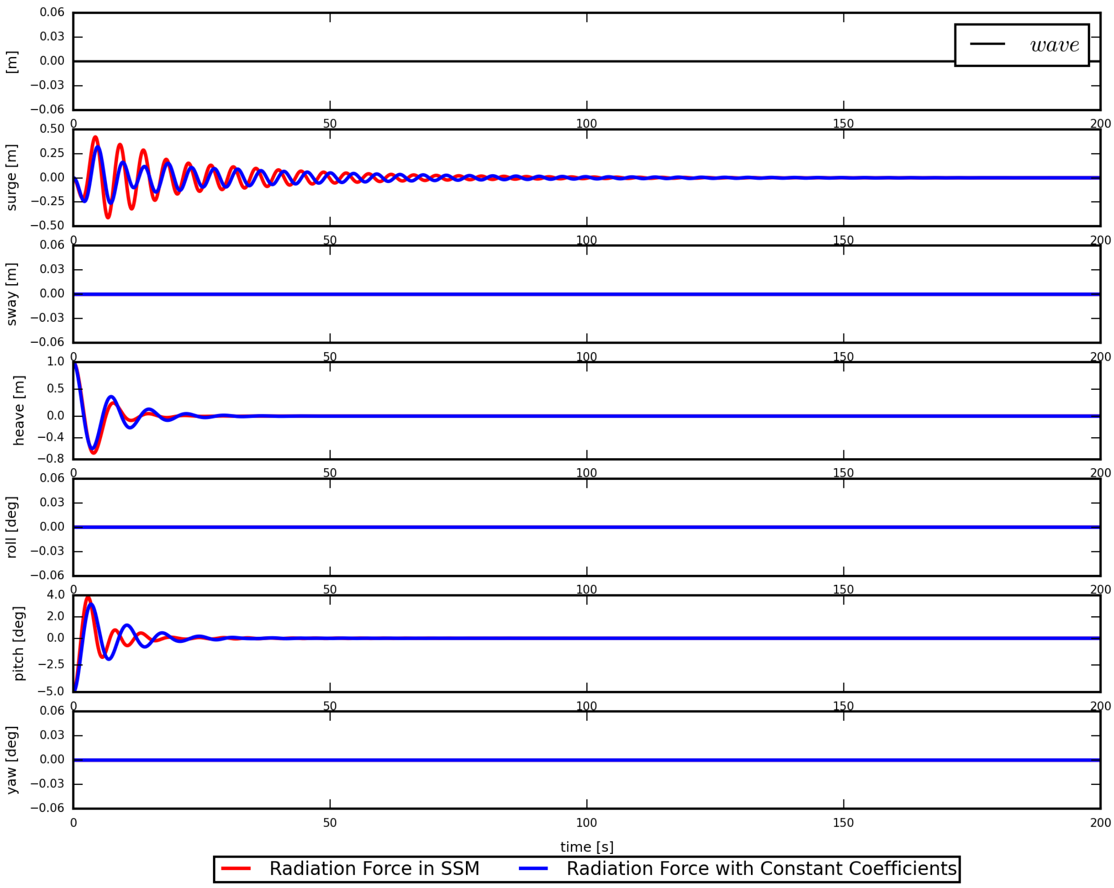

Figure 7.6: *Time Series of the Ship Motions (Free Decay)*

The radiation force can be presented either in the identified state space model or as the function of constant added mass and damping coefficients. Results of the simulation for these two methods show that the simulation based on the identified state-space model agrees well with the one from constant coefficients method, no significant difference is observed between the response simulation.

7.5.2 Regular Wave Scenario

In the second scenario, the response of the structure initially at rest due to harmonic incident wave (regular wave) is investigated. The initial condition for the velocity and response were set to zero which is consistent with the object to understand the response from incident wave force. Typical time-domain response plots for six degrees of freedom at different wave-direction has been plotted in the following figures for the wave-direction 0^o, $,45^o$ and 90^o, which are also called heave wave, quartering wave and beam wave respectively. The wave frequency is assumed as $\omega = 1\ rad/s$.

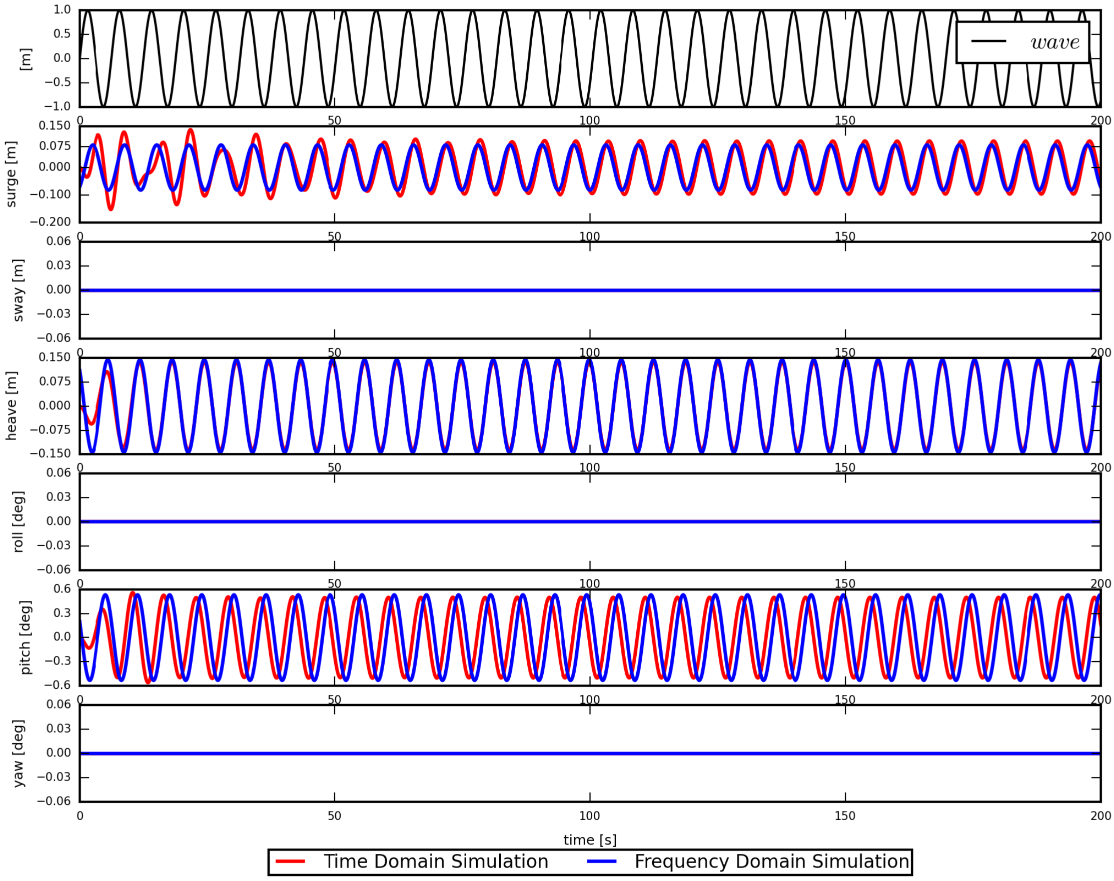

Figure 7.7: *Time Series of Ship Motions for* $\omega = 1^{rad}/_{s}$ *(Head Wave)*

The response simulation plots for quartering and beam waves are attached in the Appendix. It is observed that the simulation fits well with the harmonically generated response RAO based on the frequency domain simulation after a transitional period.

7.5.3 Irregular Wave Scenario

Finally, the response of the vessel in the open sea, which is normally described by the wave spectrum, is studied to simulate the realistic situation. Here, the sea state is described using a Jonswap spectrum with $8s$ peak wave period and $3m$ significant wave height.

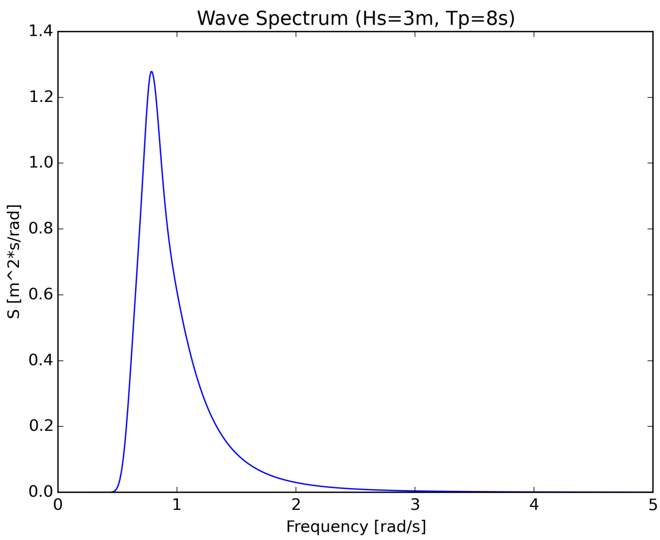

Figure 7.8: *Wave Spectrum of the Irregular Wave*

$$S(\omega) = 155\frac{H_{1/3}^2}{T_1^4\omega^5}\exp(\frac{-944}{T_1^4\omega^4})(3.3)^{\gamma}$$
$$\gamma = \exp[-(\frac{0.191\omega T_1 - 1}{2^{0.5}\sigma})^2] \tag{7.5.1}$$

with

$$\sigma = \begin{cases} 0.07 \; if \; \omega \leq 5.24/T_1 \\ 0.09 \; if \; \omega > 5.24/T_1 \end{cases} \tag{7.5.2}$$

Wave elevation and wave loads are calculated using superposition of wave components, with wave load $\tau_{exc}(t)$ in mode j given by (Kristiansen et al., 2005):

$$\tau_j(t) = \Sigma_i K_{j,i} A_i \cos(\omega_i t + \varphi_{j,i} + \epsilon_i) \tag{7.5.3}$$

where, A_i is the amplitude of component i at frequency ω_i

$$A_i = \sqrt{2S(\omega_i) \triangle \omega} \tag{7.5.4}$$

and $K_{j,i}$, $\varphi_{j,i}$ represents force response amplitude and phase, which vary with the wave frequency and the wave direction and are calculated by WAMIT. ϵ_i is the random phase for each wave component.

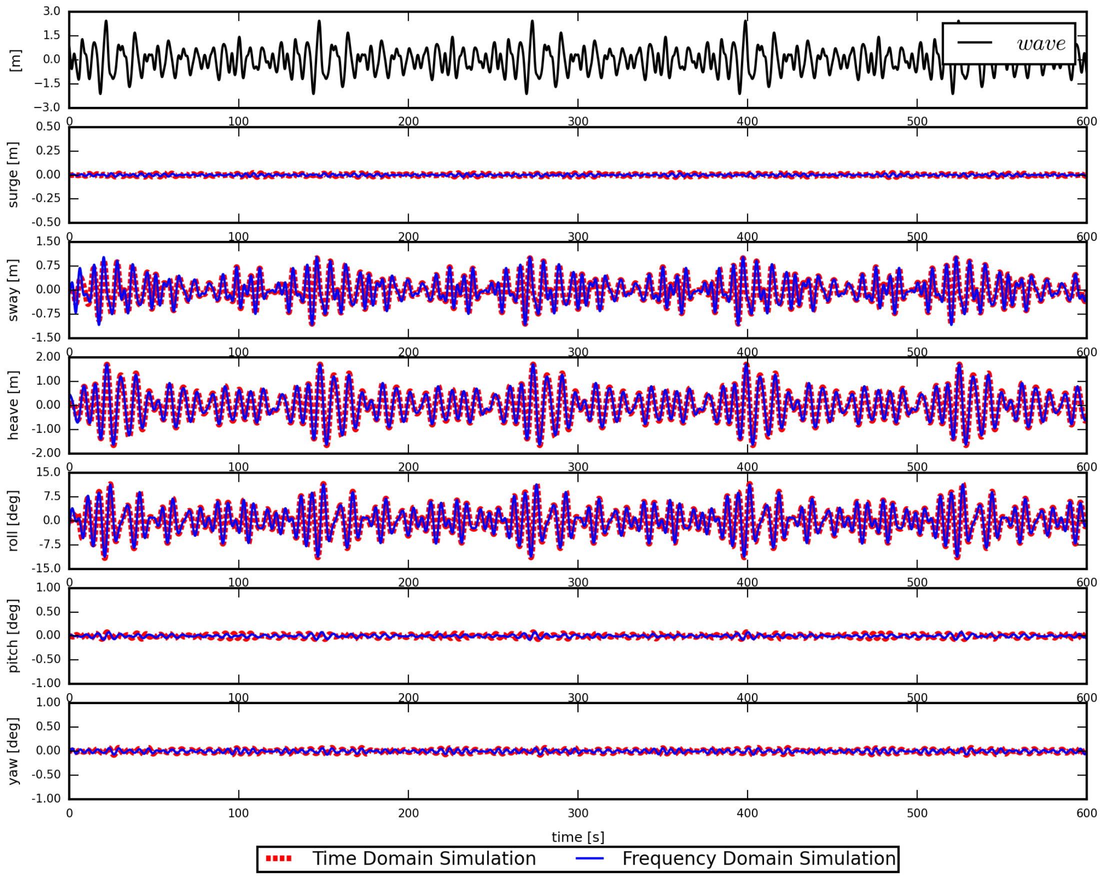

Figure 7.9: *Time Series of Ship Motions for Irregular Wave (Beam Wave)*

For the irregular wave scenario, the same observations can be identified that the time domain analysis is identical with the frequency domain analysis.

7.6 Concluding Remarks

In this case study, the theoretical basis of the methodology used in the paper has been validated. The equation of motion constructed by Kane's method is exactly identical with the sea-keeping model. The emphasis has been paid on the methods that replace the convolution terms by the state-space model, a comparison between the two methods shows that the new constrained frequency domain subspace identification technique has successfully satisfy the system properties. Finally, the identified state space model is incorporated into the equations of motion and give the time domain simulation of a moored barge, the results are identical with the conventional frequency domain simulation results with a high quality. So, the state space identification methods discussed in this thesis are able to account for the fluid memory effects and give a state space form of the *Cummins equation*. The efficiency of using time domain analysis has been improved greatly without sacrifice of the accuracy.

Chapter 8

Twin Barges Case Study

8.1 Introduction

In some cases, the substructure like jacket is not transparent or the capacity of one barge is not enough for the lifting-off operation, therefore a twin barges system is proposed as the alternative option to overcome these limitations.

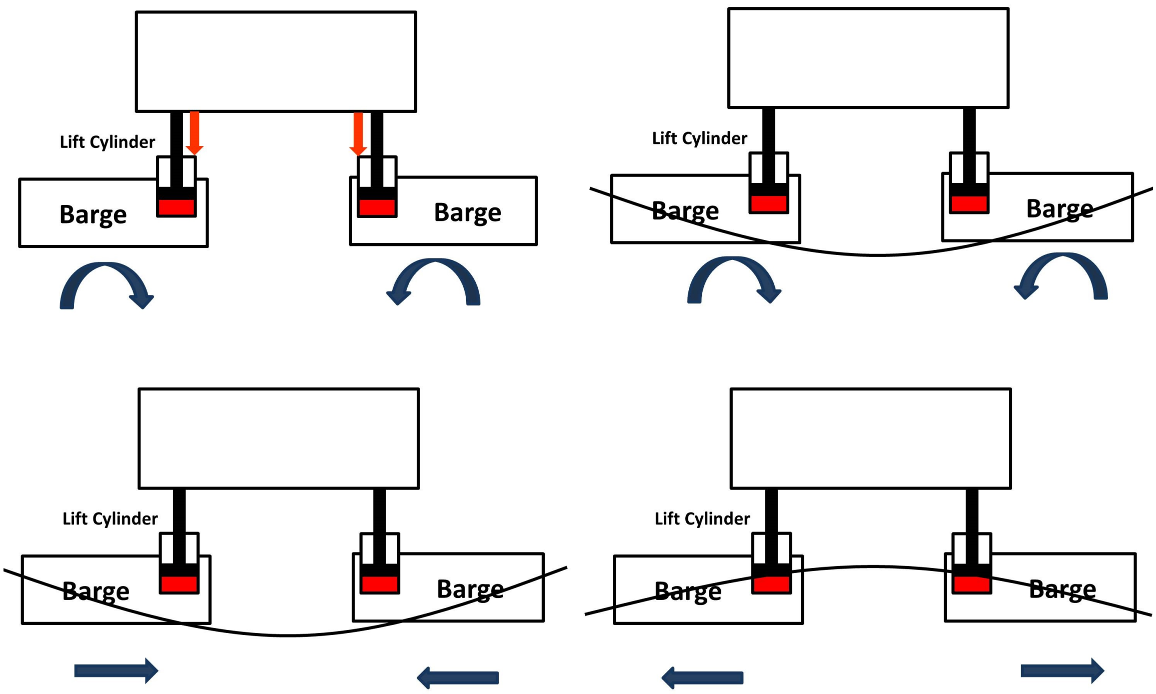

Figure 8.1: *Challenges of Free Floating Twin Barges Lift Off System*

However, the moment induced by the topside would result in excessive relative roll, which maybe causes undesirable mistake in the operations. Besides, the twin barges system will be faced with other challenges same with the semi-submersible vessel, especially under the beam wave situation.

In order to eliminate the threat from the excessive relative sway and roll, two rigid bars are used to hinged connect the twin barges. Therefore, the innovative concept developed by Mammoet Global Engineering is designed for the removal of topside on the jacket, which consists of two connected standard barges in a catamaran configuration with each hull either side of the jacket. The lift is executed by means of the lift system using winches and steel booms transmitting the weight of the deck to the barges as shown in the sketches below.

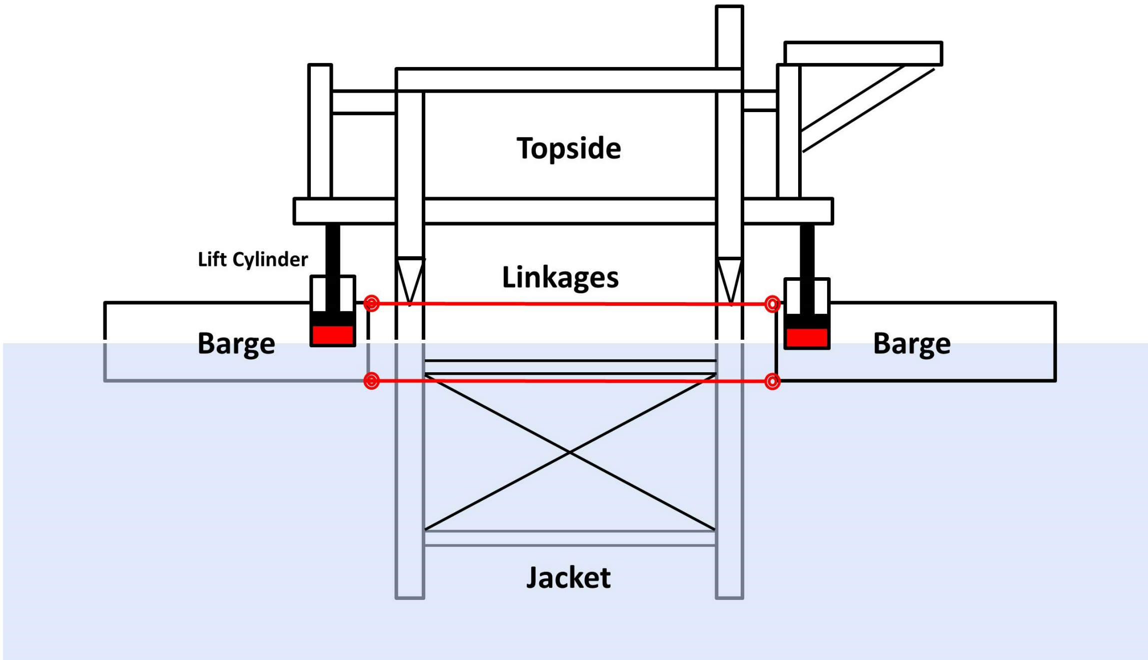

Figure 8.2: *Configuration of the Optimized Twin Barges Lift Off System*

The criterion of the catamaran configuration concept is not only related with the motion of each barge but also the relative motion of two barges in the system, in some cases, the second criterion is more critical. In order to eliminate the relative motion, the rigid bars are hinged connected between the two barges, therefore the effect of these linkages is examined on the motion of the twin barges system.

Ship Dimensions	
Length [m]	150
Width [m]	40
Draft [m]	4
Gap [m]	50

Table 8.1: *Dimensions of the Twin Barges and its Gap*

8.2 Equations of Motion

In lift-off topside decommission, the vertical motion of the system plays significant role for its successful implementation, thus the heave, roll and pitch motion should be considered carefully. In addition, the bars are connected in the sway direction, which should also be accounted for. In many situations, lashing lines are used in order to limit the horizontal motions of the barge, so in this case study, it is simplified that there are no motions in surge and yaw. The catamaran configuration barges are simplified that each barge has only four degrees of freedom: *sway, heave, roll* and *pitch* with 2 linkages.

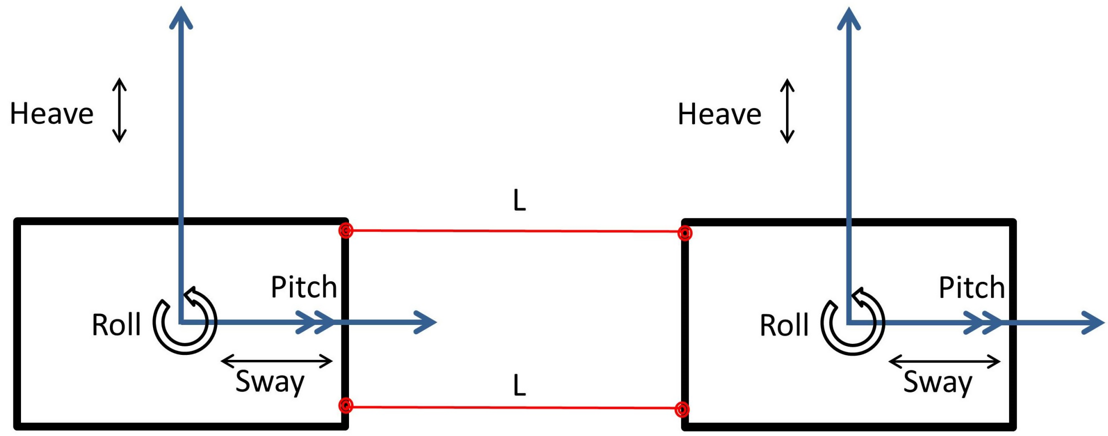

Figure 8.3: *Simplified Model for Twin Barges System with Linkages*

The equations of motion for each of the floating barges can be easily obtained from the first case study.

$$\begin{bmatrix} m & 0 & -mz_g & 0 \\ 0 & m & my_g & -mx_g \\ -mz_g & my_g & I_{xx}+mz_g^2+my_g^2 & -mx_gy_g \\ 0 & -mx_g & -mx_gy_g & I_{yy}+mz_g^2+mx_g^2 \end{bmatrix} \begin{bmatrix} \dot{u}_y \\ \dot{u}_z \\ \dot{u}_{xx} \\ \dot{u}_{yy} \end{bmatrix} = \begin{bmatrix} f_y \\ f_z \\ \tau_{xx} \\ \tau_{yy} \end{bmatrix} \tag{8.2.1}$$

in which, u_y, $,u_z$, u_{xx}, u_{yy} are the velocity in the sway, heave, roll and pitch direction. The f_y, f_z, τ_{xx}, τ_{yy} are the hydrodynamic forces or moments with respect to these motion.

Here, the bars are assumed as rigid, so the length of the bar is kept constant, which results in two holonomic constraints:

$$\begin{aligned} (x_{p1}-x_{p2})^2+(y_{p1}-y_{p2}+L)^2+(z_{p1}-z_{p2})^2-L^2=0 \\ (x_{p3}-x_{p4})^2+(y_{p3}-y_{p4}+L)^2+(z_{p3}-z_{p4})^2-L^2=0 \end{aligned} \tag{8.2.2}$$

in which, the x_p, y_p, z_p are the coordinates of the hinged points on the barge in the h-frame, which can be derived from the motions of barge.

$$\begin{aligned} x_p &= z_b \cdot \theta \\ y_p &= y - z_b \cdot \phi \\ z_p &= z - x_b \cdot \theta + y_b \cdot \phi \end{aligned} \tag{8.2.3}$$

where, the x_b, y_b, z_b are the coordinates of the hinged points on the barge in the body-fixed frame, and y, z, ϕ, θ are the sway, heave, roll and pitch of the barge respectively. The two holonomic constraints can eliminate two independent degrees of freedom by substituting the differentiated Eq: 8.2.2 into the equation of motion Eq: 8.2.1, normally, the sway and roll of either barge can be chosen as the dependent degrees to be eliminated.

8.3 System Identification of the Fluid Memory Effect

8.3.1 Data Preparation

The added mass and damping coefficients can be obtained using the hydrodynamic software WAMIT in frequency domain, which is based on potential theory. As mentioned in the first case study, the original data should be preprocessed before identification, which generally consists of two important steps: data setting and scaling.

There are 8 degrees of freedom considered in the catamaran configuration system, so the full transfer function matrix is 8 by 8. Due to the hydrodynamic interaction between the two barges, the transfer function becomes much more complicated than the single barge situation, which means there is more information contained in the transfer function which should be identified in the state space model. So, in order to maintain a high accuracy of the identified model, the full transfer function matrix is divided into 3 parts, a sway-sway 2×2 matrix, a heave-roll 4×4 matrix and a yaw-yaw 2×2 matrix.

Following the data setting, the data should be transformed into a proper scale which can be substituted into the convex optimization solver. In general, the power conservative scaling transformation can provide successful scaling factor:

$$\begin{aligned} K^S_{ik}(j\omega) &= \alpha_i \alpha_k K_{ik}(j\omega) \\ K^S(j\omega) &= \alpha^T K(j\omega)\alpha \end{aligned} \tag{8.3.1}$$

with $\alpha = diag(\alpha_1,\ \alpha_2,\ ..,\alpha_n)$. The coupling term weights α_i are chosen such that the mean magnitude of the diagonal elements of the scaled matrix, mean $\alpha_i^2|K_{ii}(j\omega)|$, is unity. This weighting scheme reflects the fact that the degrees of freedom associated with small radiation forces are not necessarily less important and should thus be given a larger weight to compensate. At the same time, insignificant off-diagonal elements are given less weight. It is worth noting that since the scaling transformation is power conservative, K will be passive provided that K^S is still passive. We can therefore use the scaled transfer matrix in the passivity enforcement as well.

8.3.2 Identification Results

Once the identification data is prepared well, the order of the state space model can be decided following the QR-factorization and singular value decomposition, normally, the singular value below 1% of the maximum should be ignored. In practice, the capacity of convex optimization solver is limited, which can only estimate a state space model with 24 orders for maximum. So, in some cases, the accuracy decreases due to the solver limitation.

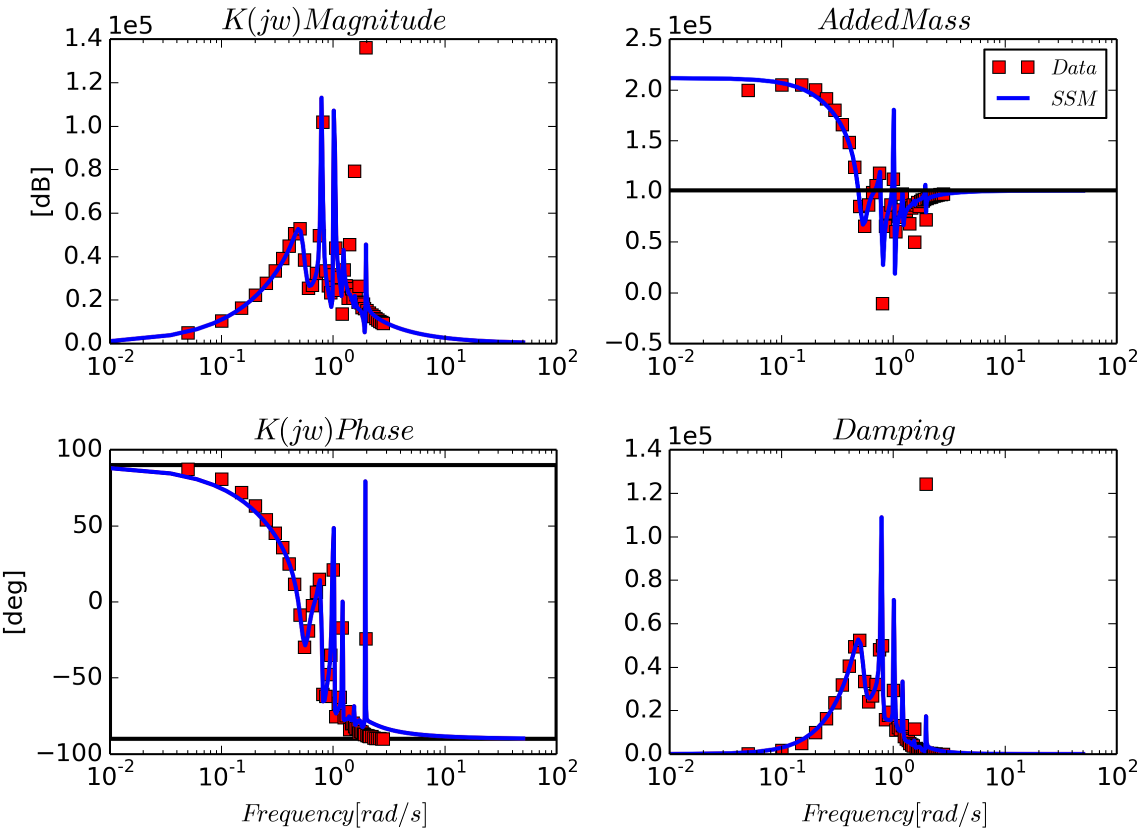

Figure 8.4: *Identification Results for Heave1-Heave1*

The above figure shows the identification result for the heave1- heave1 coupling term, from which it is obvious to see that the identified state space model can fit the original data well. The quality of fit is about 85% and the major deviation happens in the high frequency region where the wave energy is low and has insignificant influence on the barge motion. Thus the identified model is considered to be reliable.

8.3.3 Impulse Response Function Validation

The identified state-space model describes the linear time-invariant system of fluid memory effect, which also can be converted back to the impulse response function to validate the identified SSM fits the original data very well in time domain.

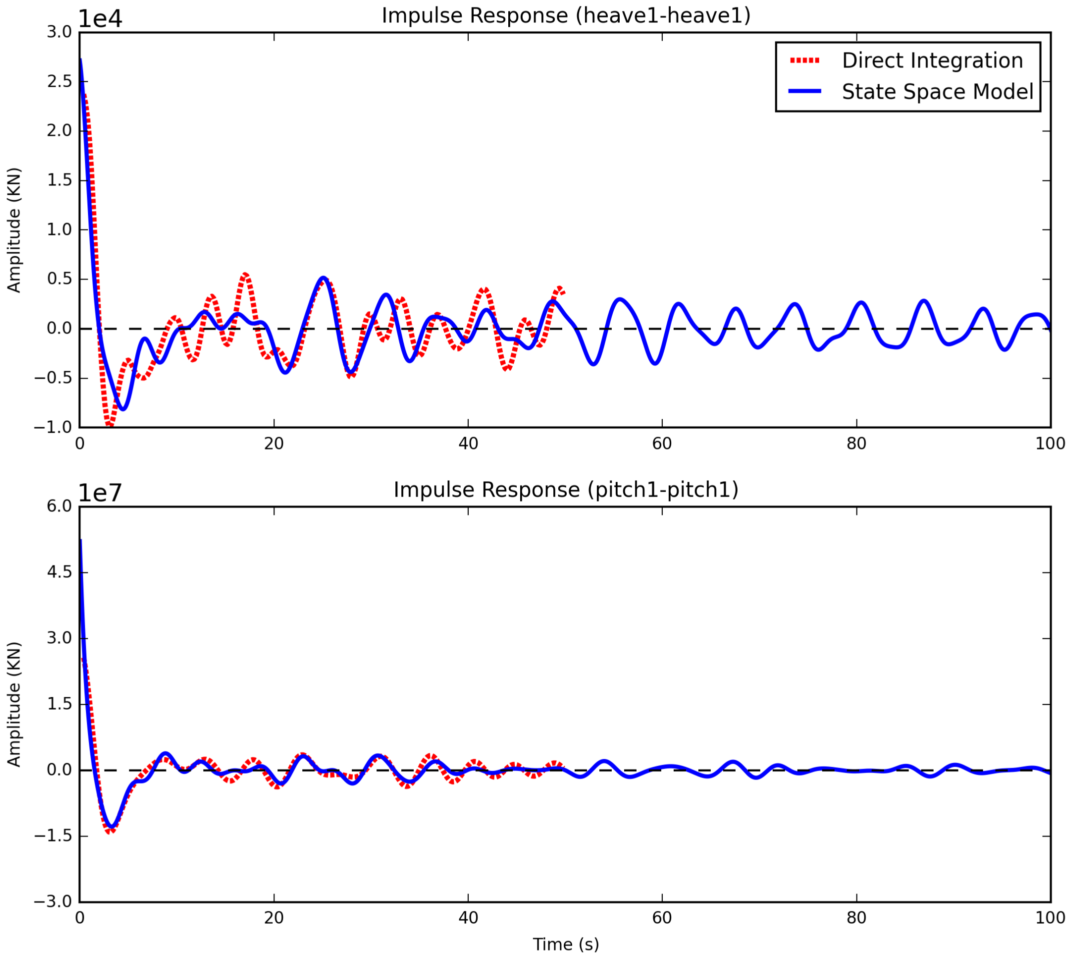

Figure 8.5: *Impulse Response Function Validation for Heave and Pitch*

Even though some discrepancies are observed in the impulse response plot, which is possibly due to the solver capacity that is limited into 24 orders, the identification state space model captures the major trend of the impulse response in time series, so it is considered as reliable to replace the convolution term in the *Cummins equation.*

8.4 State-Space Model of EoM

The identified state-space model of fluid memory effect can be incorporated into the equations of motion to obtain a uniform format in state space model:

$$\begin{bmatrix} I & 0 & 0 \\ 0 & \mathbf{I_{n\times n}} & 0 \\ 0 & 0 & M + A_{inf} \end{bmatrix} \begin{bmatrix} \dot{q} \\ \dot{\mathbf{x}} \\ \dot{u} \end{bmatrix} = \begin{bmatrix} u \\ \bar{\mathbf{A}}\mathbf{x} + \bar{\mathbf{B}}\mathbf{u} \\ \bar{\mathbf{C}}\mathbf{x} + \bar{G}q + \tau_{exc} \end{bmatrix} \tag{8.4.1}$$

where, the emphasized terms are the fluid memory effect and n is the new states number in the state space model of the fluid memory effect. The holonomic constraints Eq: 8.2.2 are taken into consideration into the EoM.

8.5 Simulation of the Dynamic Response

In order to have a deep insight of the effect from the linkages on the barge motion, three different scenarios are investigated to compare it with the free floating twin barges system (without linkages).

- Free Decay Scenario
- Regular Wave Scenario
- Irregular Wave Scenario

8.5.1 Free Decay Scenario

In this scenario, it is assumed that the structure is in the calm water without incoming waves. A initial displaced condition in heave and pitch of the first barge corresponding to $1m$ and 1^o is considered. The objective is to simulate the transient response of the vessel after it is released from this condition.

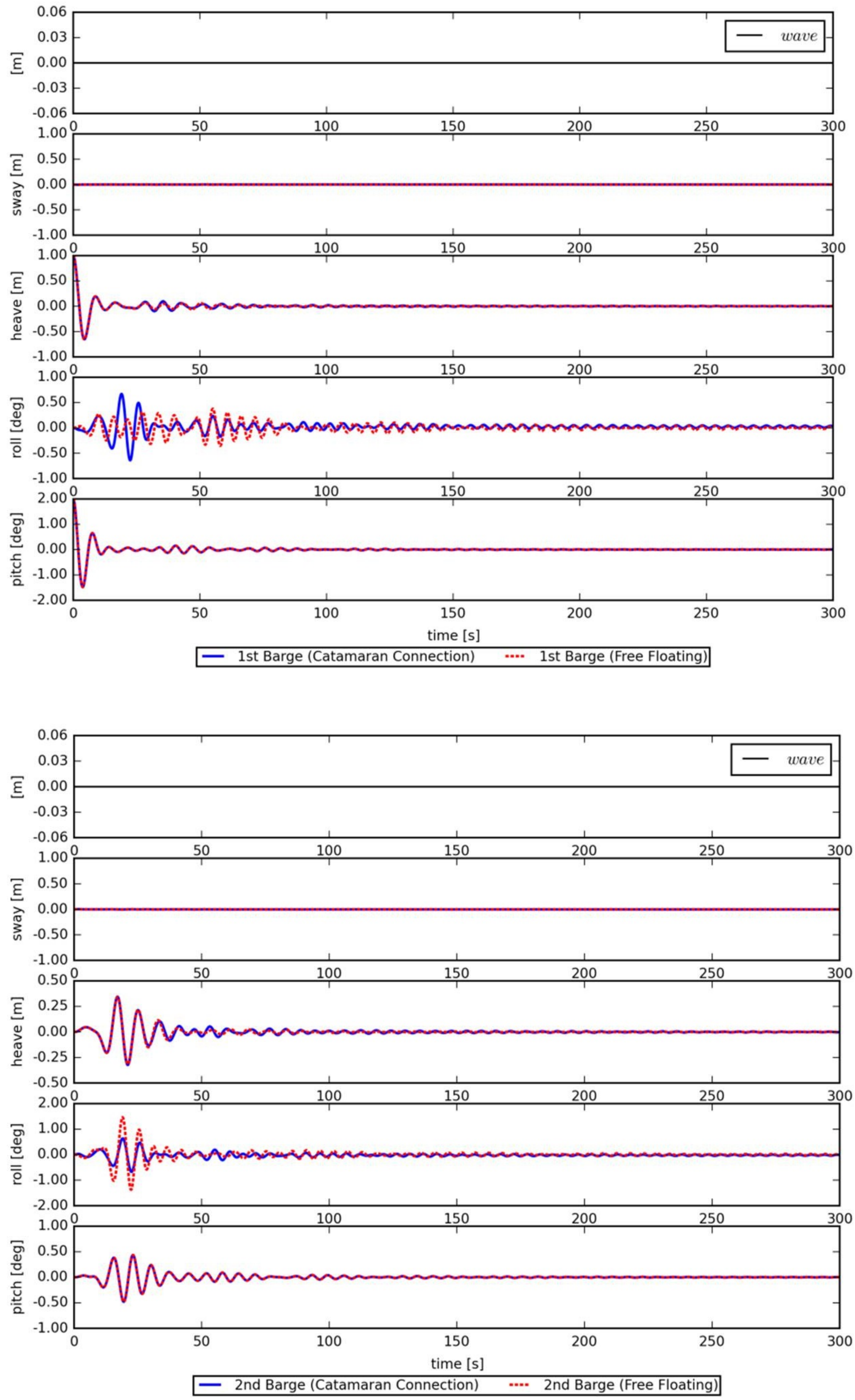

Figure 8.6: *Comparison of the Ship Motions for Two Systems (Free Decay)*

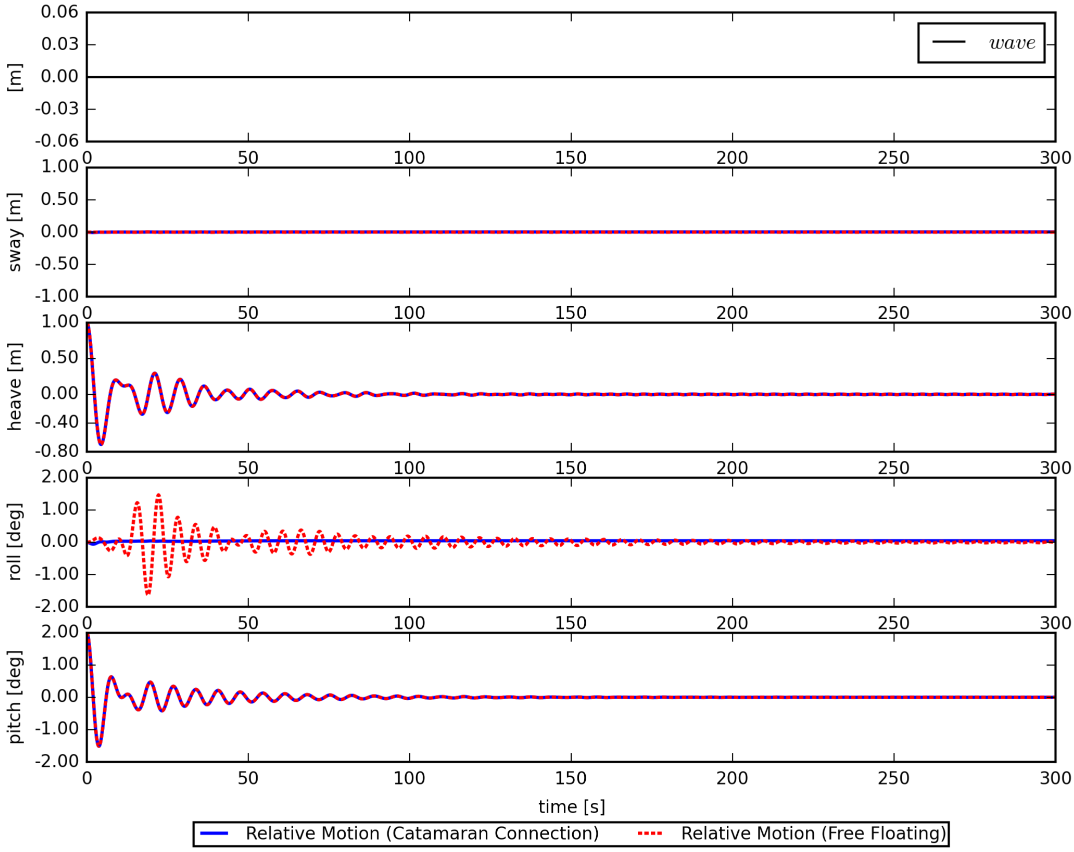

Figure 8.7: *Comparison of the Relative Motions for Two Systems (Free Decay)*

In this situation, the linkages do not have significant effect on the motion for individual barge, but the relative motion of roll has been successfully restricted.

8.5.2 Regular Wave Scenario

In the second scenario, the response of the structure initially at rest due to harmonic incident wave (regular wave) is investigated. The initial condition for the velocity and response were set to zero which is consistent with the object to understand the response from incident wave force. Typical time-domain response plots for 4 degrees of freedom at different wave-direction has been plotted in the following figures for the wave-direction 0^o, $,45^o$ and 90^o, which are also called heave wave, quartering wave and beam wave respectively. The wave frequency is assumed as $\omega = 1\ rad/s$.

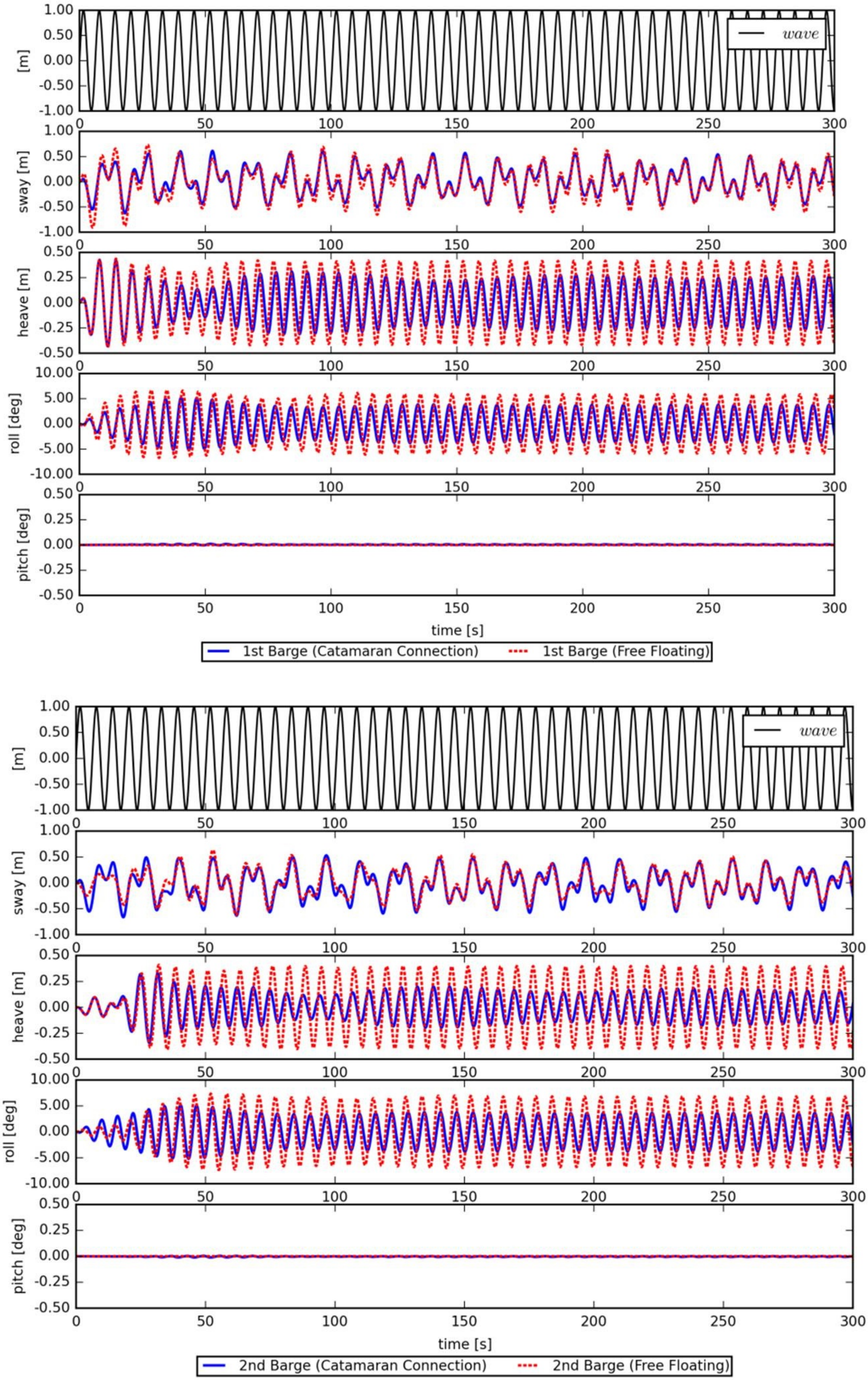

Figure 8.8: *Comparison of the Ship Motions for Two Systems (Beam Wave)*

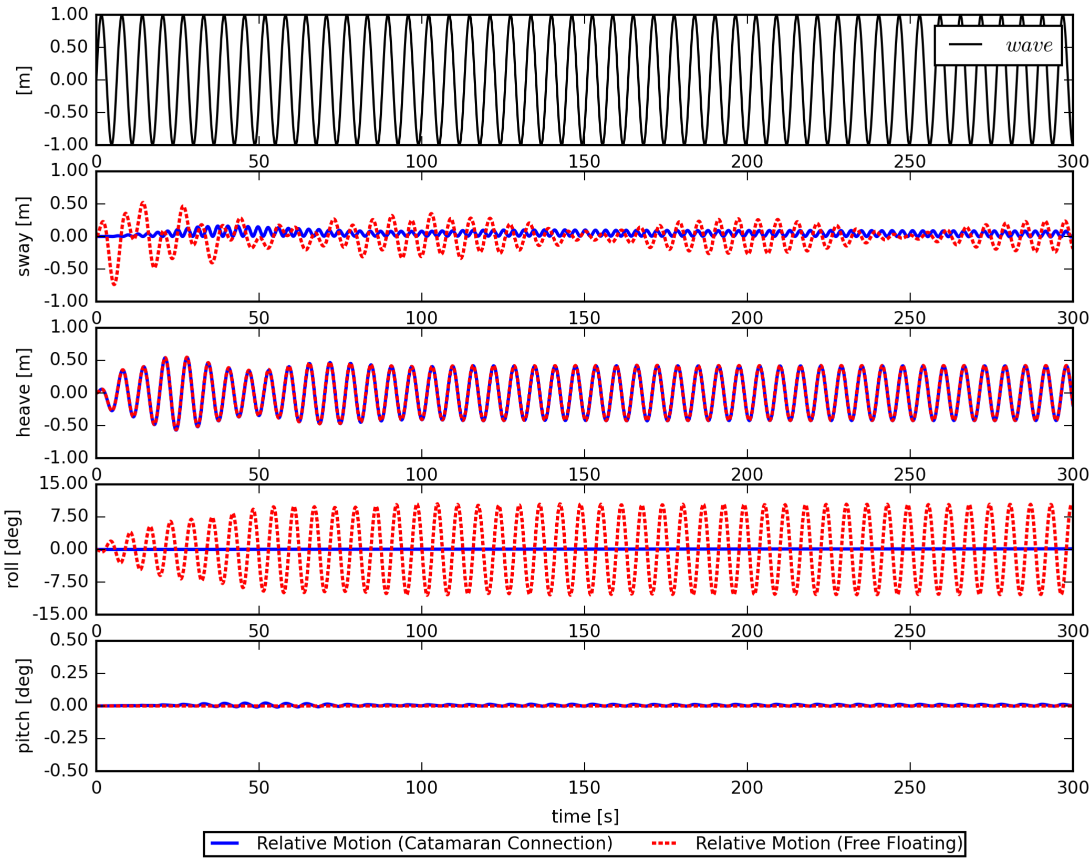

Figure 8.9: *Comparison of the Relative Motions for Two Systems (Beam Wave)*

Here, the motion analysis due to the beam wave is taken as an example to inspect the effect of linkages. It is obvious to notice that the motion responses in sway and roll for each barge have been eliminated greatly. What is more, the relative sway and roll have been restricted significantly.

8.5.3 Irregular Wave Scenario

Finally, the response of the vessel in the open sea, which is normally described by the wave spectrum, is studied to simulate the realistic situation. Here, the sea state is still described using a Jonswap spectrum with $8s$ peak wave period and $3m$ significant wave height which is same with the first case study.

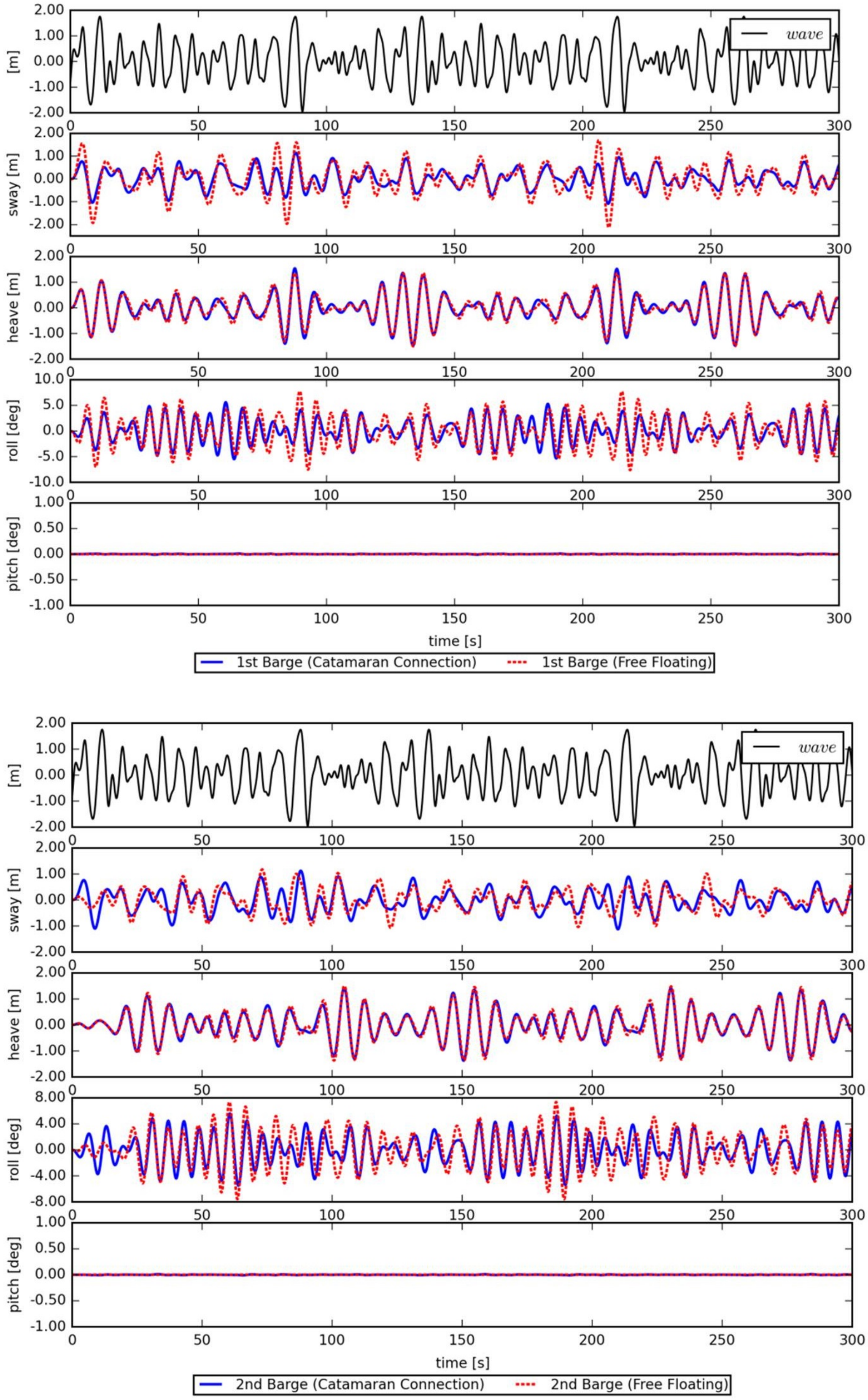

Figure 8.10: *Comparison of the Ship Motions for Two Systems (Beam Wave)*

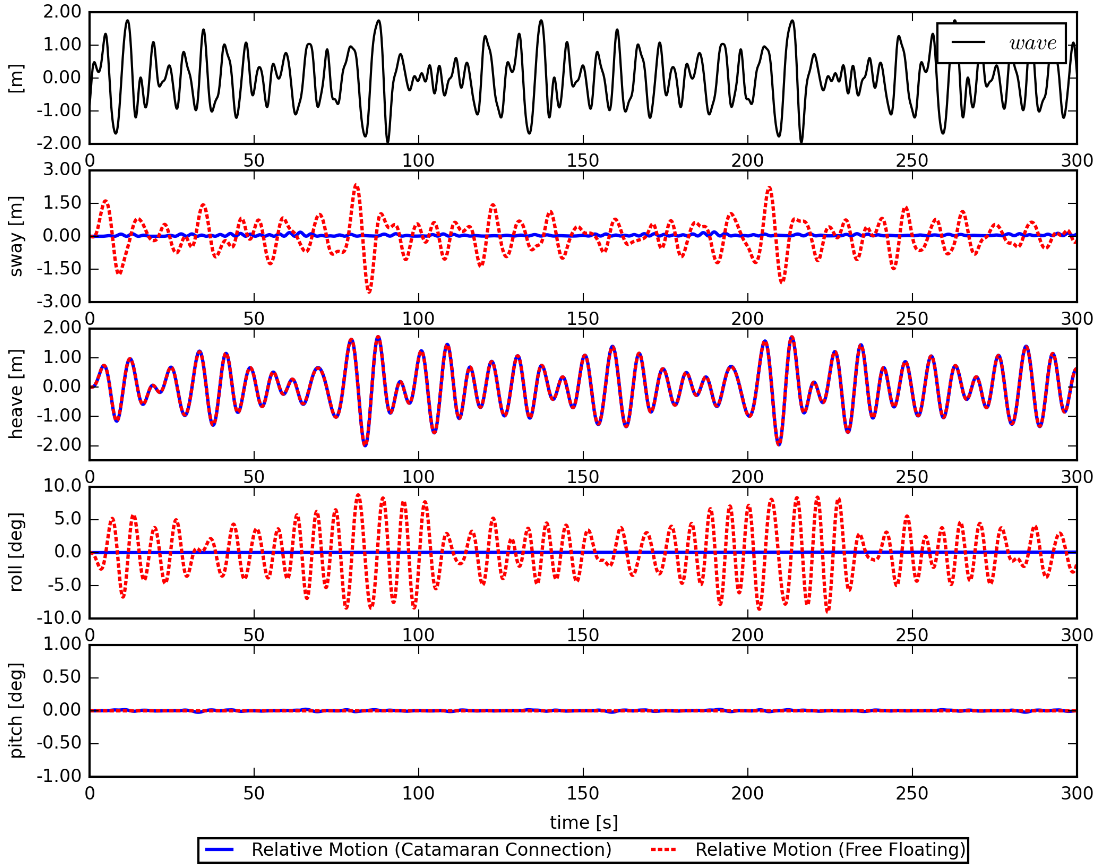

Figure 8.11: *Comparison of the Relative Motions for Two Systems (Beam Wave)*

The same effect of linkages in regular wave scenario can be observed here. The motion of each barge almost enforced synchronously in the sway and roll direction, however, the magnitude of the motions for each barge is not affected greatly.

8.6 Concluding Remarks

In this case study, it is the first time to apply the constrained system identification technique into a multibody case, the identification results show that this technique is reliable to estimate a state space model to replace the convolution term in the *Cummin equation*. Three different scenarios have been further studied to examine the effect of linkages on the motion response of the twin barges system. The motion simulation shows that the catamaran configuration barges can restrict the relative sway and roll significantly. So, the sway and roll for both barges in this system keep synchronous, and the heave and pitch can almost move freely. The goal of using hinged barges can be achieved successfully to reduce the risks due to the excessive relative sway and roll.

Chapter 9

Load Transfer Case Study

9.1 Introduction

During the lift phase, the topside is transferred onto the barge by using the active lift cylinders pre-installed on the barges when the prevailing sea state is suitable, and then towed to decommissioning site. In this phase, when the system is excited by waves, the lift cylinders will make intermittent impact with the topside deck. In addition, the barge may interact with the jacket by impacting with the fenders attached on the jacket legs. In order to ensure an efficient and safe topside decommissioning operation, it is critical to predict the resulting force and dynamics of the system with high confidence. In this case study, two simplified load transfer models are implemented by ignoring the horizontal impacts, which is useful as a preliminary step to demonstrate the methodology to investigate the dynamic responses arising in a lift-off decommissioning operation.

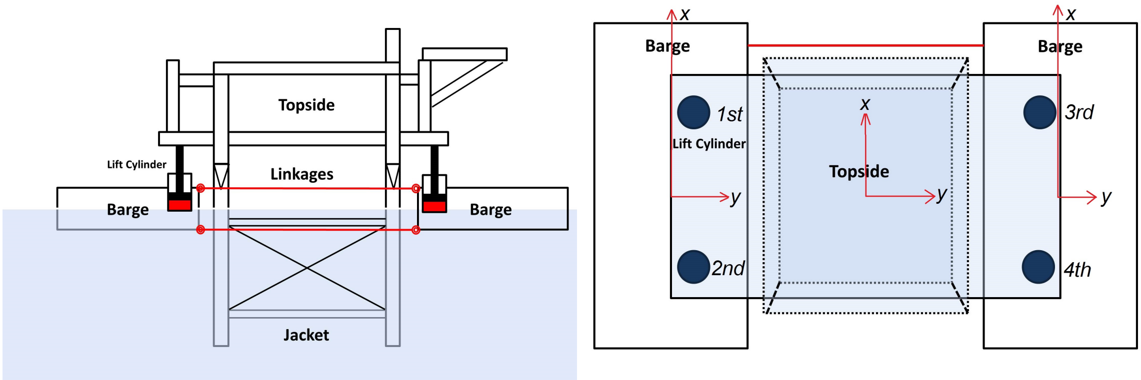

Figure 9.1: *Configuration of the Twin Barges Lift Off System (Left: Aft-side View; Right: Top View)*

Fig 9.1 illustrates the general configuration for decommissioning a topside on Jacket by the twin barges lift off method, in which two lift cylinders are pre-installed on each barge. The main parameters are provided as following.

Topside	Weight	Inertia of Moment (I_{xx})	Inertia of Moment (I_{yy})
	4000 ton	$1.5 \times 10^8\ kg \cdot m^2$	$1.5 \times 10^8\ kg \cdot m^2$
Lift Cylinder	Label	Coordinates (*Barge-fixed*)	Coordinates (*Topside-fixed*)
	$1st$	$(10, 10)$	$(10, -30)$
	$2nd$	$(-10, 10)$	$(-10, -30)$
	$3rd$	$(10, -10)$	$(10, 30)$
	$4th$	$(-10, -10)$	$(-10, 30)$

Table 9.1: *Parameters of the Twin Barges Lift-Off System*

Lift off operations generally can be divided into different stages: docking, premating, first contact, 50% of integrated topside weight transferred, last contact between support points and postmating. Numerical simulation of the lift off operations has commonly been conducted for the various stages, the 0% load transfer and 100% load transfer stage are studied in this thesis.

9.2 0% Load Transfer Stage

9.2.1 Simplified Two Bodies Model

Due to no load transferred on the barge, the topside is assumed to be fixed on the jacket, so the model consists of only two barges. During this stage, the wave-induced interaction between the lift cylinders and the deck is similar to a soft impact oscillator that has been extensively studied(Chen et al., 2014).

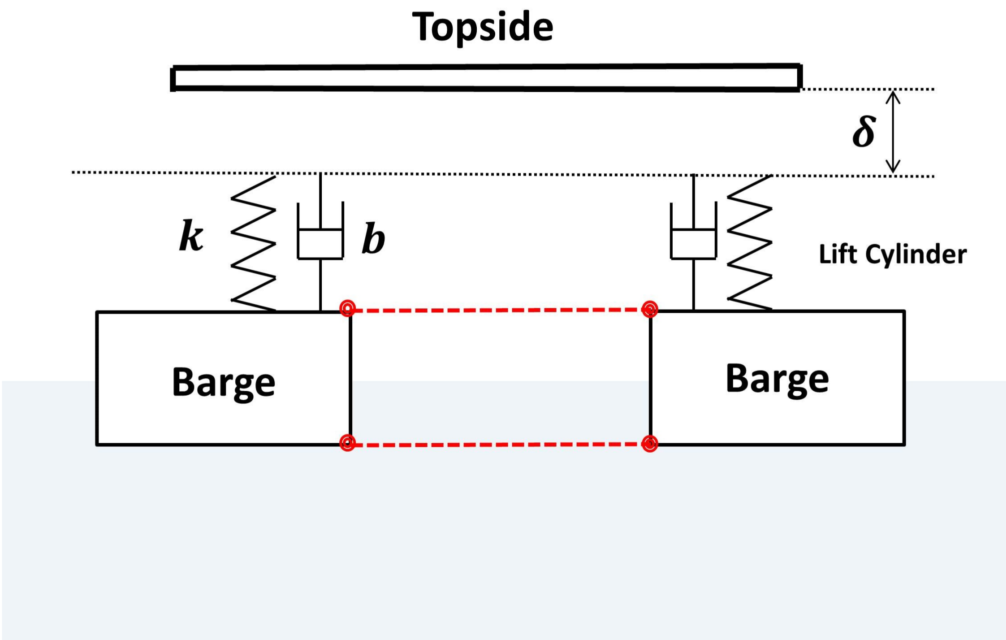

Figure 9.2: *Simplified Model at 0% Load Transfer Stage*

Fig: 9.2 describes the simplified impact model based on a typical impacting oscillator, in which the lift cylinders has been modeled as a dash-pot system with spring stiffness k and damping coefficient b. So, the impact force for each lift cylinder can be expressed as:

$$F = \begin{cases} 0, & z \leq \delta \\ b\dot{z} + k(z - \delta), & z > \delta \end{cases} \tag{9.2.1}$$

where, z is the vertical movement of the lift cylinder and δ is the original clearance gap between the deck and lift cylinder. In order to highlight the dynamic effects, the damping coefficient b is set as zero and the stiffness k is in a lower condition. Besides, the δ is assumed as 0 corresponding to the first contact between the topside and the lift cylinders. So the impact force can be expressed in an alternative form:

$$F = \sum_{i=1}^{4} \mathcal{H}(z_i) \cdot k \cdot z_i \tag{9.2.2}$$

in which $\mathcal{H}$ is the heaviside function that

$$\mathcal{H}(z) = \begin{cases} 0, & z \leq 0 \\ 1, & z > 0 \end{cases} \tag{9.2.3}$$

and $z = z_b - x_{LC} \times \theta_b + y_{LC} \times \phi_b$, $z_b,\ \phi_b,\ \theta_b$ are corresponding to heave, roll and pitch of the barge and $x_{LC},\ y_{LC}$ stands for the coordinates of the lift cylinder in the body fixed frame respectively.

The moment induced by the impact force can be easily obtained:

$$\begin{aligned} M_{xx} &= \sum_{i=1}^{4} \mathcal{H}(z_i) \cdot k \cdot z_i \cdot y_{LCi} \\ M_{yy} &= \sum_{i=1}^{4} \mathcal{H}(z_i) \cdot k \cdot z_i \cdot x_{LCi} \end{aligned} \tag{9.2.4}$$

Substitute the impact force and moments into the Eq: 8.2.1 to derive the EoMs for load transfer model:

$$\begin{bmatrix} m & 0 & -mz_g & 0 \\ 0 & m & my_g & -mx_g \\ -mz_g & my_g & I_{xx} + mz_g^2 + my_g^2 & -mx_g y_g \\ 0 & -mx_g & -mx_g y_g & I_{yy} + mz_g^2 + mx_g^2 \end{bmatrix} \begin{bmatrix} \dot{u}_y \\ \dot{u}_z \\ \dot{u}_{xx} \\ \dot{u}_{yy} \end{bmatrix} = \begin{bmatrix} f_y \\ f_z + \mathbf{F} \\ \tau_{xx} + \mathbf{M_{xx}} \\ \tau_{yy} + \mathbf{M_{yy}} \end{bmatrix} \tag{9.2.5}$$

During the load transfer stage, the hydrodynamic forces are not affected by the impact between the topside and the lift cylinder, so the identified radiation force in the second case study can applied to this case directly. Combining the above equation with the identified state space model to get:

$$\begin{bmatrix} I & 0 & 0 \\ 0 & I_{n\times n} & 0 \\ 0 & 0 & M + A_{inf} \end{bmatrix} \begin{bmatrix} \dot{q} \\ \dot{x} \\ \dot{u} \end{bmatrix} = \begin{bmatrix} u \\ Ax + Bu \\ Cx + Gq + \tau_{\mathbf{exc}} \end{bmatrix} \tag{9.2.6}$$

Finally, the holonomic constraints of linkages Eq: 8.2.2 are incorporated into the governing equations.

9.2.2 Simulation of the Dynamic Response

In the beginning of the lift off operation, the stiffness is weak, purposely so, so as to shielding the barges from possibly excessive dynamics events. The stiffness of lift cylinder is assumed as $10^2\ KN/m$ and two scenarios are taken into consideration here: regular wave scenario and irregular wave scenario.

- **Regular Wave Scenario**

In the first scenario, the response of the structure initially at rest due to harmonic incident wave (regular wave) is investigated. The initial condition for the velocity and response were set to zero which is consistent with the object to understand the response from incident wave force. Typical time-domain response plots for 4 degrees of freedom at different wave-direction has been plotted in the following figures for the wave-direction 90^o, which is also called beam wave. The wave height is $1m$ and the wave frequency is assumed as $\omega = 1.25\ rad/s$.

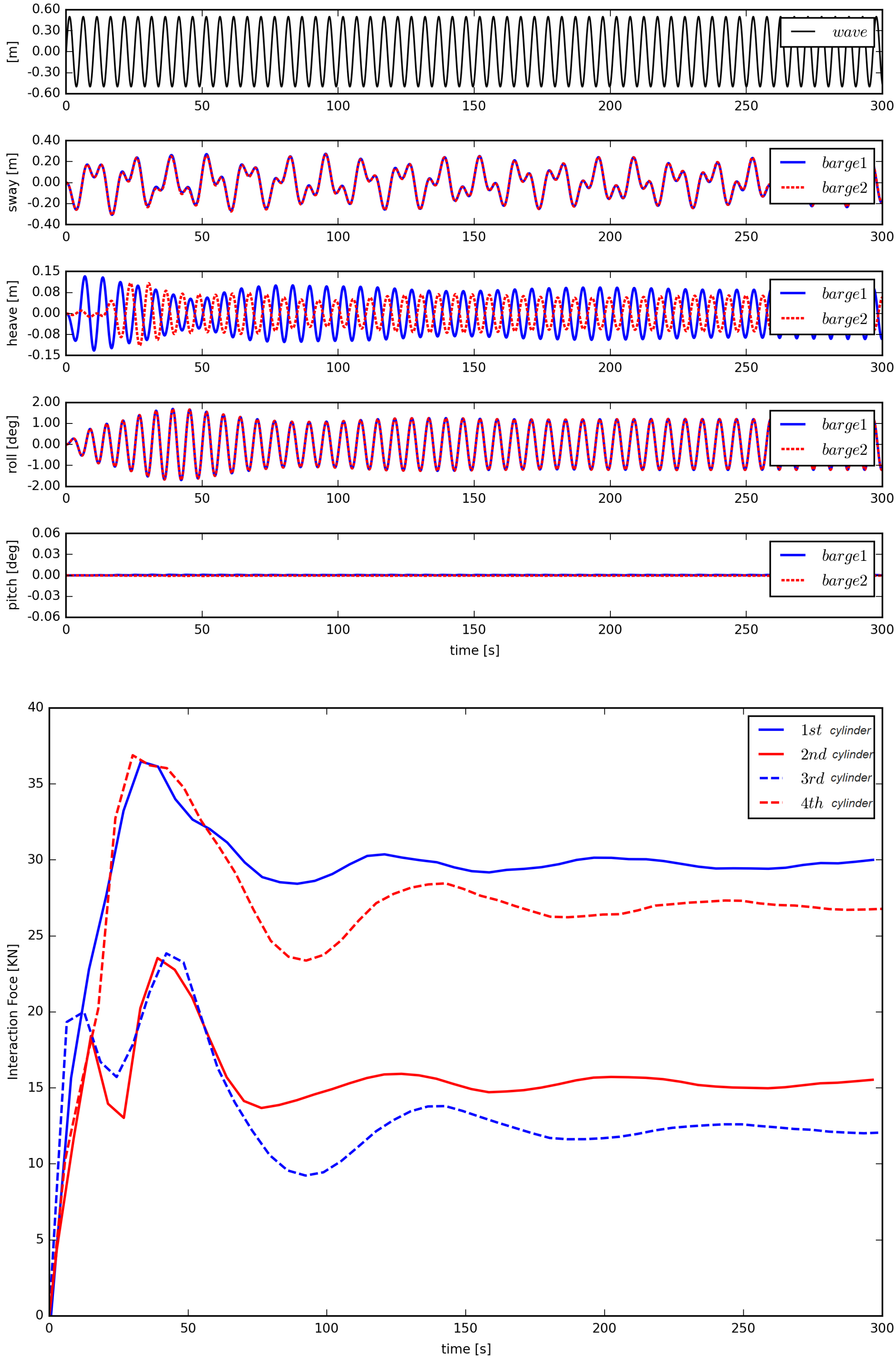

Figure 9.3: *Ship Motions and Interaction Forces at 0% Load Transfer Stage (Regular Beam Wave)*

- **Irregular Wave Scenario**

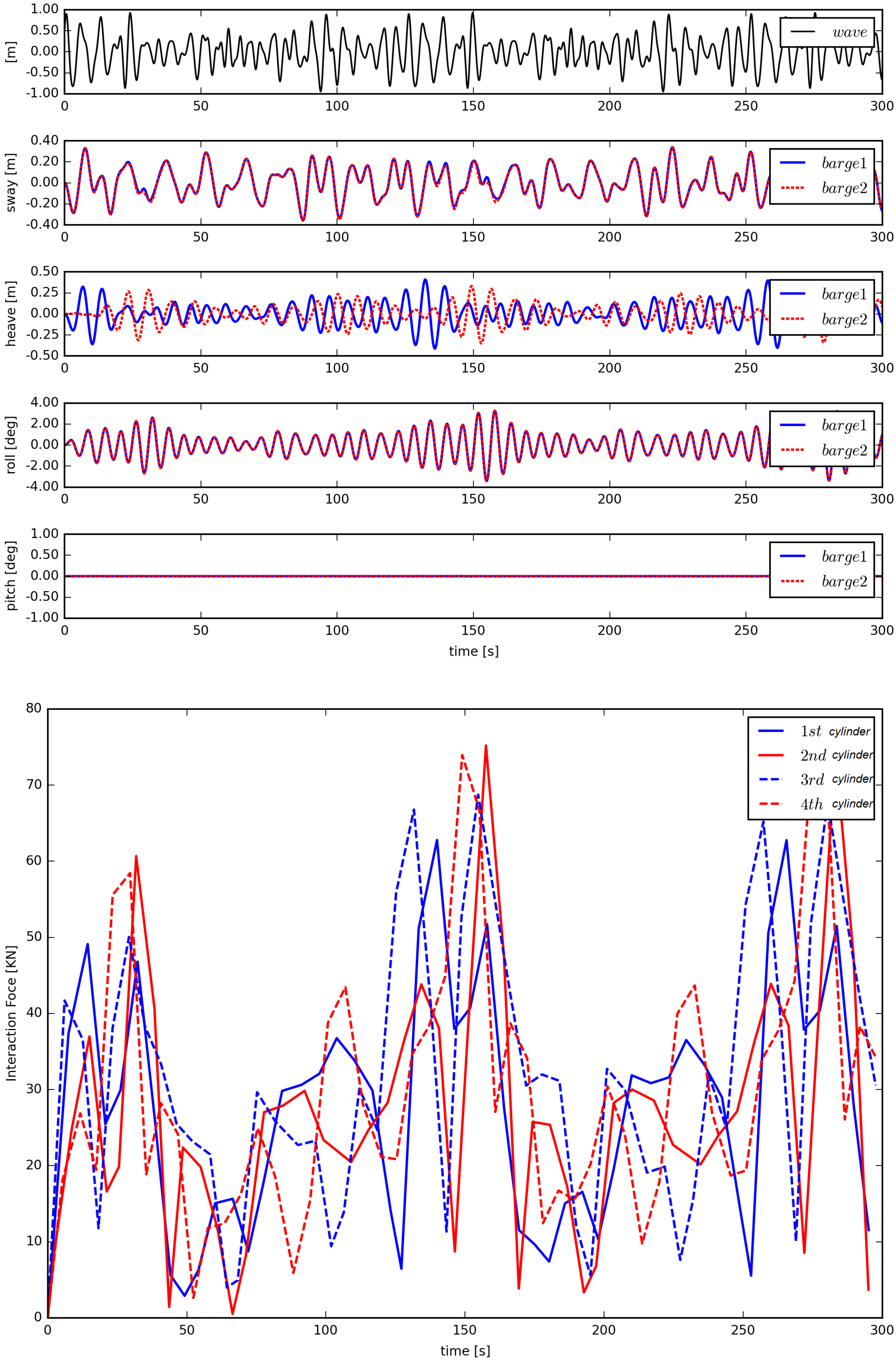

Figure 9.4: *Ship Motions and Interaction Forces at 0% Load Transfer Stage (Irregular Beam Wave)*

Finally, the response of the vessel in the open sea, which is normally described by the wave spectrum, is studied to simulate the realistic situation. Here, the sea state is described using a Jonswap spectrum with $6s$ peak wave period and $1.5m$ significant wave height because the lift off operation is normally executed in a quite mild sea state. The maximum relative motion and interaction force can be found in the time series.

9.3 100% Load Transfer Stage

9.3.1 Simplified Three Bodies Model

In the end of the lift off operations, weight of the topside is fully transferred on the barge to form a three bodies system consisting of two barges and the topside. The interaction between the barge and topside due to the lift cylinders is primarily governed by the relative motion and acceleration between topside and the barges. These motions can be adequately described by introducing a 3 degrees of freedom (*heave, roll* and *pitch*) topside into the twin barges system. So, in total 11 DoFs need to be considered.

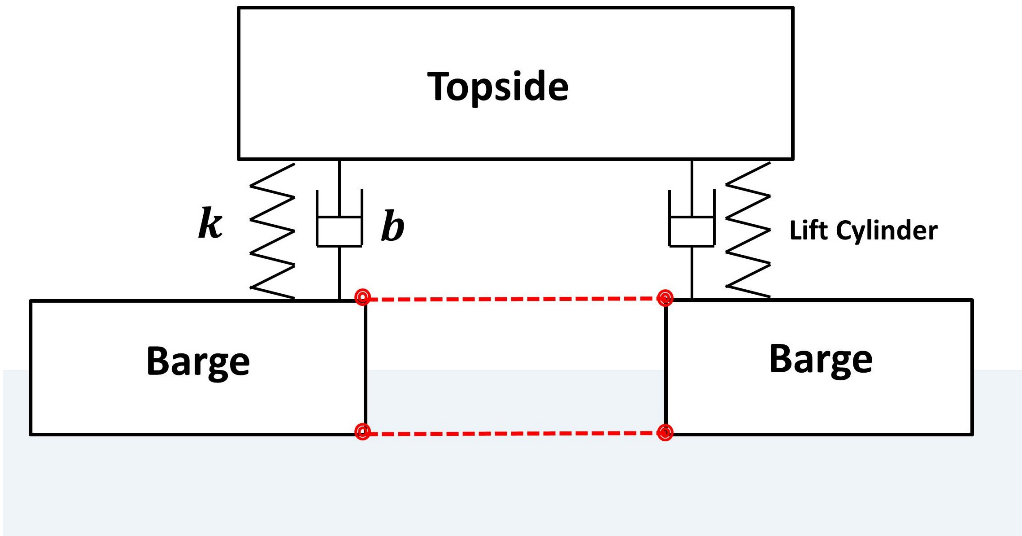

Figure 9.5: *Simplified Model at* 100% *Load Transfer Stage*

The governing equations for the topside can be easily obtained only taking the lift cylinders into consideration:

$$\begin{bmatrix} m_p & 0 & 0 \\ 0 & I_p^{xx} & 0 \\ 0 & 0 & I_p^{yy} \end{bmatrix} \begin{bmatrix} \ddot{z}_p \\ \ddot{\phi}_p \\ \ddot{\theta}_p \end{bmatrix} = \begin{bmatrix} F_p - m_p \cdot g \\ M_p^{xx} \\ M_p^{yy} \end{bmatrix} \tag{9.3.1}$$

in which, z_p, ϕ_p, θ_p are corresponding to *heave, roll* and *pitch* of the topside respectively.

The force acting on the topside from the lift cylinders can be expressed as following:

$$\begin{aligned} F_p &= \sum_{i=1}^{4} k \cdot (z_b^i - z_p^i + \delta_i) + b \cdot (v_b^i - v_p^i) \\ M_p^{xx} &= \sum_{i=1}^{4} (k \cdot (z_b^i - z_p^i) + b \cdot (v_b^i - v_p^i)) \cdot y_p^i \\ M_p^{yy} &= \sum_{i=1}^{4} (k \cdot (z_b^i - z_p^i) + b \cdot (v_b^i - v_p^i)) \cdot x_p^i \end{aligned} \tag{9.3.2}$$

in which, z_b, z_p are the vertical motion of the end of the lift cylinders on the barge and topside respectively and v_b, v_p corresponding to their velocity. x_p, y_p are the position of the lift cylinders in the topside-fixed frame. δ_i is the initial strain of the cylinder from the preload.

The forces from the lift cylinder as well act on the barge, substitute the forces into the governing equations of the twin barges:

$$\begin{bmatrix} m & 0 & -mz_g & 0 \\ 0 & m & my_g & -mx_g \\ -mz_g & my_g & I_{xx}+mz_g^2+my_g^2 & -mx_gy_g \\ 0 & -mx_g & -mx_gy_g & I_{yy}+mz_g^2+mx_g^2 \end{bmatrix} \begin{bmatrix} \dot{u}_y \\ \dot{u}_z \\ \dot{u}_{xx} \\ \dot{u}_{yy} \end{bmatrix} = \begin{bmatrix} f_y \\ f_z+\mathbf{F_b} \\ \tau_{xx}+\mathbf{M_b^{xx}} \\ \tau_{yy}+\mathbf{M_b^{yy}} \end{bmatrix} \tag{9.3.3}$$

in which,

$$\begin{aligned} F_b &= -F_p \\ M_b^{xx} &= -\sum_{i=1}^{4}(k\cdot(z_b^i-z_p^i)+b\cdot(v_b^i-v_p^i))\cdot y_b^i \\ M_b^{yy} &= -\sum_{i=1}^{4}(k\cdot(z_b^i-z_p^i)+b\cdot(v_b^i-v_p^i))\cdot x_b^i \end{aligned} \tag{9.3.4}$$

Finally, the holonomic constraints of linkages Eq: 8.2.2 are incorporated into the governing equations.

9.3.2 Simulation of the Dynamic Response

Before the final lift phase, the preload (pressure building) collectively pushed by the cylinders should be greater than the topside's weight against its bottom structure - quick-release (QR) locks take the extra preload as tension force, so as keeping the topside detached to its bottom support. Normally, the quick-release (QR) locks can take the 20% of the topside's weight. The purpose of the preload is to produce an additional uplift of the topside by approximately 1 meter.

The stiffness of the lift cylinder is decided by the desired preload and uplift:

$$k_{LC} = \frac{(preload-1)}{\Delta u\cdot n_{LC}}\cdot m_p\cdot g = \frac{(1.2-1)}{1\times 4}\times 4000\times 10 = 2\times 10^3 {}^{KN}\!/\!{}_{m} \tag{9.3.5}$$

Due to the barge is gonna have a deeper draft after the load transfer finished, so some redundancy needs to be taken into account. Here k_{LC} is set as $3\times 10^3 {}^{KN}\!/\!{}_{m}$ for each lift cylinder, and preload is set as the 120% of the topside weight, which is equivalent with a original strain of the lift cylinders with $5m$. The critical damping therefore is decided as $b_{LC} = \frac{2\sqrt{n_{LC}\times k_{LC}m_p}}{n_{LC}} = 3.5\times 10^3 {}^{KN\cdot s}\!/\!{}_{m}$.

Three simulation cases are made: the unlinked system in regular wave, the linked system in regular wave and the linked system in irregular wave. Their results are plotted in the end of this chapter.

Comparing the dynamic response for the unlinked system (Fig: 9.6) with the linked system (Fig: 9.7) in the same regular wave situation, in which wave height is $1m$ and the wave frequency is assumed as $\omega = 1.25\ rad/s$, it is significant to observe that:

1. For the unlinked system, the motions of the second barge especially in the direction of sway and roll are smaller than the first one due to the wave dissipated by the first barge, so the relative sway and roll are significant between two barges, which result in the obvious oscillation of the topside so that the safety clearance between the topside and the jacket is violated sometimes.
2. For the linked system, the linkages can keep the motions synchronous in the roll and sway directions, so the vertical elevation of the topside can reach to the equilibrium point quicker. Besides, the magnitude of the motions for each barge are also to be constrained greatly.
3. The effect of the damping has been examined here, it is obvious to notice that increasing the damping coefficient can decrease the transitional period to reach equilibrium point, so, the critical damping can be adopted taking into account the efficiency.
4. The above observations confirm the concerns that the unlinked system is of high possibilities to produce some undesirable mistakes in the lift off operation.

Finally, the irregular wave scenario is taken into consideration. The simulation results show that:

1. The topside raises above safety clearance quickly after the release of the topside weight.
2. The roll motion of the topside stay within a mall bound: $\phi_p < 1.3[deg]$, this confirms the stability of this system.

- **Regular Wave Scenario without Linkages**

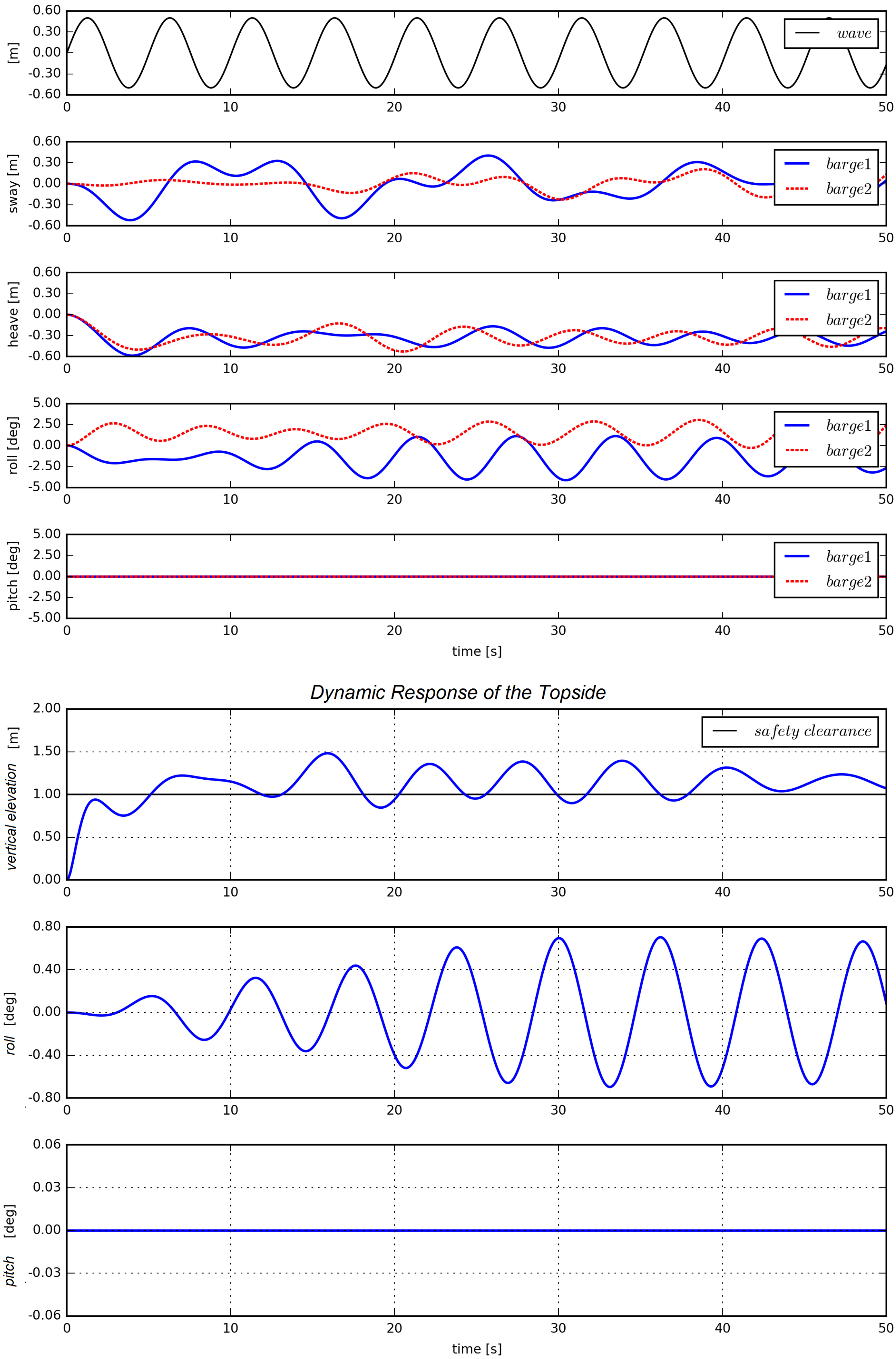

Figure 9.6: *Dynamic Response of the System without Linkages (Above: Barge; Below: Topside)*

- **Regular Wave Scenario with Linkages**

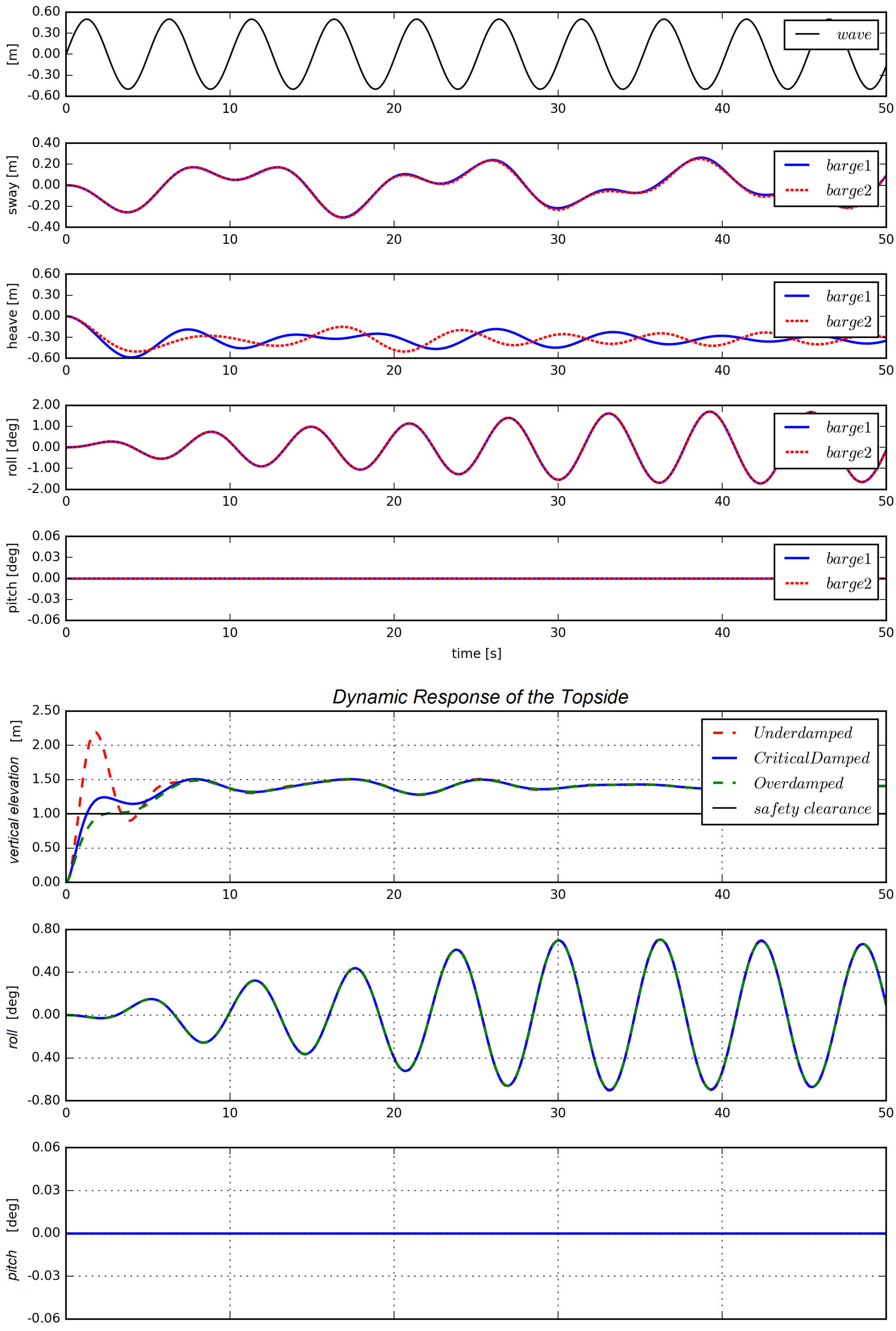

Figure 9.7: *Dynamic Response of the System with Linkages (Above: Barge; Below: Topside)*

- **Irregular Wave Scenario with Linkages**

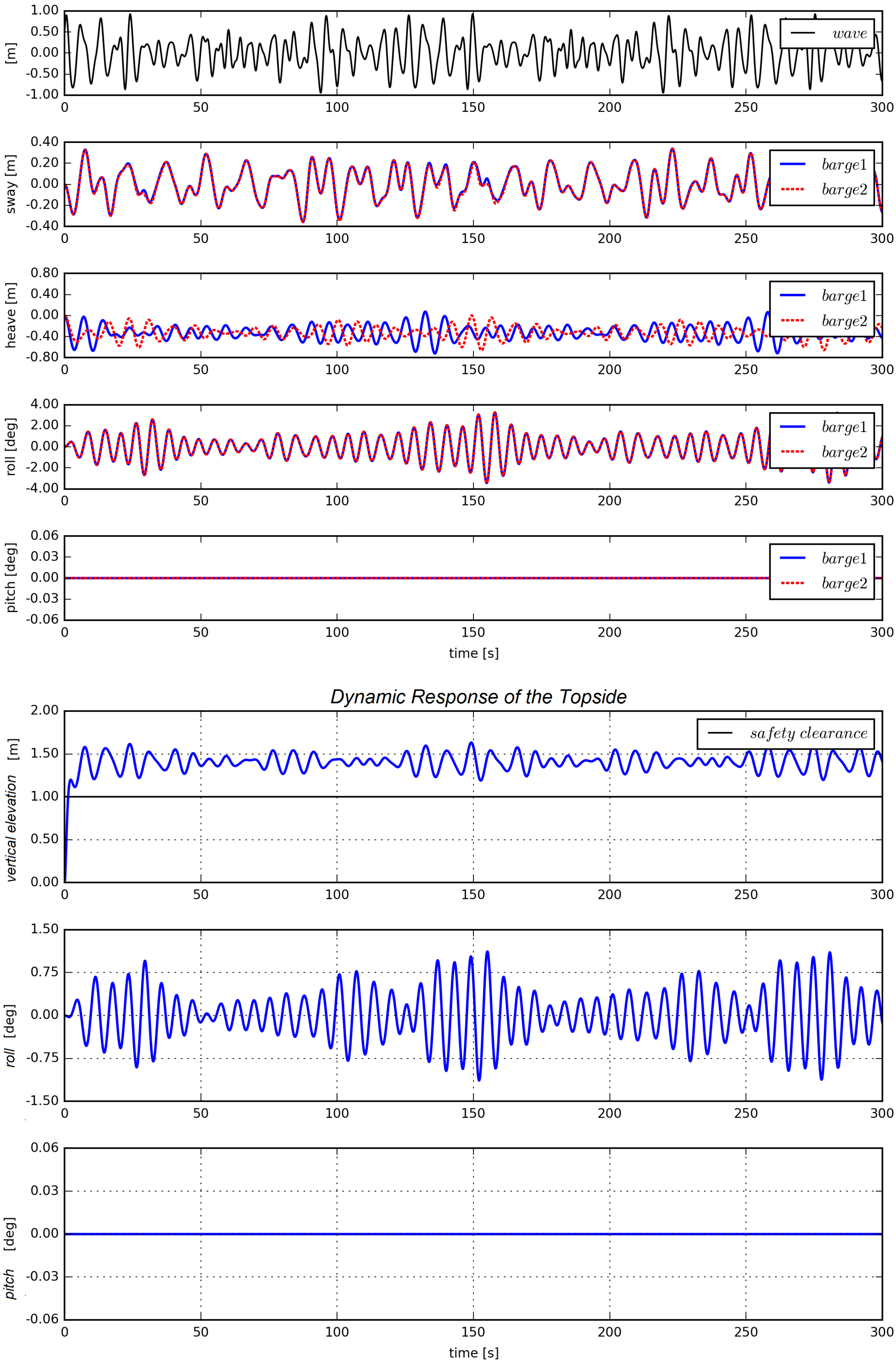

Figure 9.8: *Dynamic Response of the System with Linkages (Above: Barge; Below: Topside)*

9.4 Concluding Remarks

This case briefly introduces the methodology to analyze the load transfer stage based on the *Cummins equation*. The maximum relative motion and interaction forces can be found in the simulation results. Moreover, it is observed here that the topside heave is mainly affected by barge heave and roll, in the synchronized barge roll, the topside heave is more regular and a safety clearance is quicker attained. Besides, the topside roll is primarily decided by the different barge heave. Consequently, the synchronized barge roll makes little improvement to this.

Chapter 10

Conclusions and Recommendations

In the offshore industry, the float over installation is gaining popularity for installing a large deck onto an offshore platform due to its relatively lower operational cost and higher installation capacity. The inverse operation for offshore decommissioning using the similar way also attracts a lot of attention for the growing offshore decommissioning market. Normally, the frequency domain analysis is widely used in the preliminary stage of decommissioning operation, however, marine operations generally involve non-linearity such as the nonlinear mooring system or the nonlinear interaction from the topside. The *Cummins equation* provides a reliable way to analyze the dynamic response in time domain by incorporating the fluid memory effect as a convolution term rather than the frequency-dependent added mass and damping. For the purpose of simulation and design of motion control system, it is beneficial to approximate the fluid memory effect by a so called linear time-invariant state-space model. For the models to reflect reality better, physical properties are translated to certain model properties (prior knowledge) which are to be enforced when constructing these models.

Janssen et al. (2014) addressed the problem of constructing the state space model from software generated frequency domain hydrodynamic data by means of subspace system identification enforcing the following model properties in a multi-input multi-output (MIMO) system identification method.

System Property:

- Stability
- Passivity ($\Re[K_{ii}(j\omega] \geq 0$)
- Strictly Proper (high frequency asymptotic behavior)
- Zero at s = 0 (low frequency asymptotic behavior)

This identification strategy is incorporated into this thesis, substituting the identified state space model into the *Cummins equation* gives the equations of motion in a fully state space model, which is the basis for the simulation of the dynamic response. The first case is a linear seakeeping model, in which both of frequency domain and time domain can be applied, the simulation results validate the time domain approach is identical with the frequency domain approach, so it is considered reliable.

In the second case study, the twin barges lift off system has been studied without the linkages and with the linkages. The results show that the linkages can constraint the relative roll and sway successfully.

Finally, the load transfer is studied for two stages: 0% load transfer stage and 100% load transfer stage. For the first stage, it is still a two-bodies problem with the fixed topside, otherwise, the 100% load transfer stage should be modeled as a three-bodies system in which the topside moves.

Having performed this study, we can draw the following conclusions and make a few recommendation for future study.

Conclusions:

- The Kane's method and Lagrange method are studied to derive the EoM equivalently;
- System identification accuracy is improved and the first time to be applied to multi-body case;
- The time domain approach with identified state space model has been validated with a high accuracy and efficiency;
- The twin barges lift off system with linkages can effectively reduce the risks due to the excessive relative sway and roll;
- The load transfer stages have been studied to provide important information about the dynamic response and its interaction forces. The preliminary findings are stated:
  - Topside heave is affected by barge heave and roll. In the synchronized barge roll, the topside heave is more regular and a safety clearance is quicker attained.
  - Topside roll is primarily decided by the different barge heave. Consequently, the synchronized barge roll makes little improvement to this.

Recommendations:

- The amount of orders in the identified state space model has great influence on the efficiency and accuracy for final simulation, the order reduction methods need more attention in the future to find the best model reduction method;
- Due to the capacity limitation of convex optimization solver, the identified state space model has 24 orders at maximum, which may result in the model with low accuracy if the fluid memory effect is sophisticated;
- The original data should be prepocessed in order to be recognized by the solver, the scaling method can be improved to have a better estimation;
- The present model should be extended to do a comprehensive dynamic response analysis to asses the motions and forces under a great variety of circumstances;
- The linkage is assumed unstiffened and undamped here, which is not complete. The optimized stiffness and damping elements is forthcoming in an ongoing research by Vasileios Mathios.

Bibliography

Agüero, J. C.: 2005, *System identification methodologies incorporating constraints.* University of Newcastle.

Amirouche, F.: 2007, *Fundamentals of multibody dynamics: theory and applications.* Springer Science & Business Media.

Baruh, H.: 2000, 'Another look at the describing equations of dynamics'. *Chinese Society of Mechanical Engineers, Journal* **21**(1), 15–23.

Blundell, M. and D. Harty: 2004, *The multibody systems approach to vehicle dynamics.* Elsevier.

BP: 2011, 'Miller Decommissioning Programme'. Technical report.

Chen, M., R. E. Taylor, and Y. S. Choo: 2014, 'Time domain modeling of a dynamic impact oscillator under wave excitations'. *Ocean Engineering* **76**(0), 40 – 51.

Cummins, W.: 1962, 'The impulse response function and ship motions'. Technical report, DTIC Document.

Ekins, P., R. Vanner, and J. Firebrace: 2006, 'Decommissioning of offshore oil and gas facilities: A comparative assessment of different scenarios'. *Journal of environmental management* **79**(4), 420–438.

Faltinsen, O.: 1993, *Sea loads on ships and offshore structures*, Vol. 1. Cambridge university press.

Irvine, H. M. and H. M. Irvine: 1992, *Cable structures.* Dover Publications New York.

Janssen, R. M., H. Jansen, and J.-W. van Wingerden: 2014, 'A Novel Strategy for the Identification of Radiation Force Models'. In: *ASME 2014 33rd International Conference on Ocean, Offshore and Arctic Engineering.* pp. V01AT01A038–V01AT01A038.

Kristiansen, E., Å. Hjulstad, and O. Egeland: 2005, 'State-space representation of radiation forces in time-domain vessel models'. *Ocean Engineering* **32**(17), 2195–2216.

McKelvey, T., H. Akçay, and L. Ljung: 1996, 'Subspace-based multivariable system identification from frequency response data'. *Automatic Control, IEEE Transactions on* **41**(7), 960–979.

McKelvey, T. and S. R. Moheimani: 2005, 'Estimation of phase constrained MIMO transfer functions with application to flexible structures with mixed collocated and non-collocated actuators and sensors'. In: *Proceedings of the 16th IFAC world congress.*

Miller, D. N. and R. A. de Callafon: 2013, 'Subspace identification with eigenvalue constraints'. *Automatica* **49**(8), 2468 – 2473.

Ogilvie, T. F.: 1964, 'Recent progress toward the understanding and prediction of ship motions'. In: *5th Symposium on naval hydrodynamics.* pp. 3–80.

Osmundsen, P. and R. Tveteras: 2003, 'Decommissioning of petroleum installations-major policy issues'. *Energy policy* **31**(15), 1579–1588.

Parente, V., D. Ferreira, E. M. dos Santos, and E. Luczynski: 2006, 'Offshore decommissioning issues: Deductibility and transferability'. *Energy Policy* **34**(15), 1992–2001.

Perez, T.: 2006, *Ship motion control: course keeping and roll stabilisation using rudder and fins.* Springer Science & Business Media.

Perez, T. and T. I. Fossen: 2008, 'Joint identification of infinite-frequency added mass and fluid-memory models of marine structures'. *Modeling, Identification and Control* **29**(3), 93–102.

Pérez, T. and T. I. Fossen: 2008, 'Time-vs. frequency-domain identification of parametric radiation force models for marine structures at zero speed'. *Modeling, Identification and Control* **29**(1), 1–19.

Perez, T. and T. I. Fossen: 2009, 'Identification of Dynamic Models of Marine Structures from Frequency-domain Data Enforcing Model Structure and Parameter Constraints'. Technical report, DTIC Document.

Rogne, O. Y., T. Moan, and S. Ersdal: 2014, 'Identification of passive state-space models of strongly frequency dependent wave radiation forces'. *Ocean Engineering* **92**(0), 114 – 128.

Scottish Enterprise, D. N. S.: 2014, *Decommissioning in the North Sea - Review of Decommissioning Capacity.* ARUP.

Taghipour, R., T. Perez, and T. Moan: 2008, 'Hybrid frequency–time domain models for dynamic response analysis of marine structures'. *Ocean Engineering* **35**(7), 685–705.

Unknown: 2009, 'A brief synopsis of Kane's method and a few applications'. *Carnegie Mellon University.*

Unneland, K.: 2007, 'Identification and order reduction of radiation force models of marine structures'. Ph.D. thesis, PhD thesis, Norwegian University of Science and Technology, Department of Engineering Cybernetics.

Appendix A

CFDSI and UFDSI Comparison

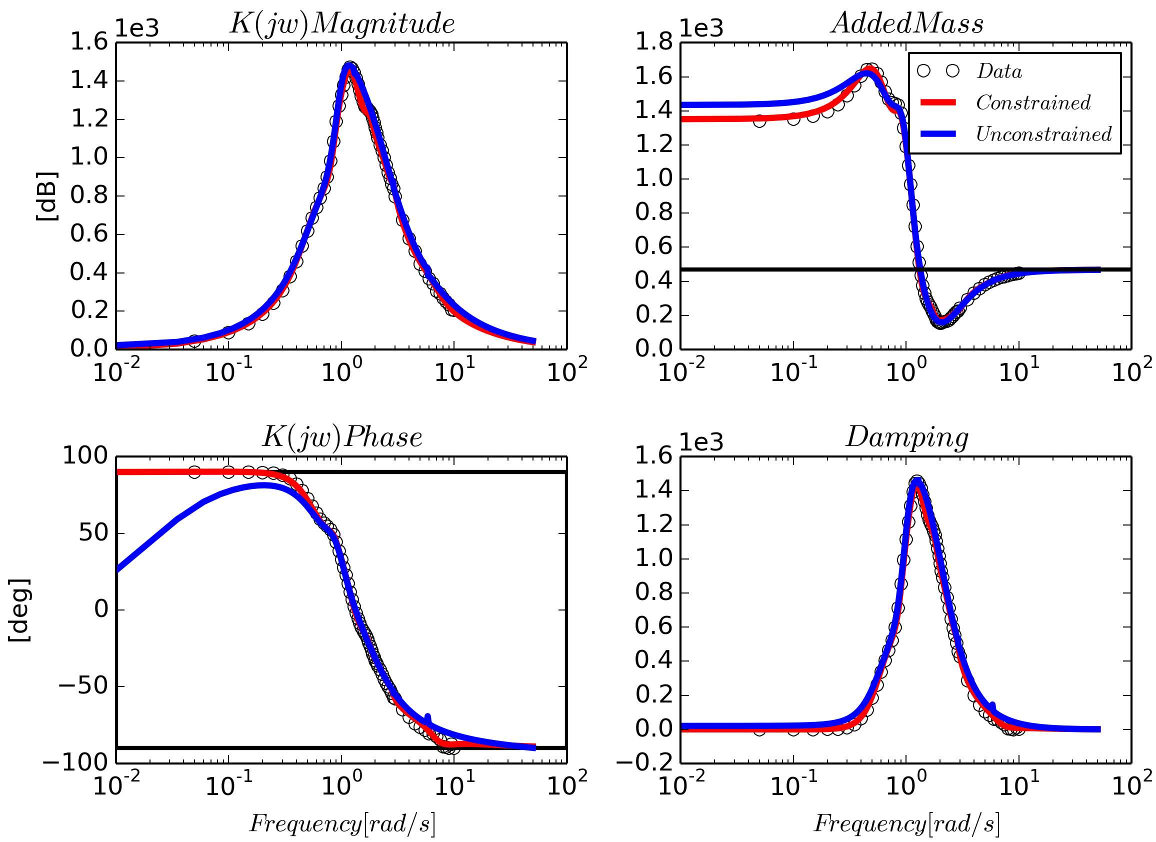

Figure A.1: *Effect of Constrained Identification Method (surge-surge)*

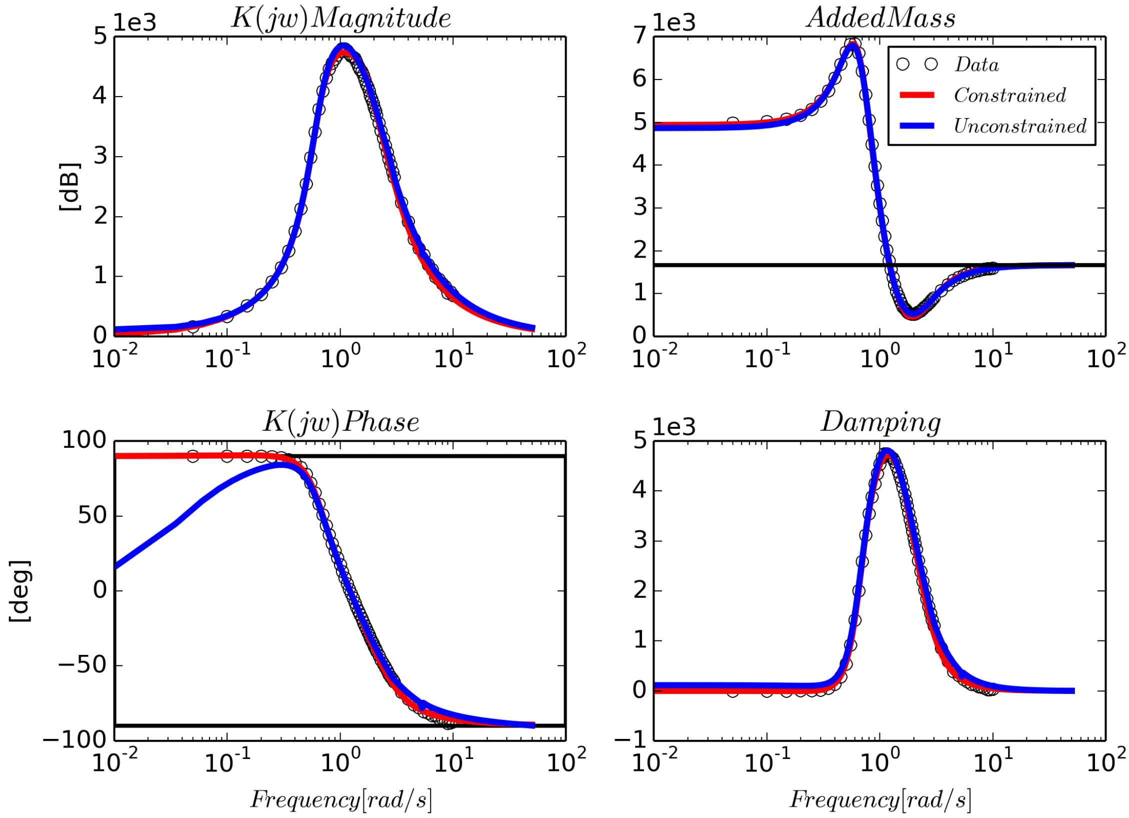

Figure A.2: *Effect of Constrained Identification Method (sway-sway)*

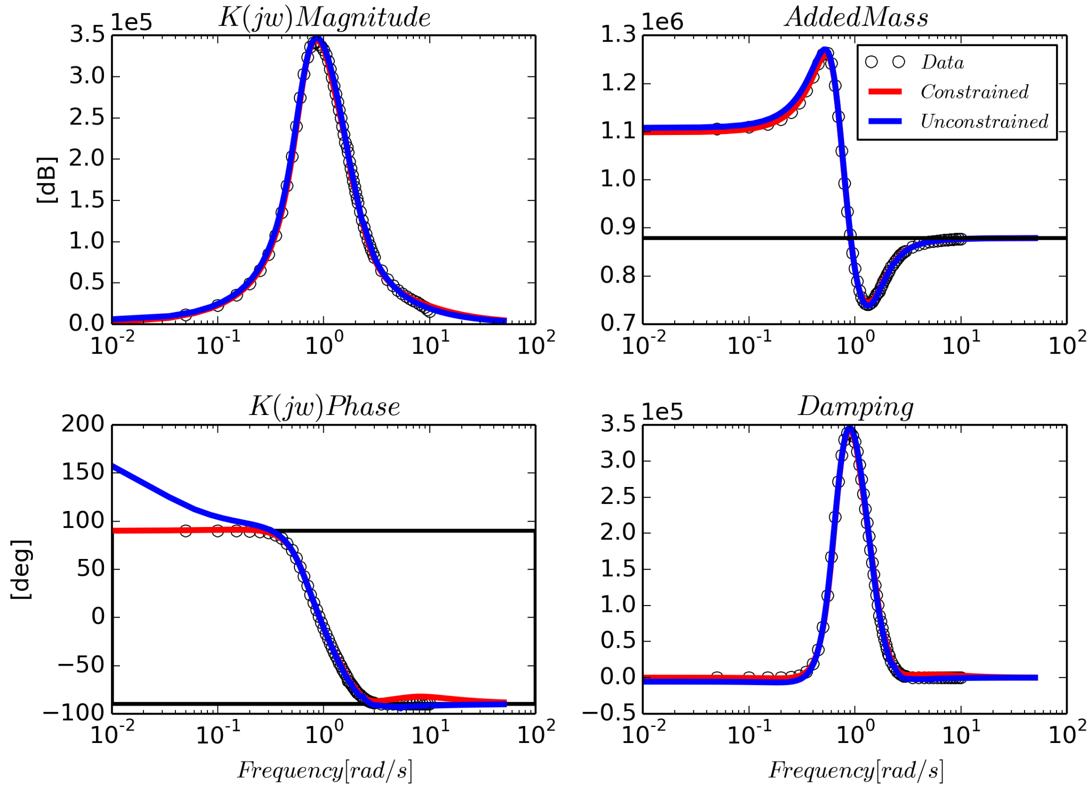

Figure A.3: *Effect of Constrained Identification Method (roll-roll)*

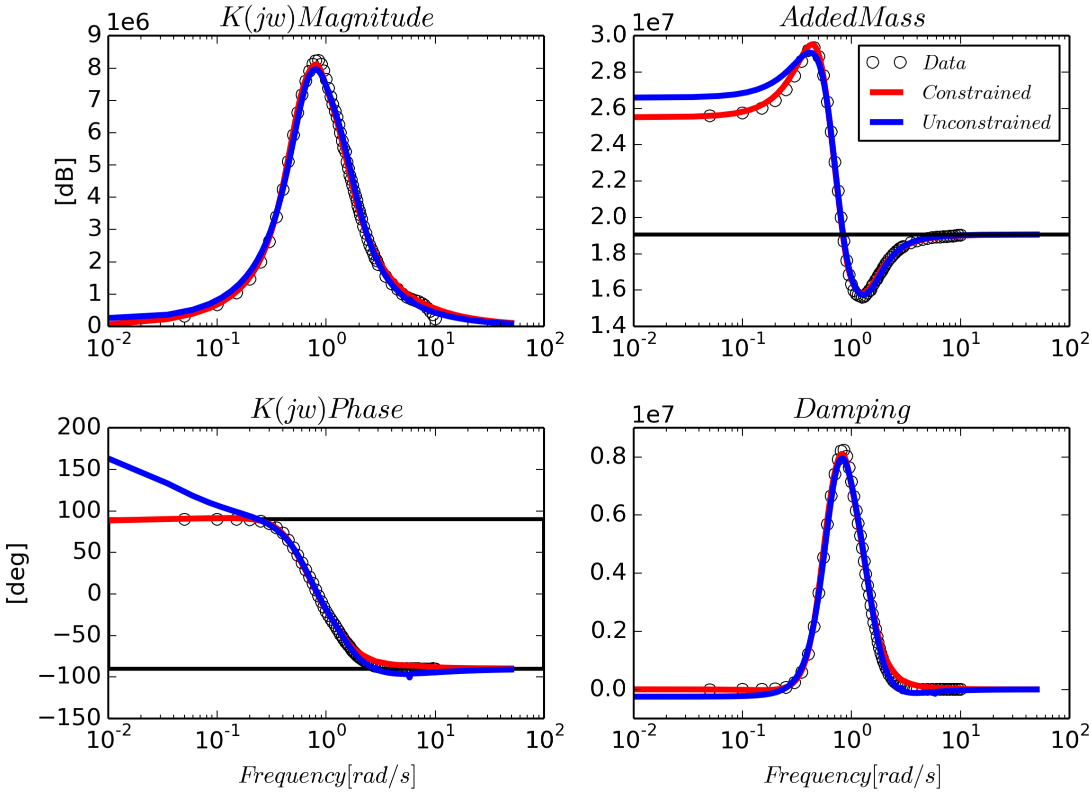

Figure A.4: *Effect of Constrained Identification Method (pitch-pitch)*

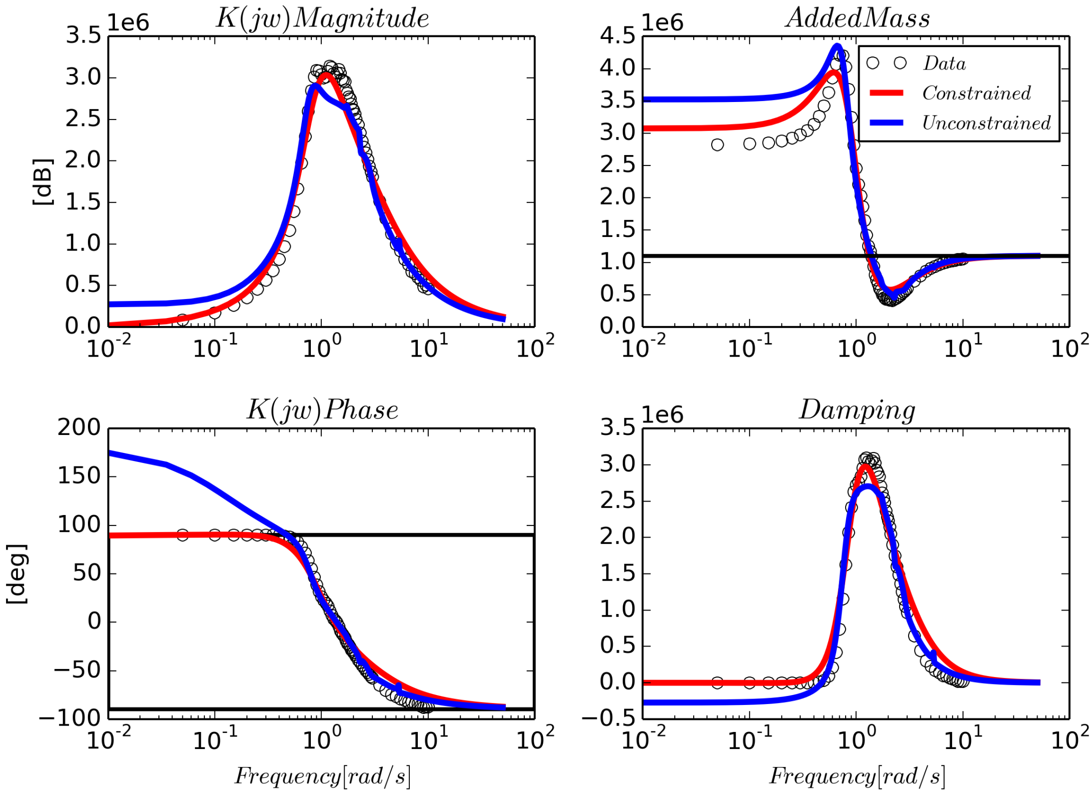

Figure A.5: *Effect of Constrained Identification Method (yaw-yaw)*

Appendix B

Twin Barges Identification

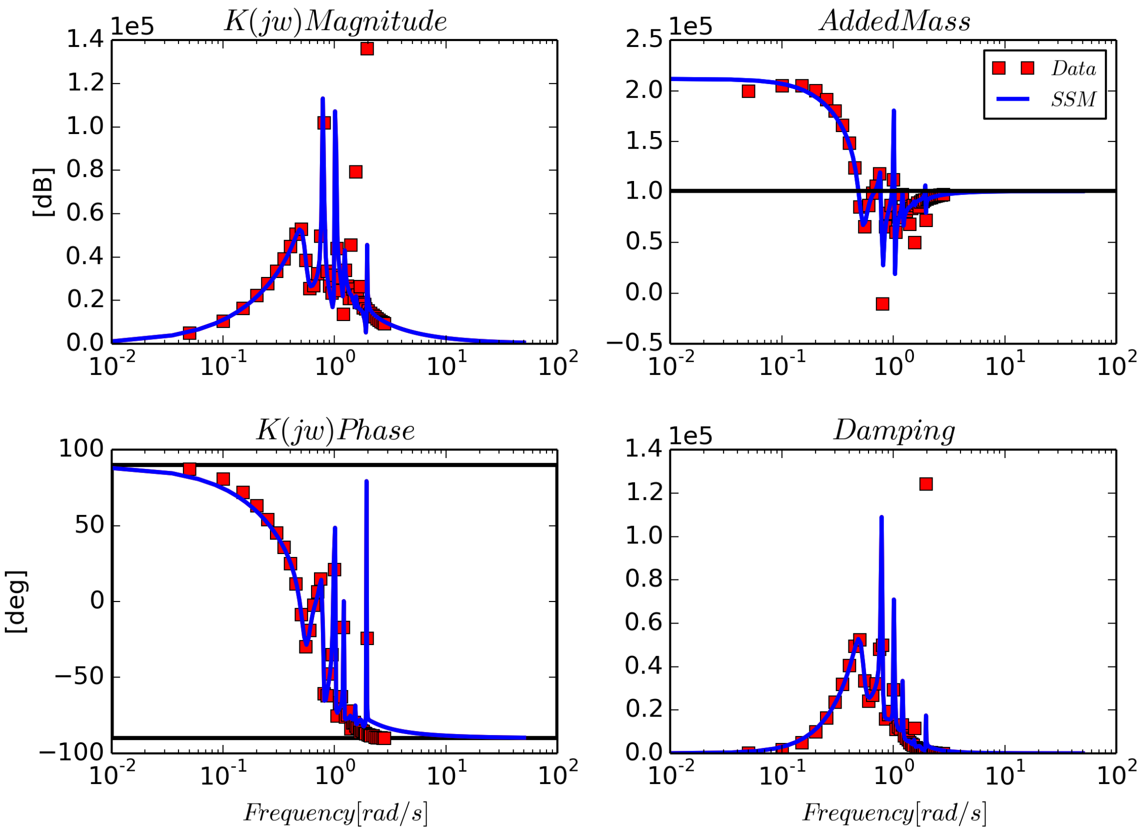

Figure B.1: *Identification Results for Heave1-Heave1*

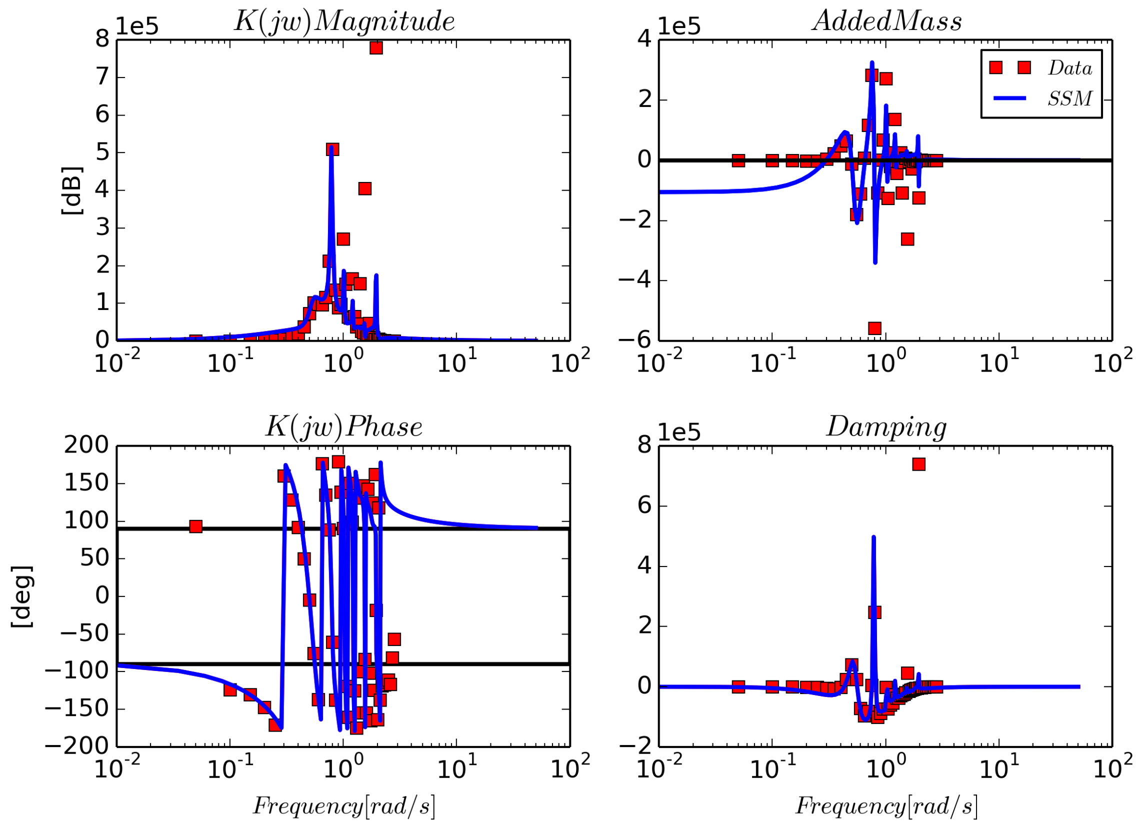

Figure B.2: *Identification Results for Heave1-Roll1*

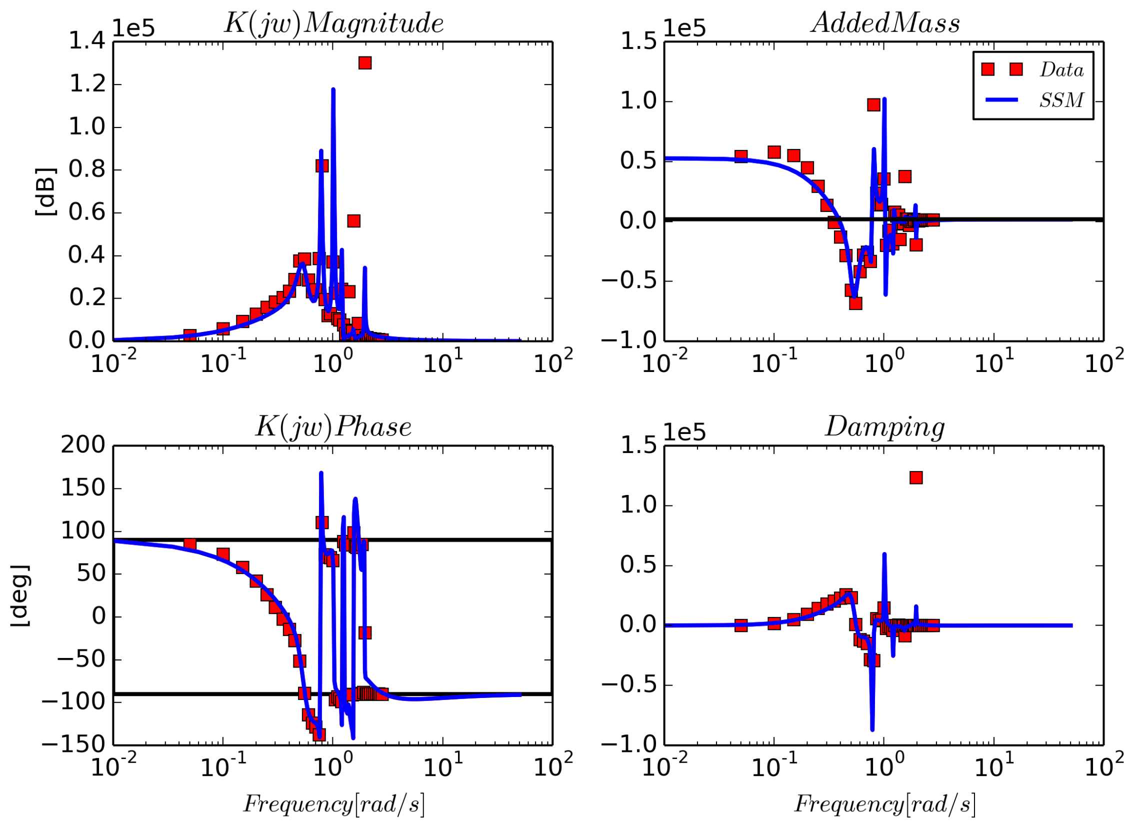

Figure B.3: *Identification Results for Heave1-Heave2*

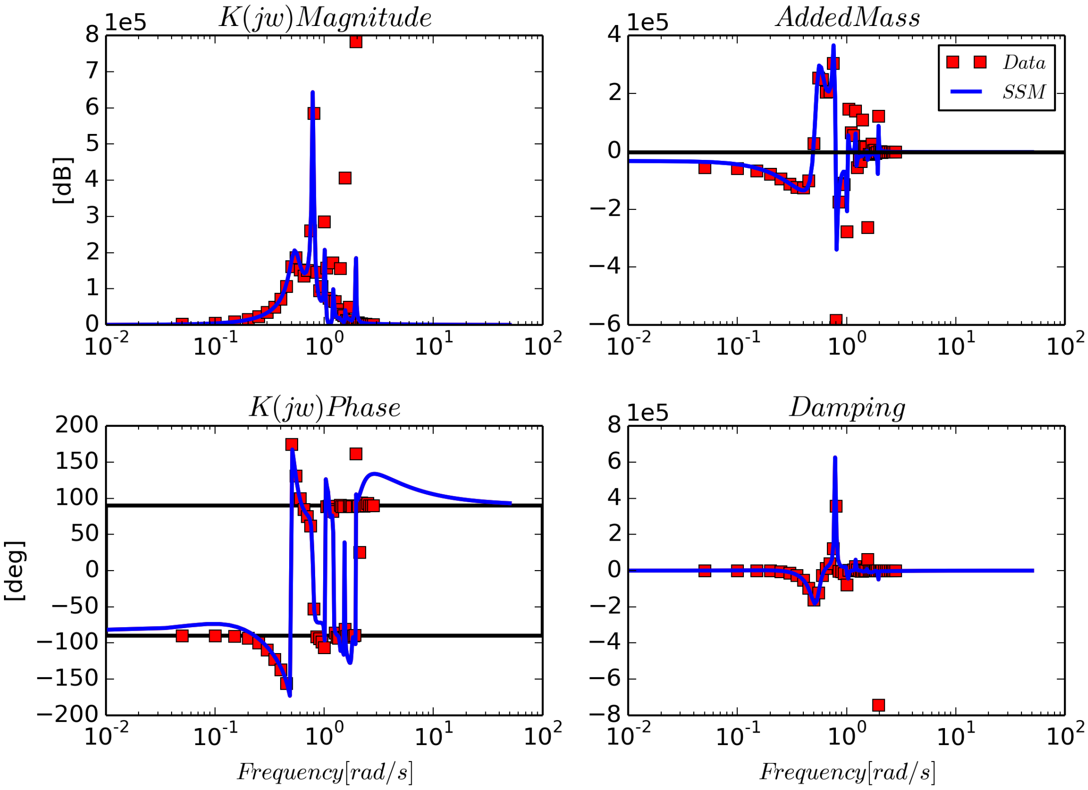

Figure B.4: *Identification Results for Heave1-Roll2*

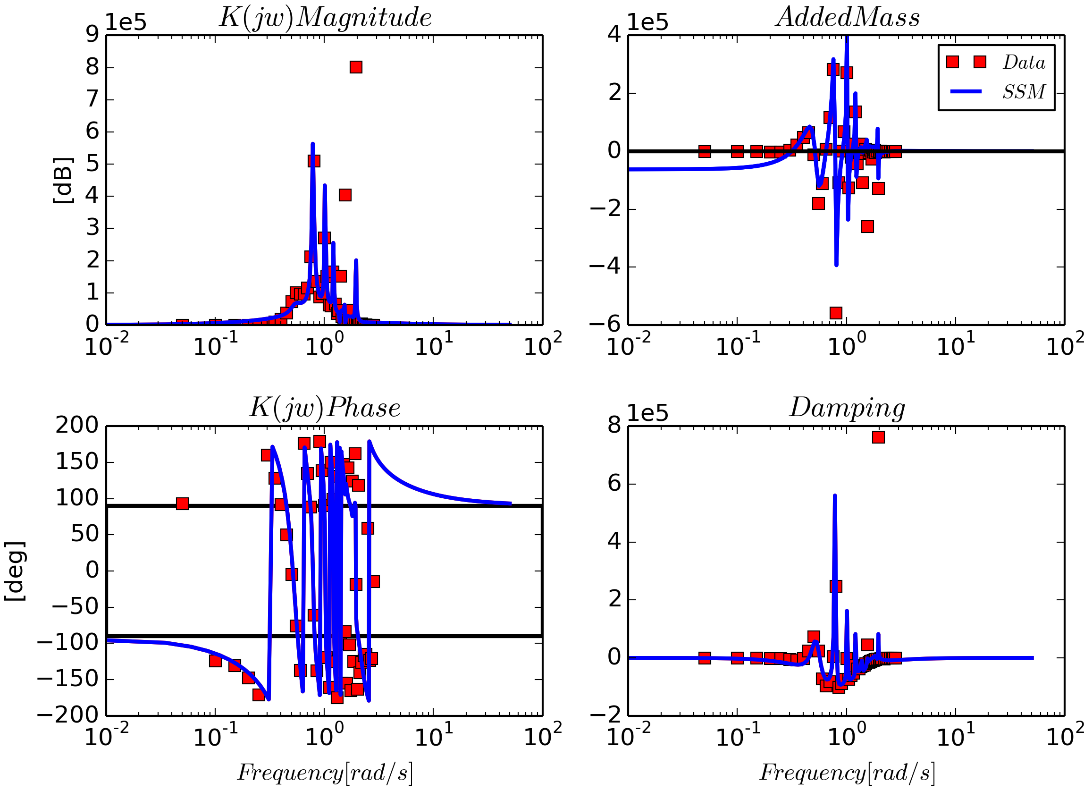

Figure B.5: *Identification Results for Roll1-Heave1*

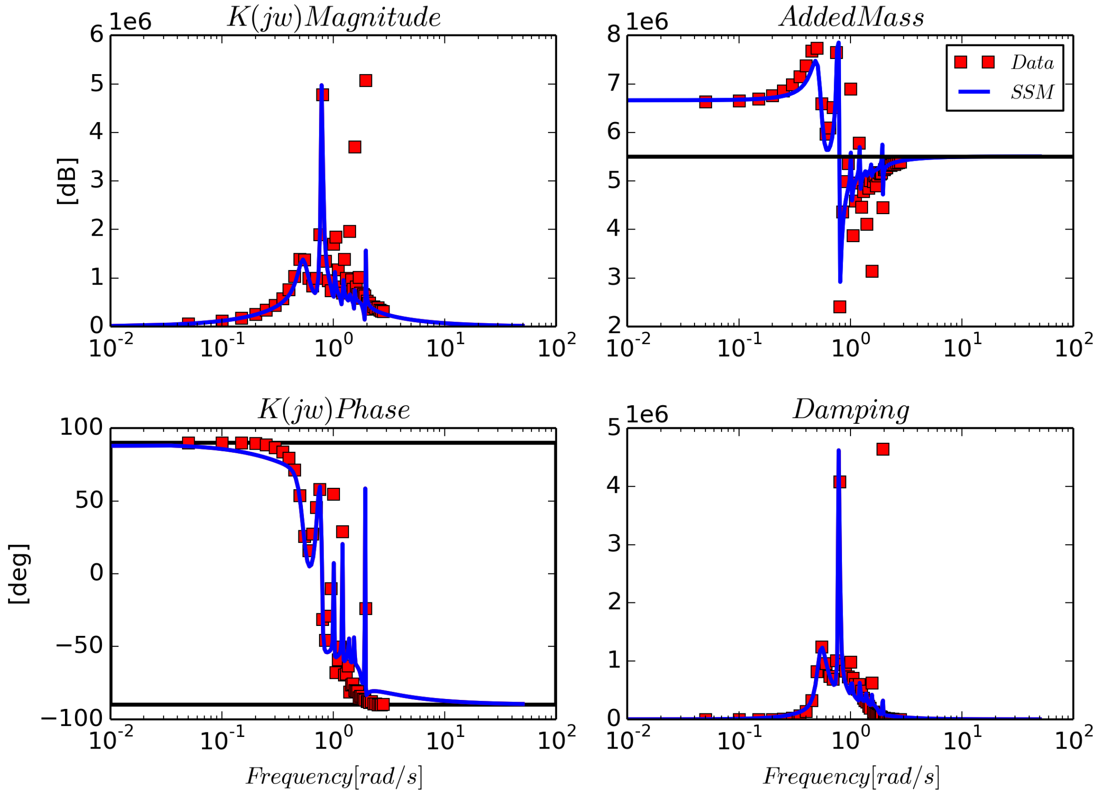

Figure B.6: *Identification Results for Roll1-Roll1*

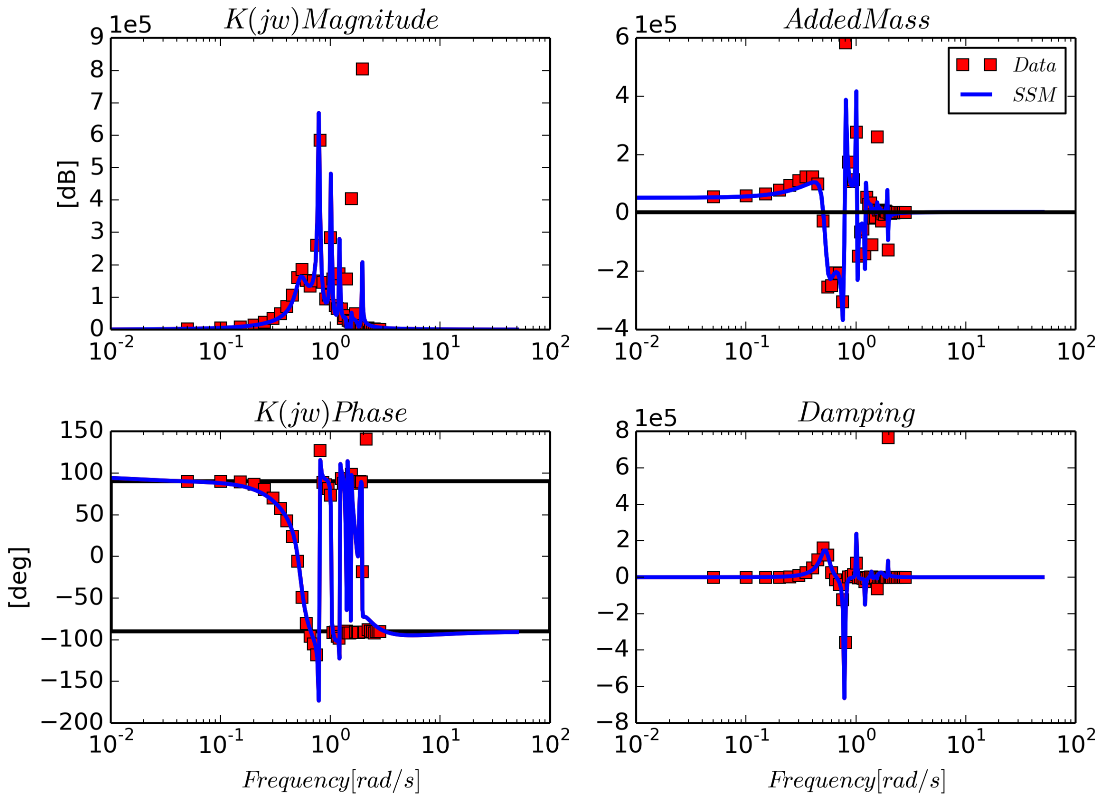

Figure B.7: *Identification Results for Roll1-Heave2*

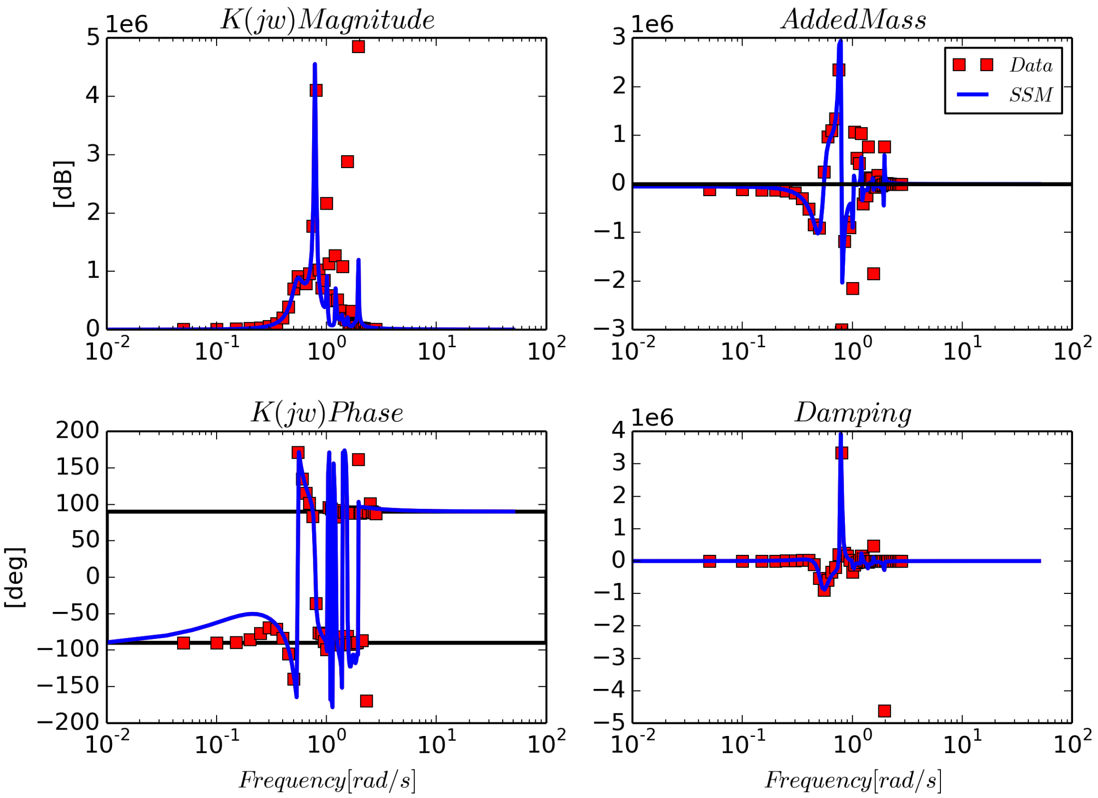

Figure B.8: *Identification Results for Roll1-Roll2*

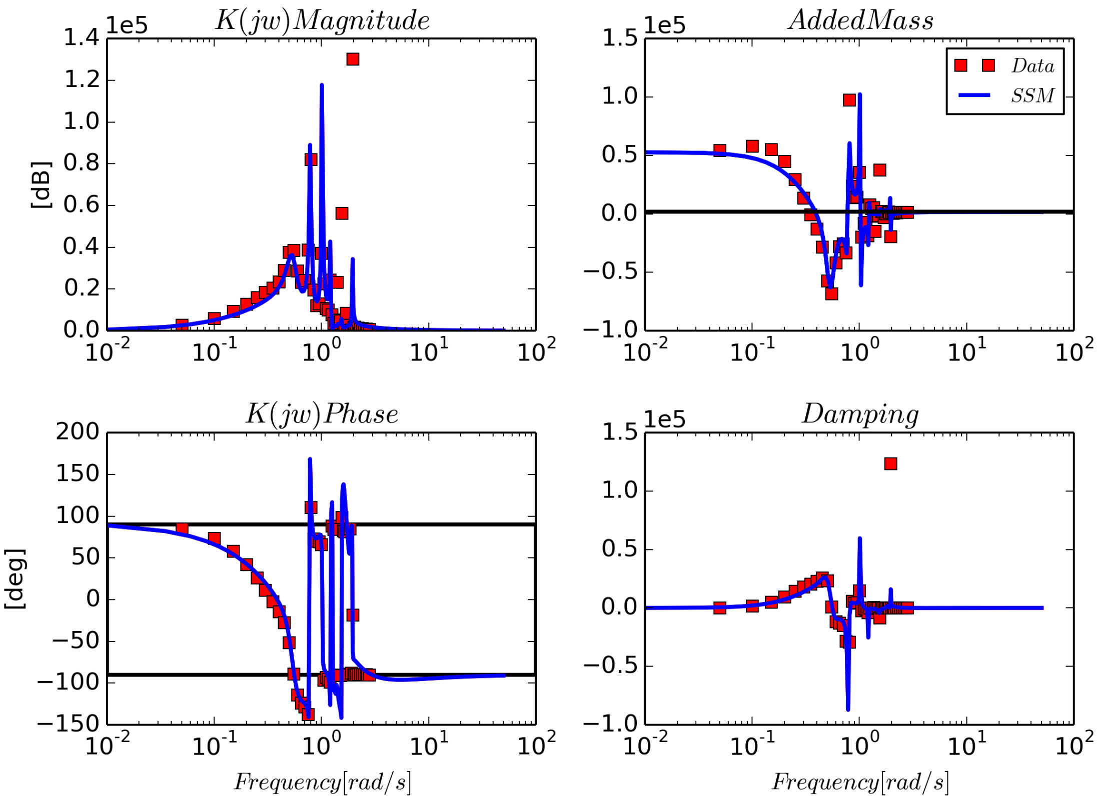

Figure B.9: *Identification Results for Heave2-Heave1*

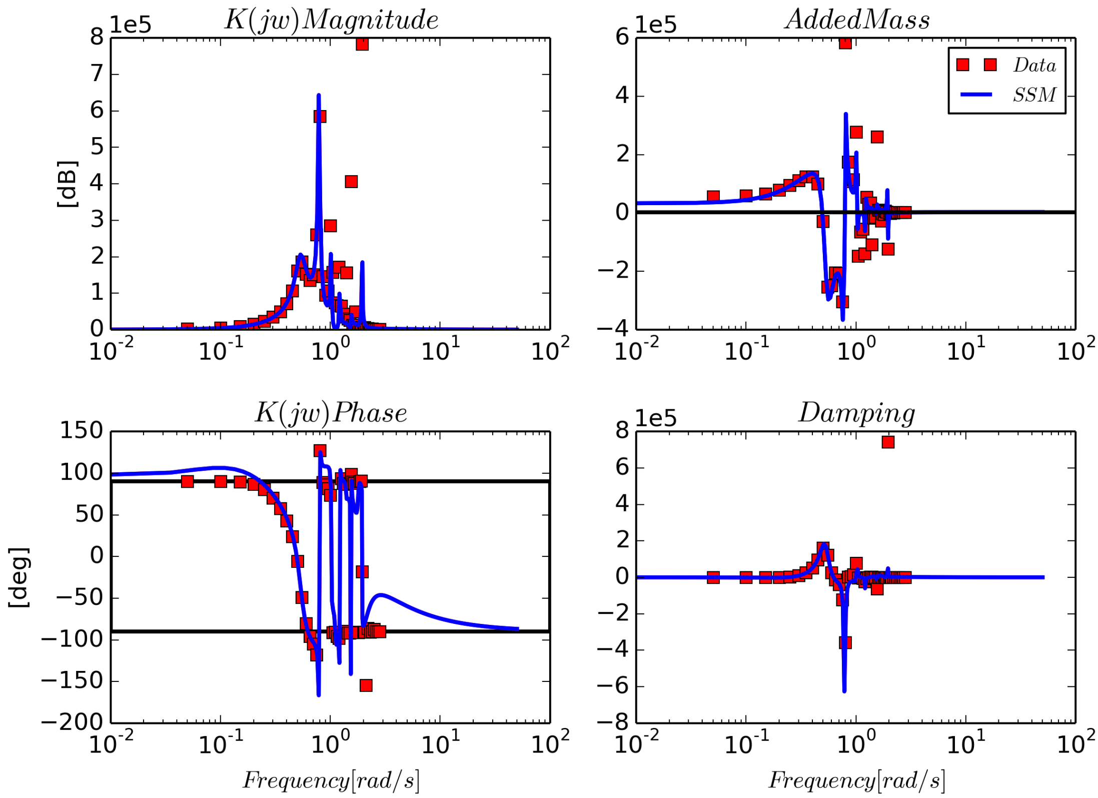

Figure B.10: *Identification Results for Heave2-Roll1*

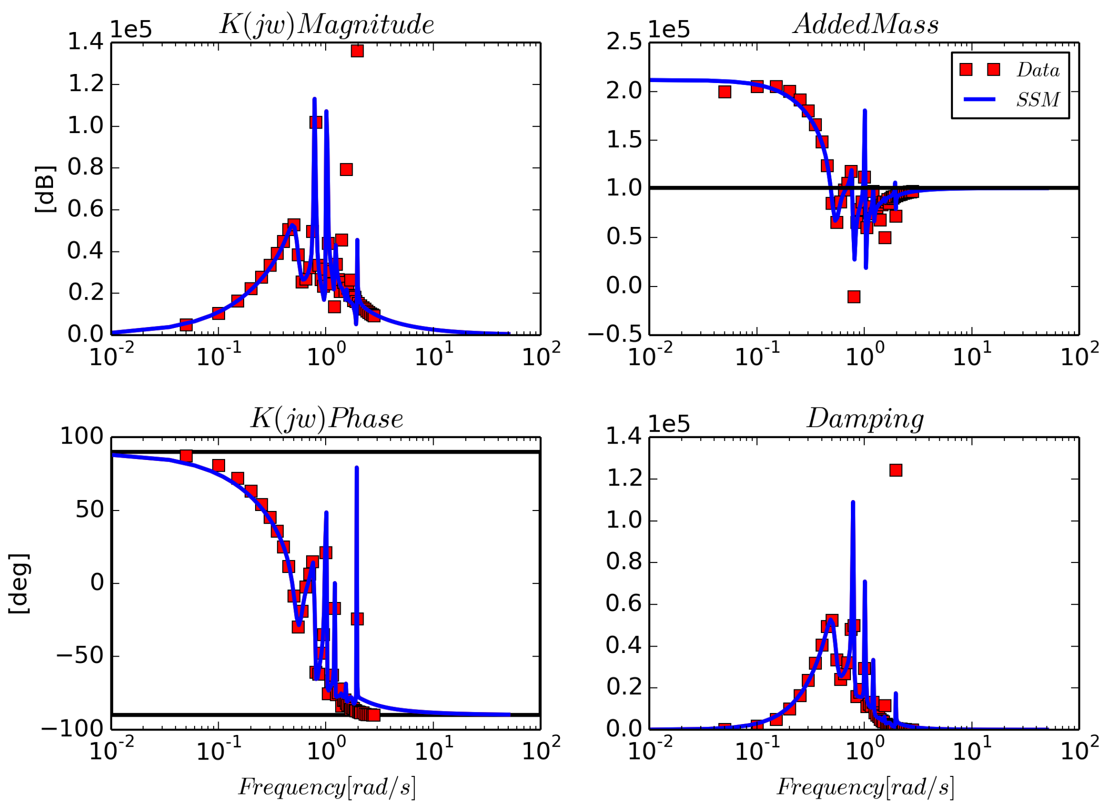

Figure B.11: *Identification Results for Heave2-Heave2*

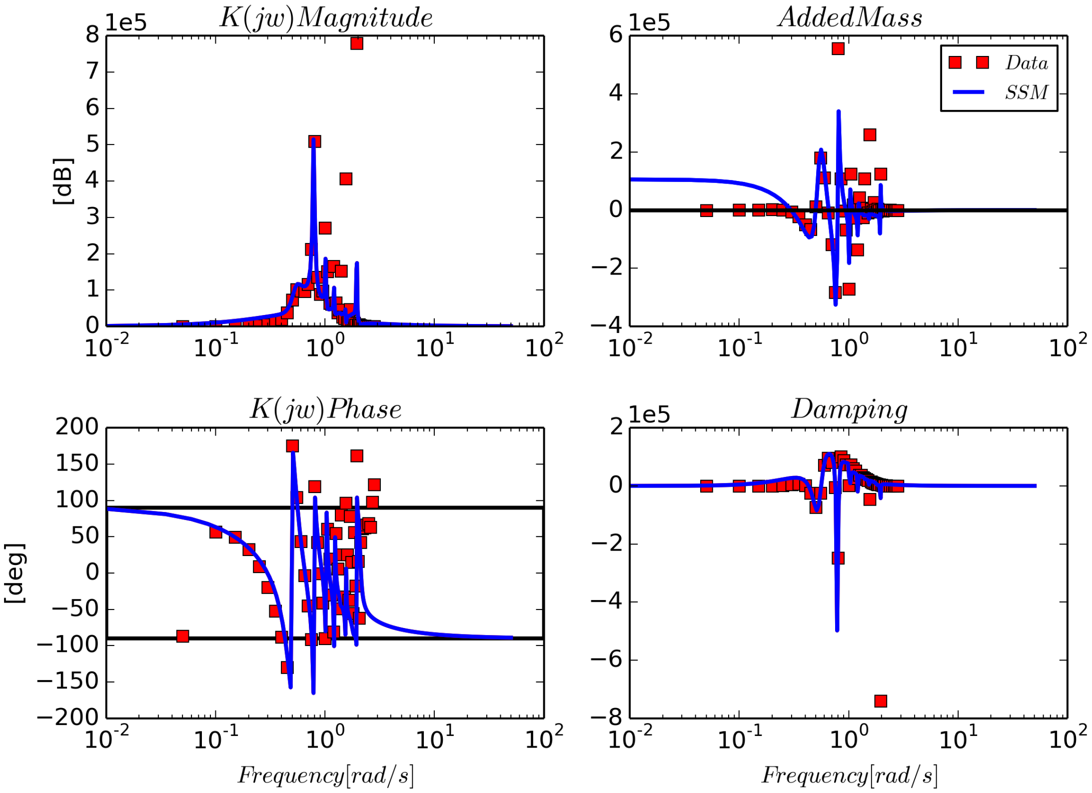

Figure B.12: *Identification Results for Heave2-Roll2*

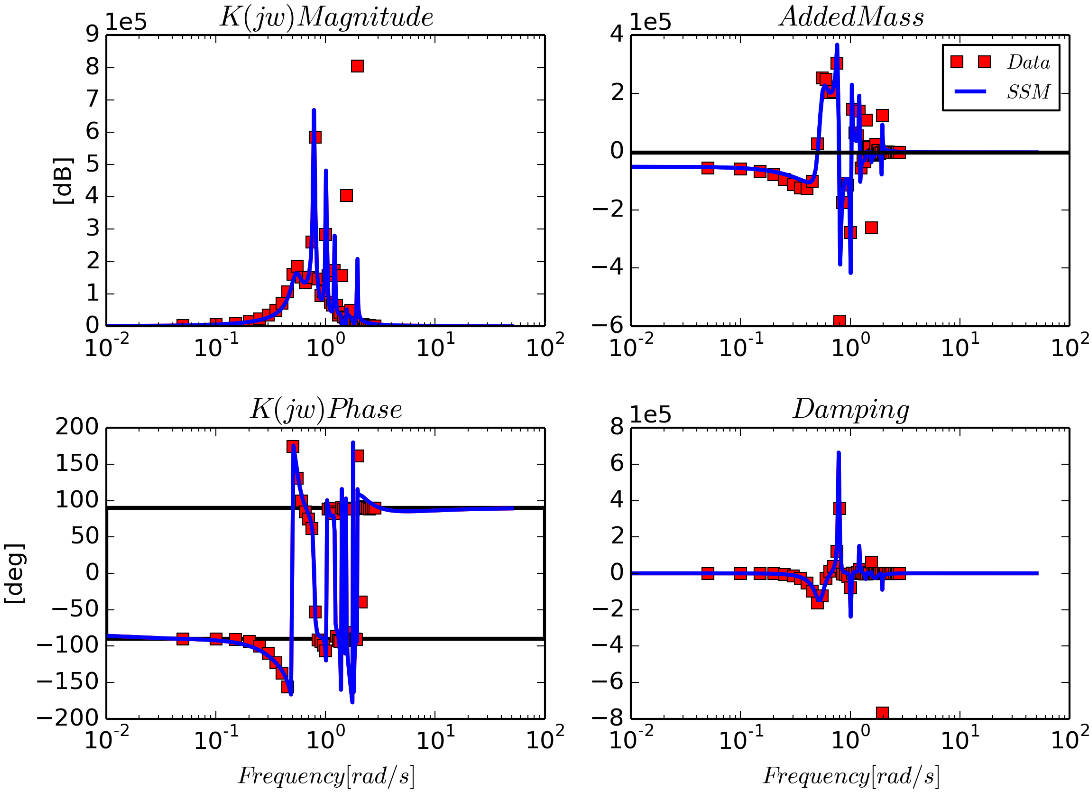

Figure B.13: *Identification Results for Roll2-Heave1*

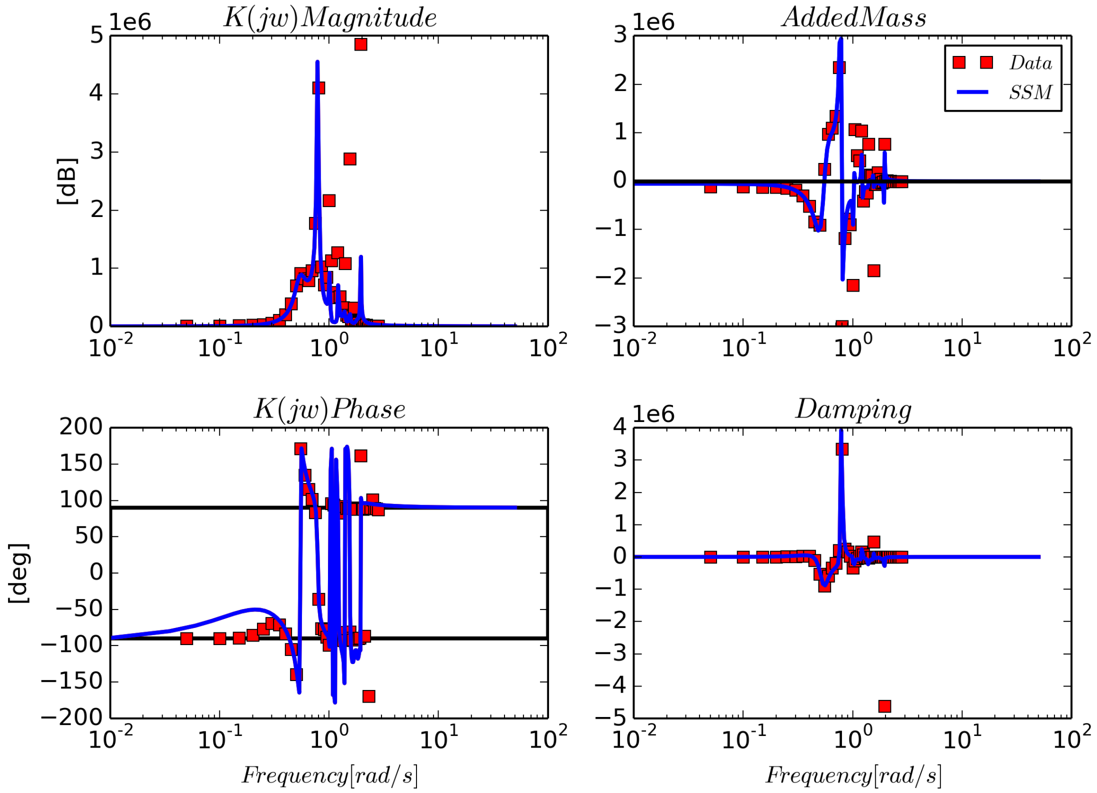

Figure B.14: *Identification Results for Roll2-Roll1*

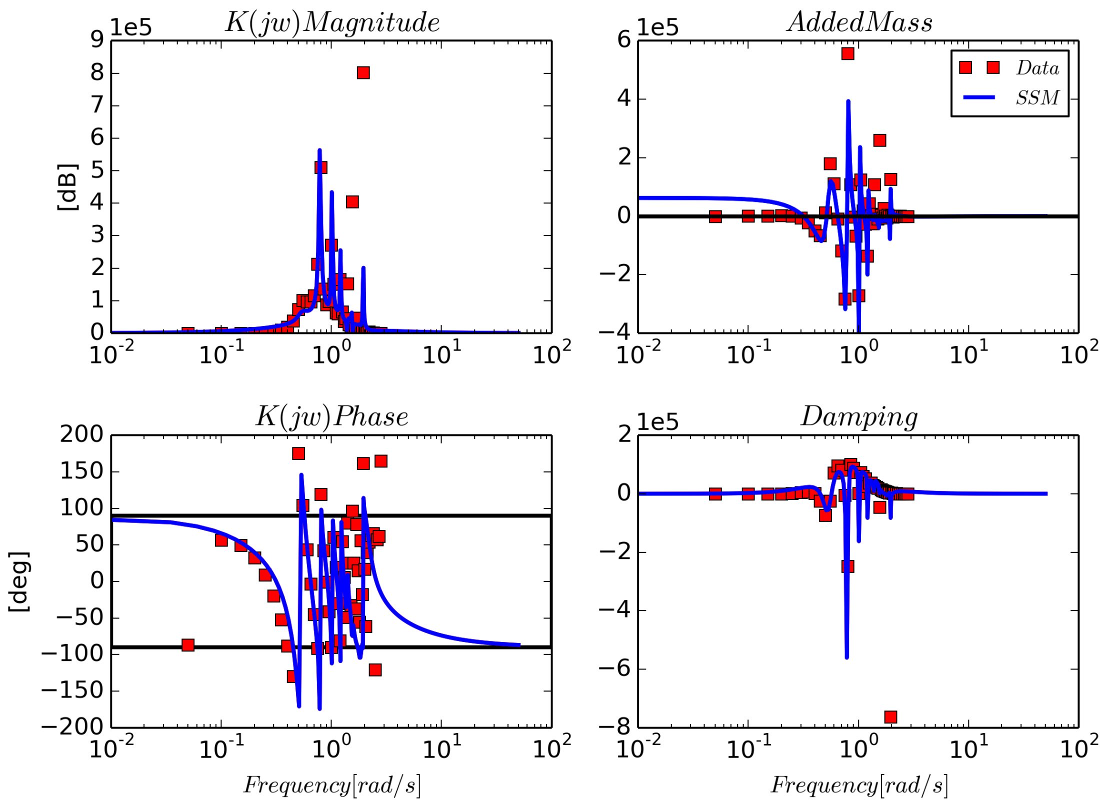

Figure B.15: *Identification Results for Roll2-Heave2*

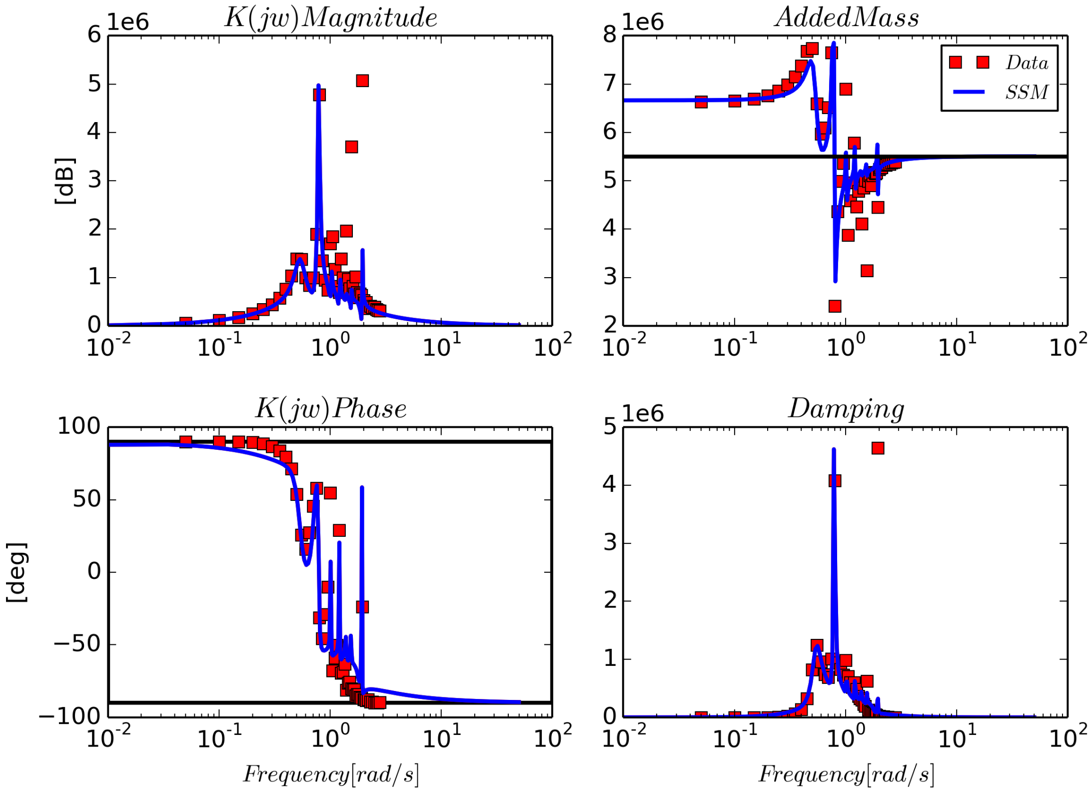

Figure B.16: *Identification Results for Roll2-Roll2*

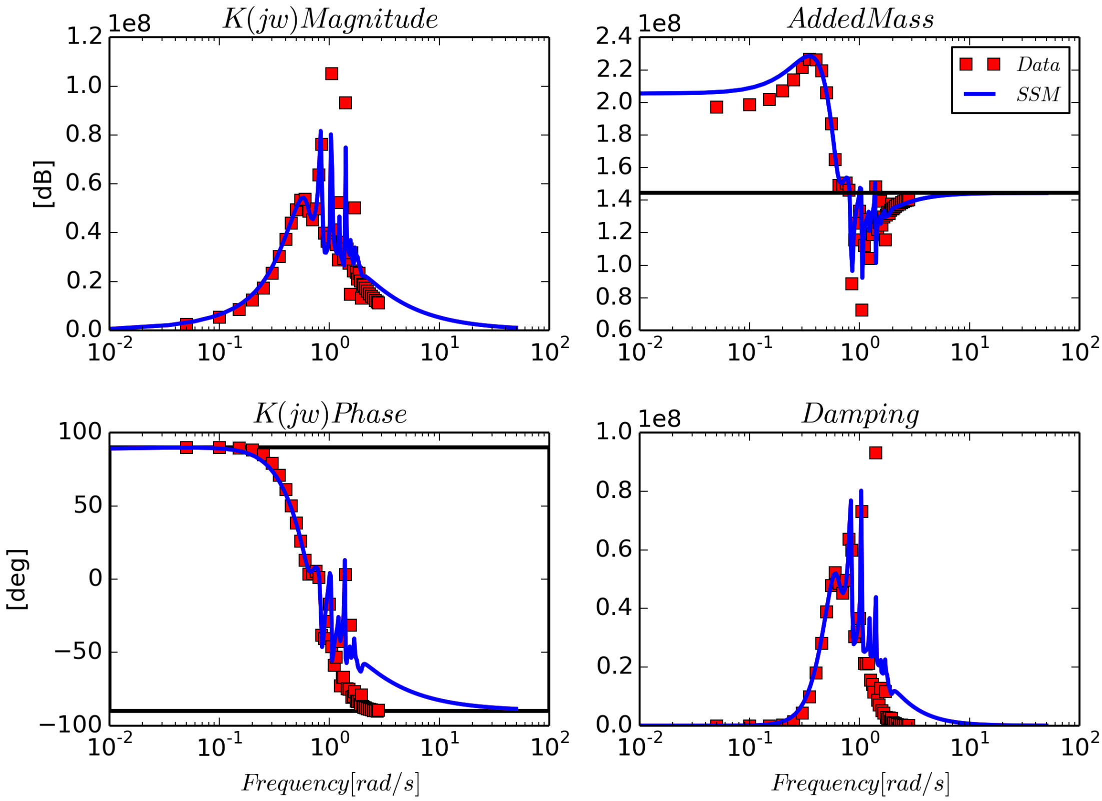

Figure B.17: *Identification Results for Pitch1-Pitch1*

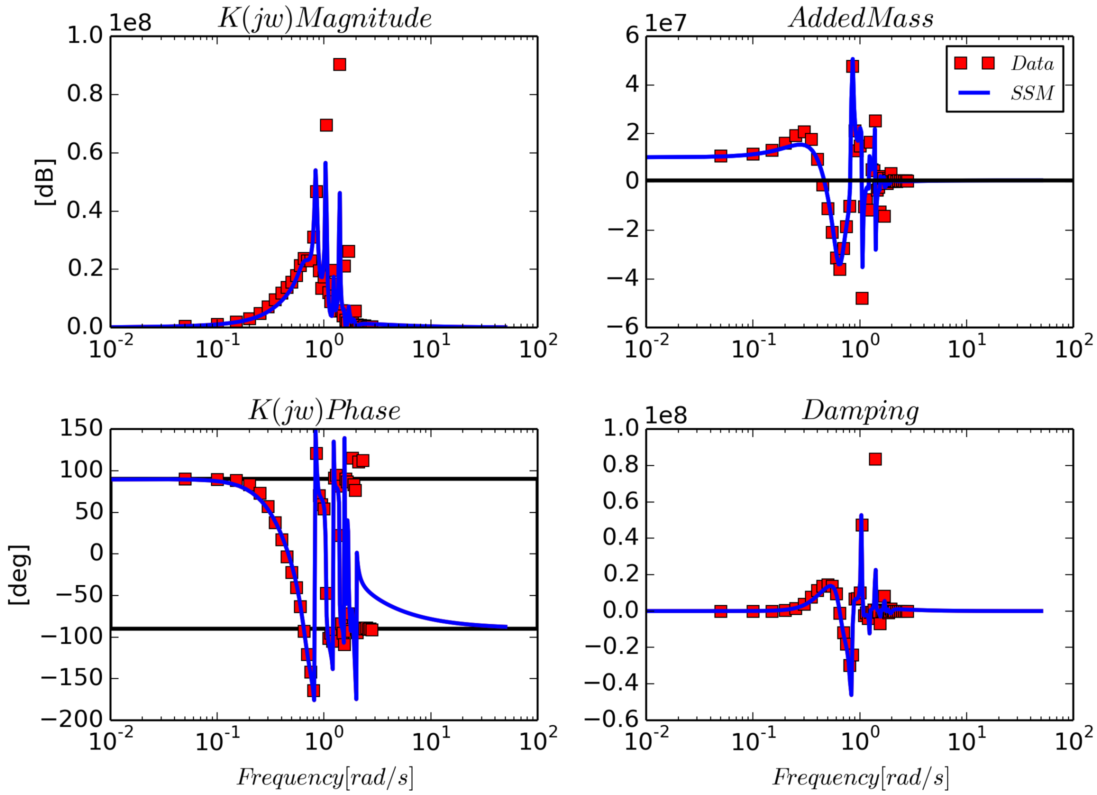

Figure B.18: *Identification Results for Pitch1-Pitch2*

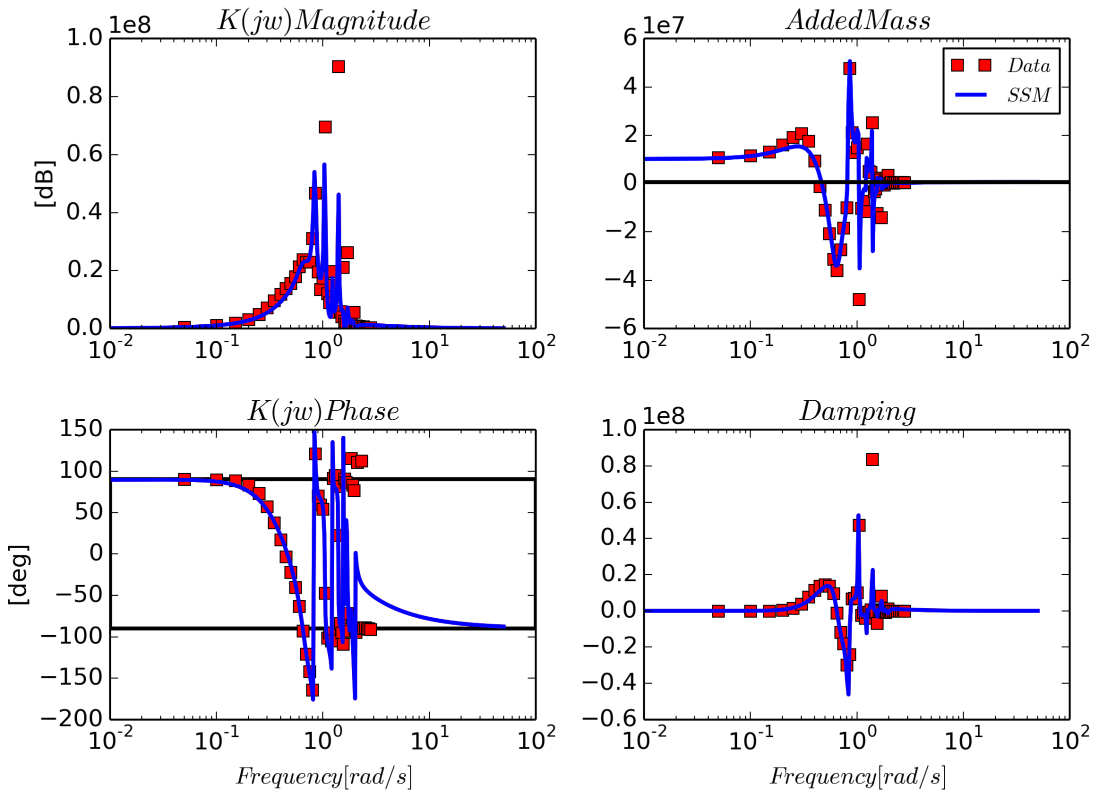

Figure B.19: *Identification Results for Pitch2-Pitch1*

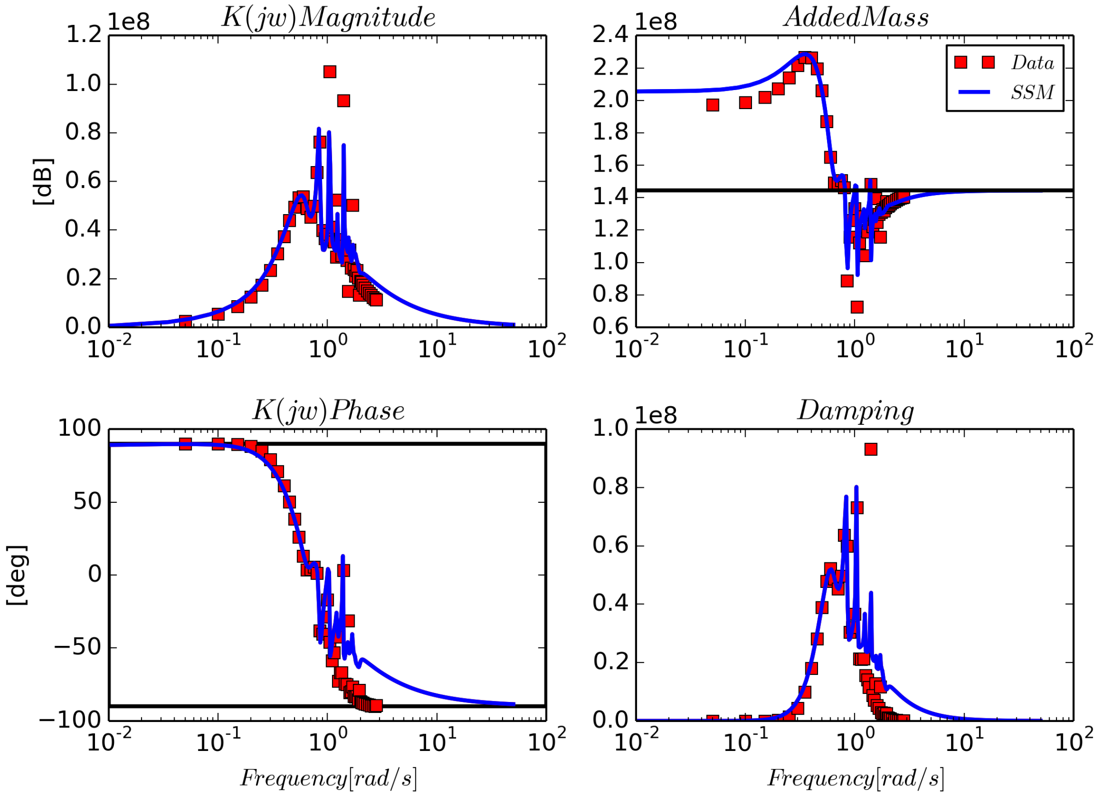

Figure B.20: *Identification Results for Pitch2-Pitch2*

Appendix C

Impulse Response Function $K(t)$

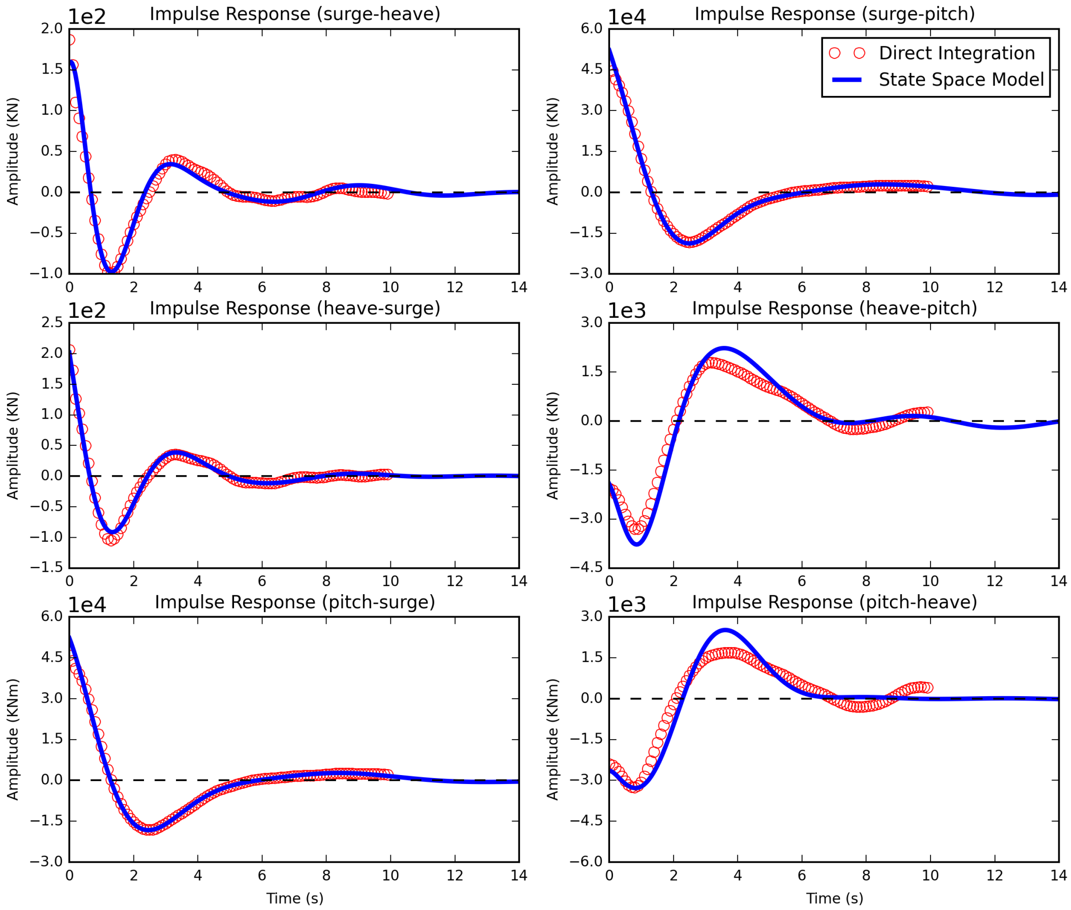

Figure C.1: *Impulse Response Function Validation for Surge, Heave and Pitch (Single Barge)*

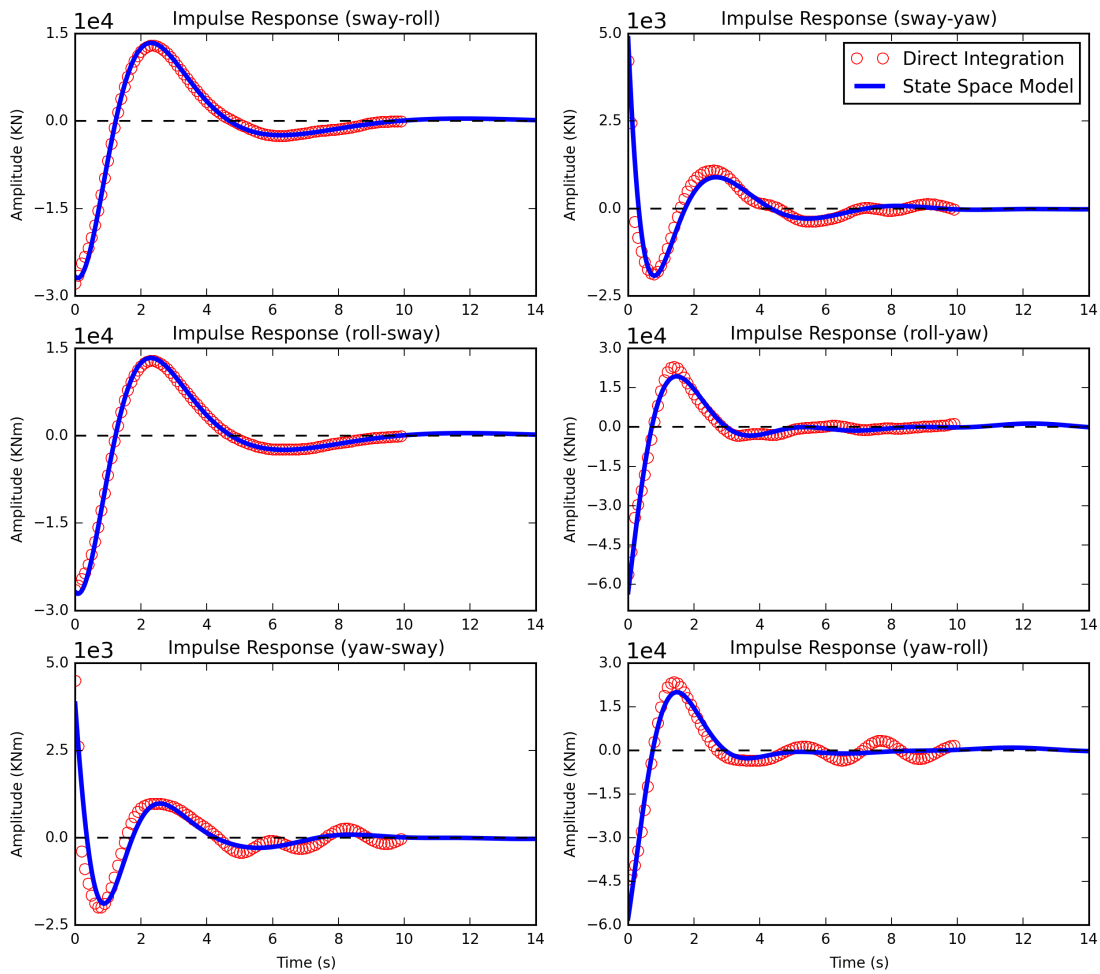

Figure C.2: *Impulse Response Function Validation for Sway, Roll and Yaw (Single Barge)*

Appendix D

Simulation of the Dynamic Response

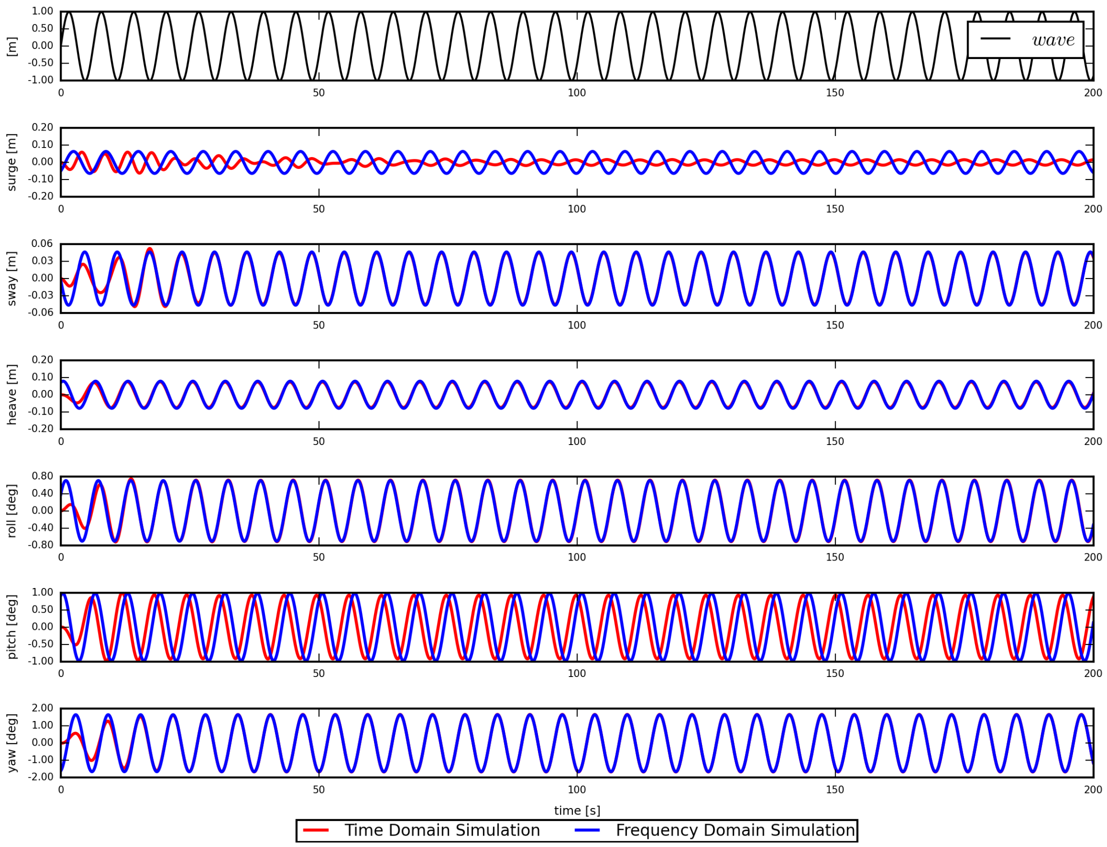

Figure D.1: *Time Series of Ship Motions for* $\omega = 1^{rad}/_{s}$ *(Quartering Wave)*

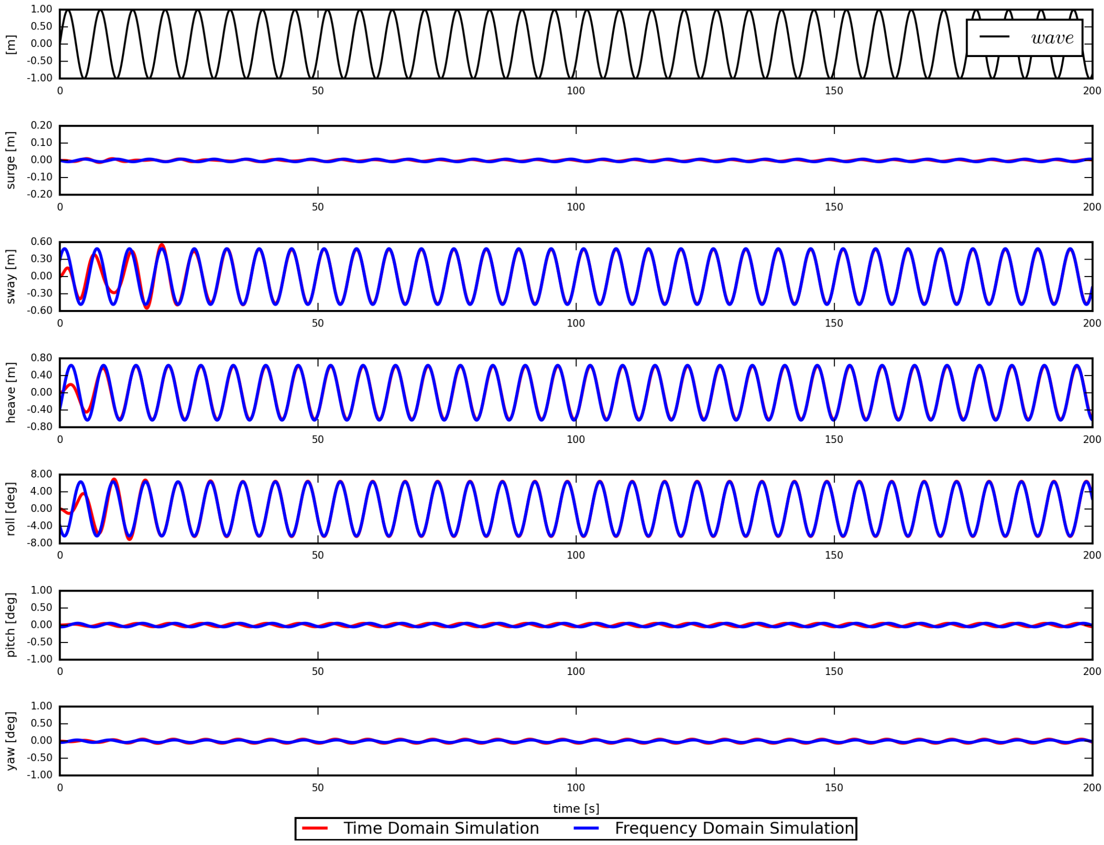

Figure D.2: *Time Series of Ship Motions for* $\omega = 1^{rad}/_{s}$ *(Beam Wave)*

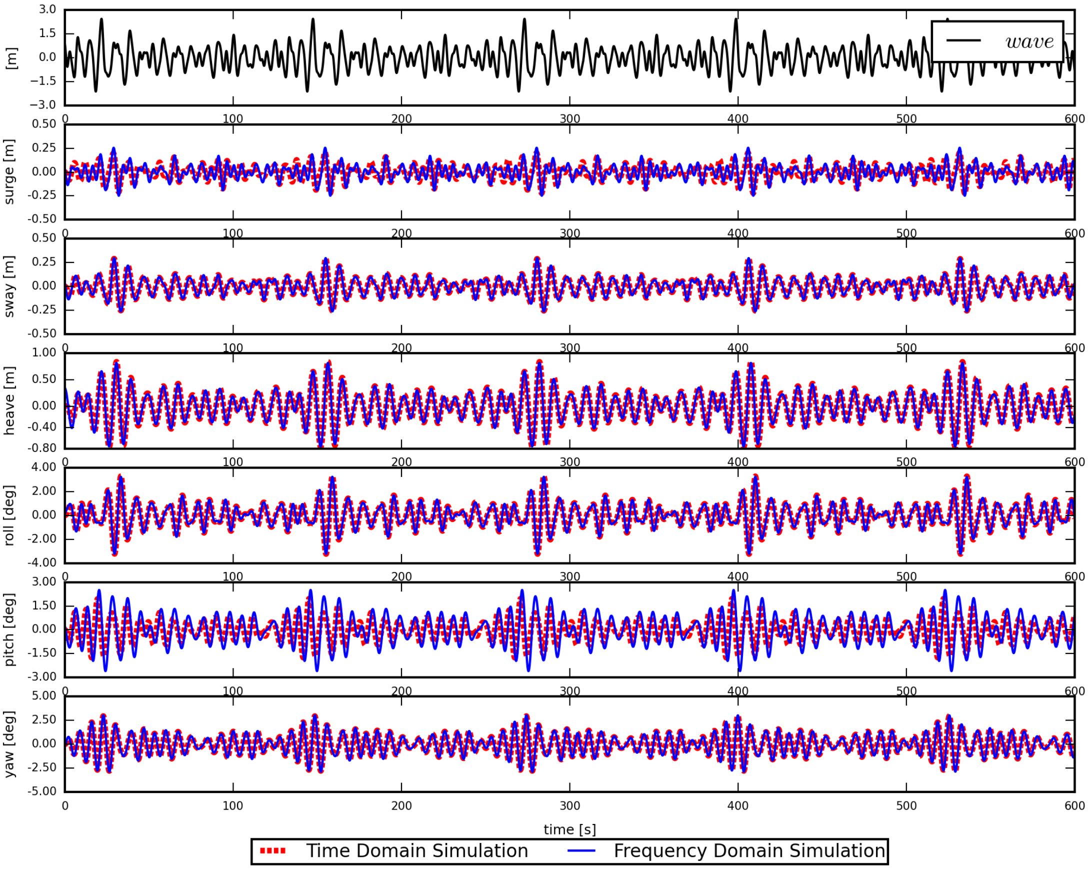

Figure D.3: *Time Series of Ship Motions for Irregular Wave (Quartering Wave)*

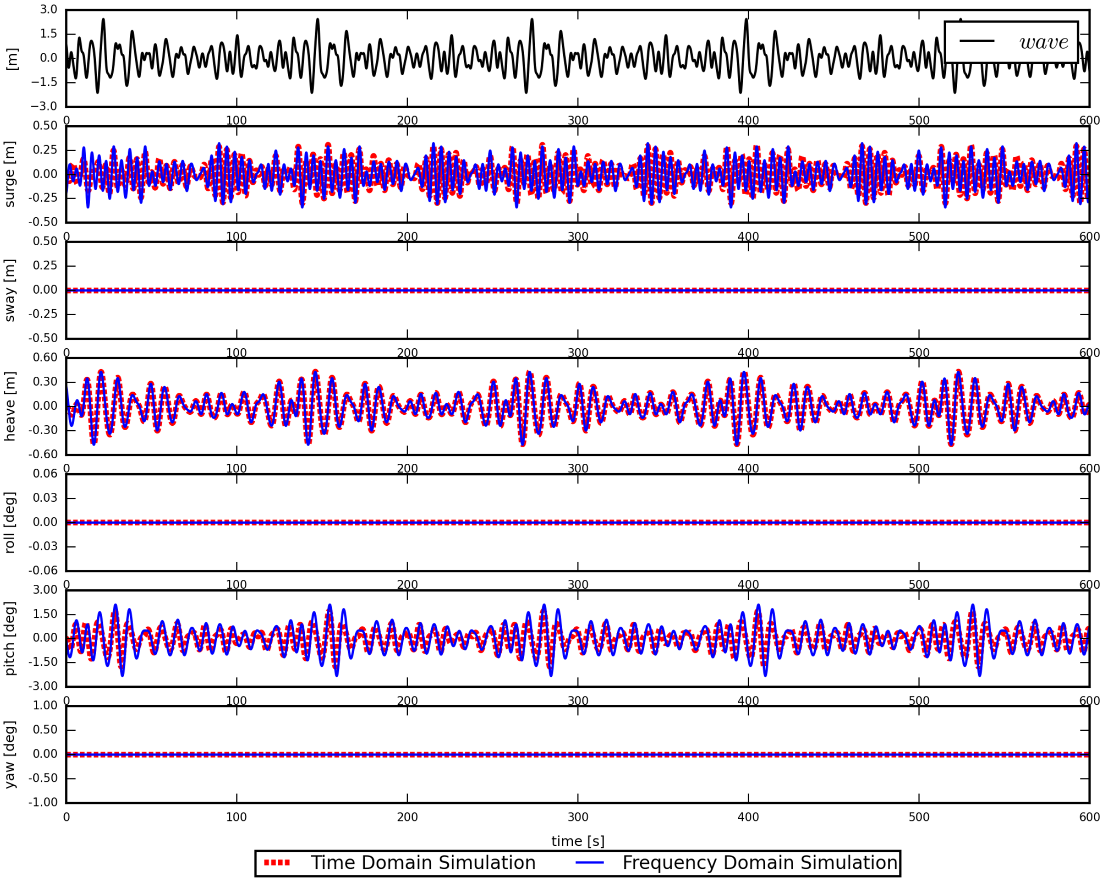

Figure D.4: *Time Series of Ship Motions for Irregular Wave (Head Wave)*

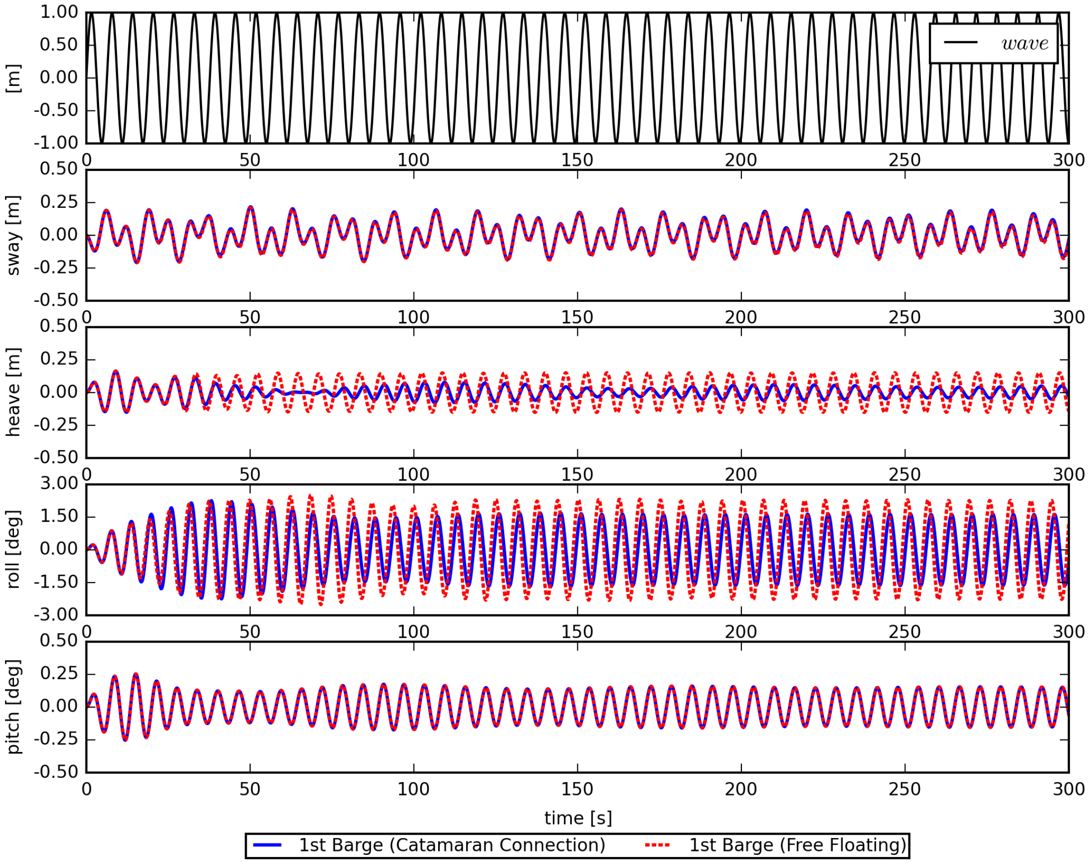

Figure D.5: *Comparison of the 1st Barge Motions for Two Systems (Head Wave)*

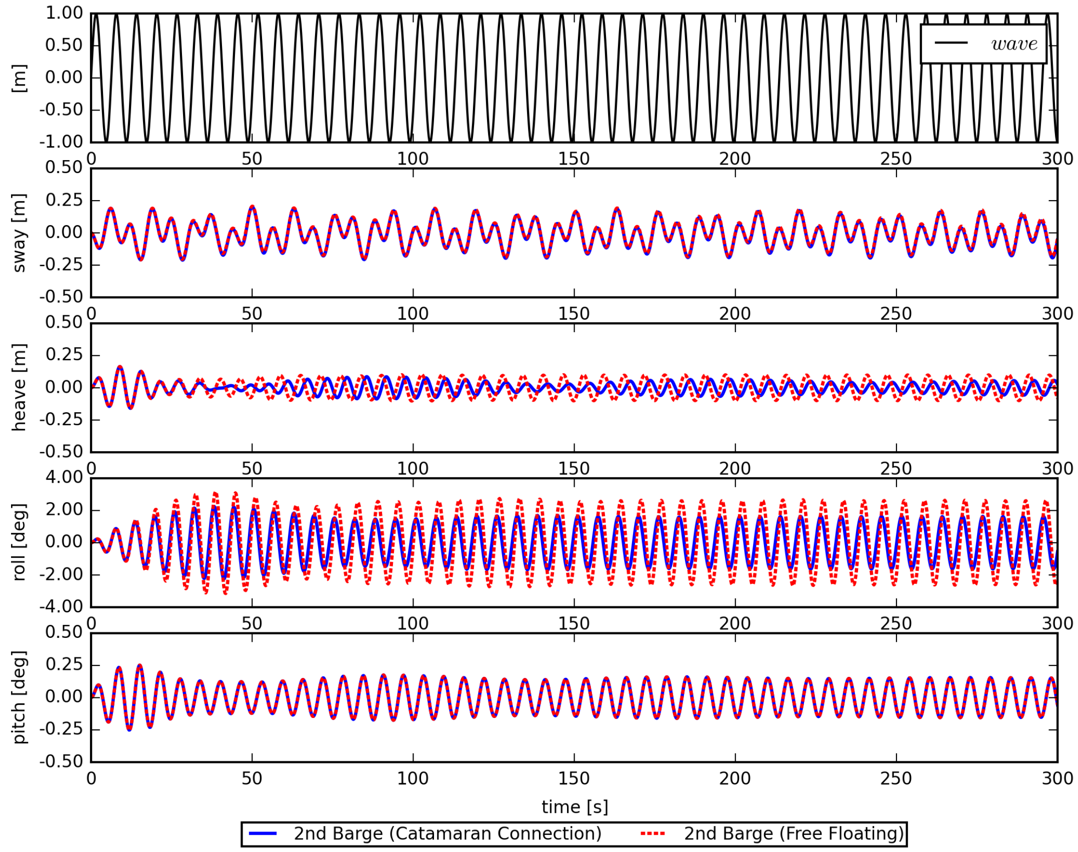

Figure D.6: *Comparison of the 2nd Barge Motions for Two Systems (Head Wave)*

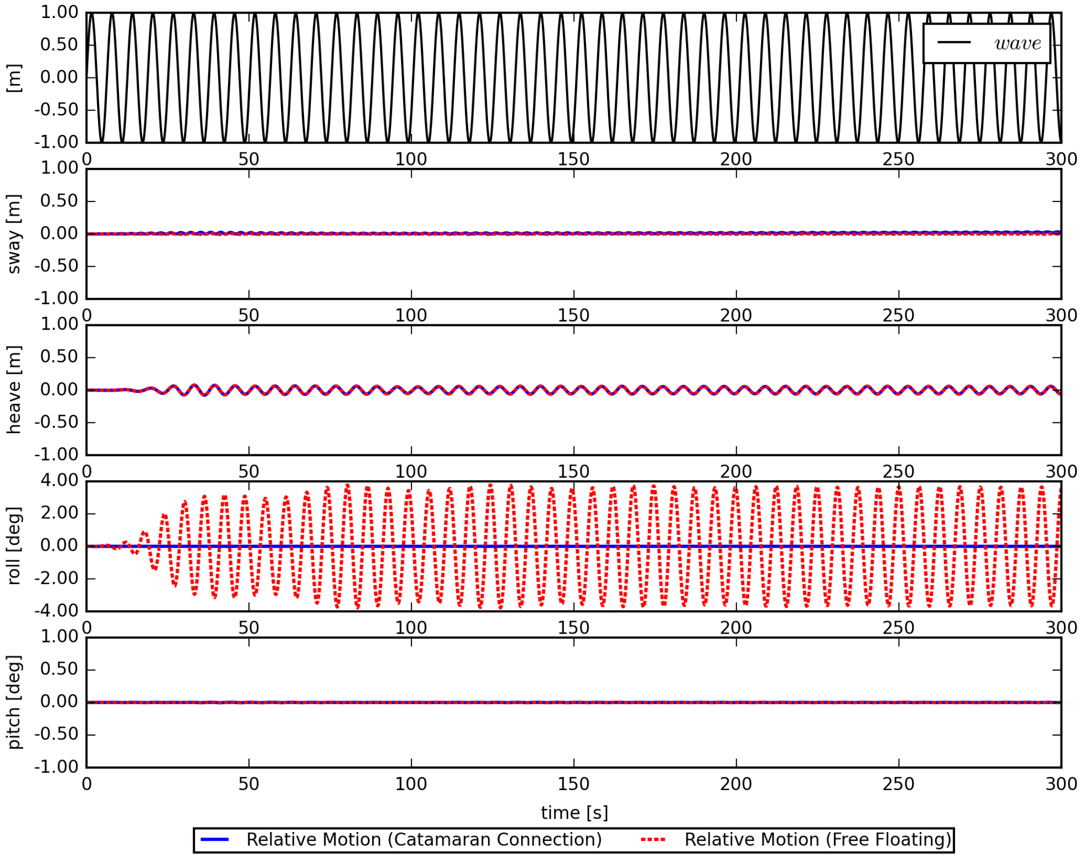

Figure D.7: *Comparison of the Relative Motions for Two Systems (Head Wave)*

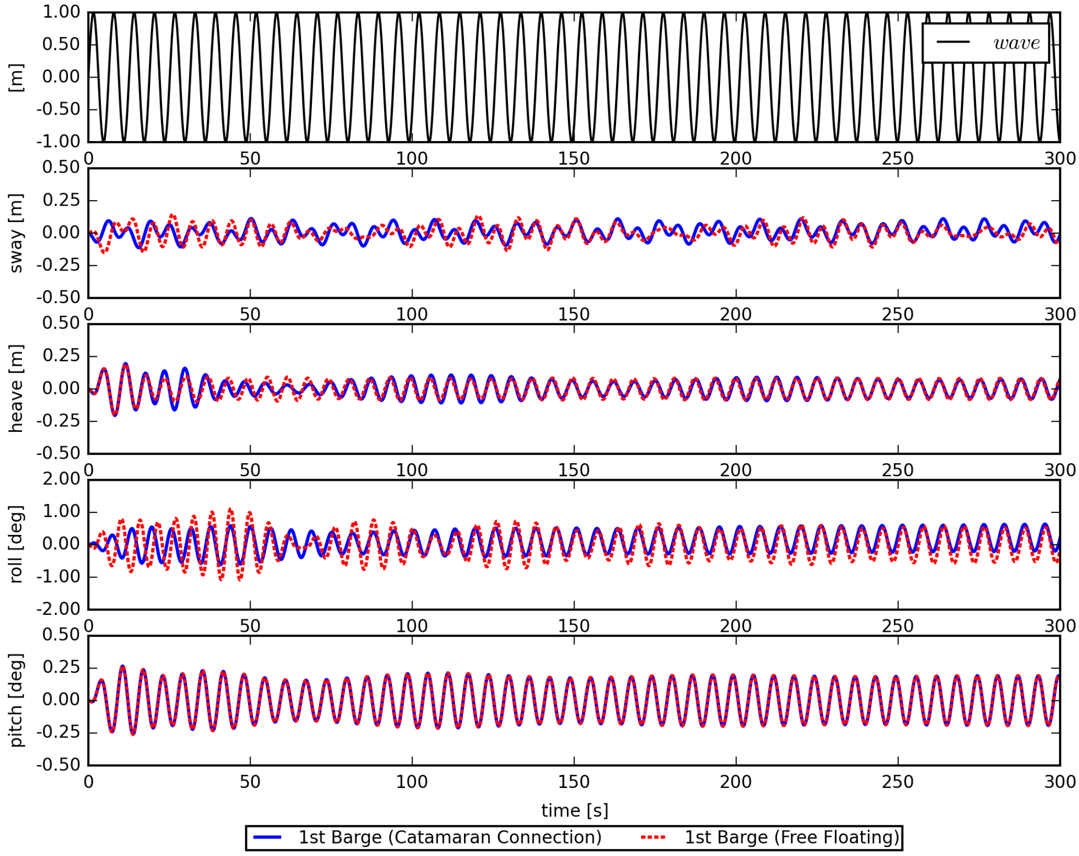

Figure D.8: *Comparison of the 1st Barge Motions for Two Systems (Quartering Wave)*

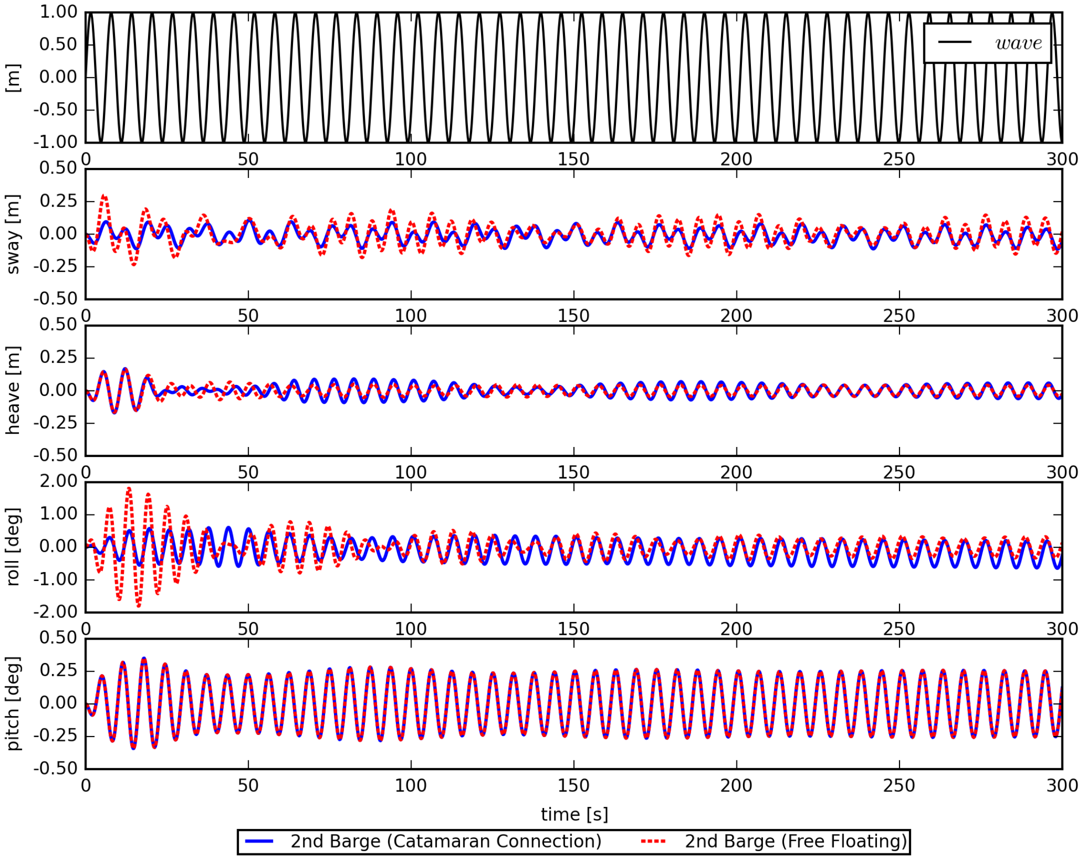

Figure D.9: *Comparison of the 2nd Barge Motions for Two Systems (Quartering Wave)*

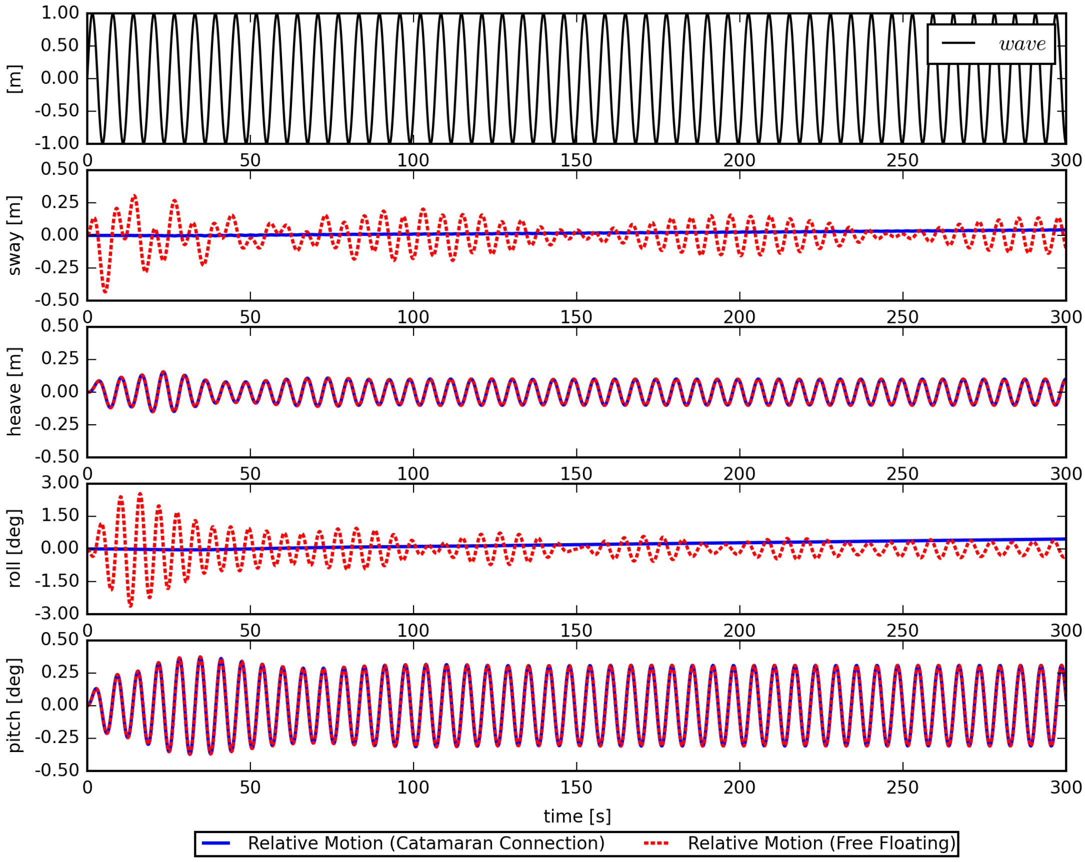

Figure D.10: *Comparison of the Relative Motions for Two Systems (Quartering Wave)*

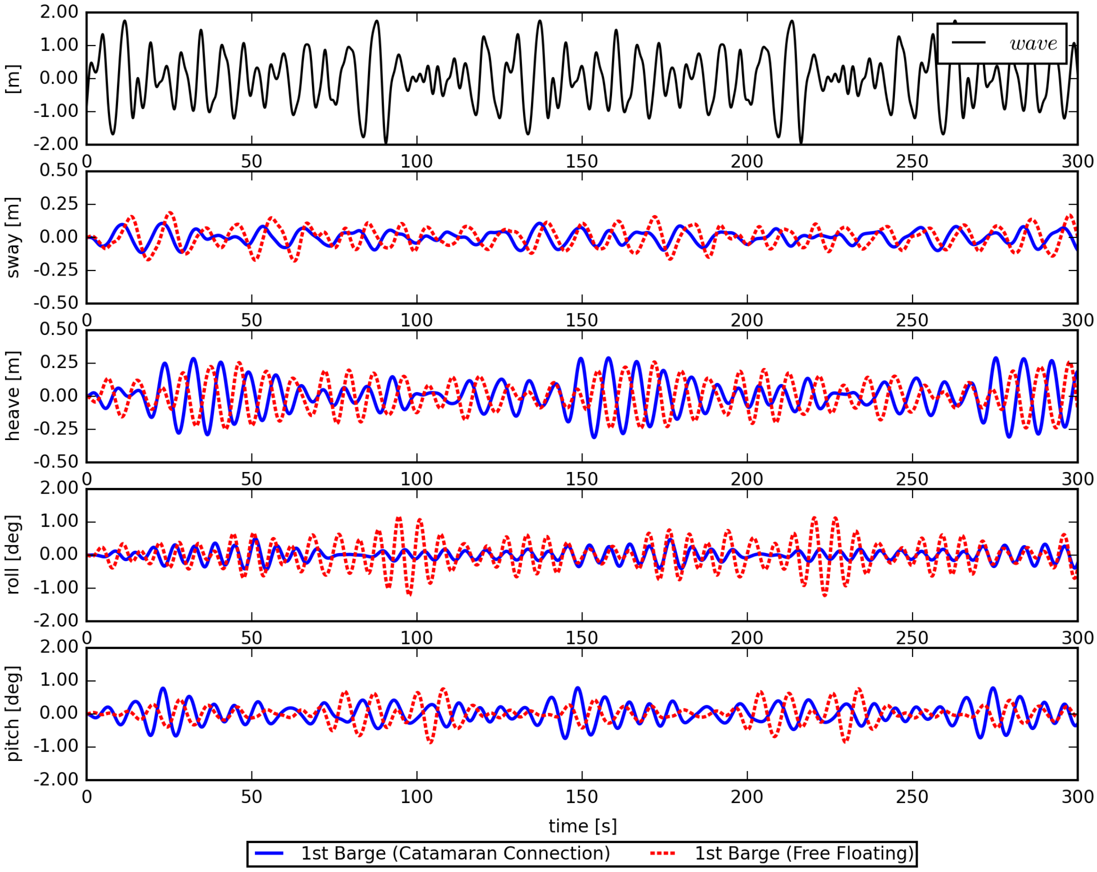

Figure D.11: *Comparison of the 1st Barge Motions for Two Systems (Irregular Head Wave)*

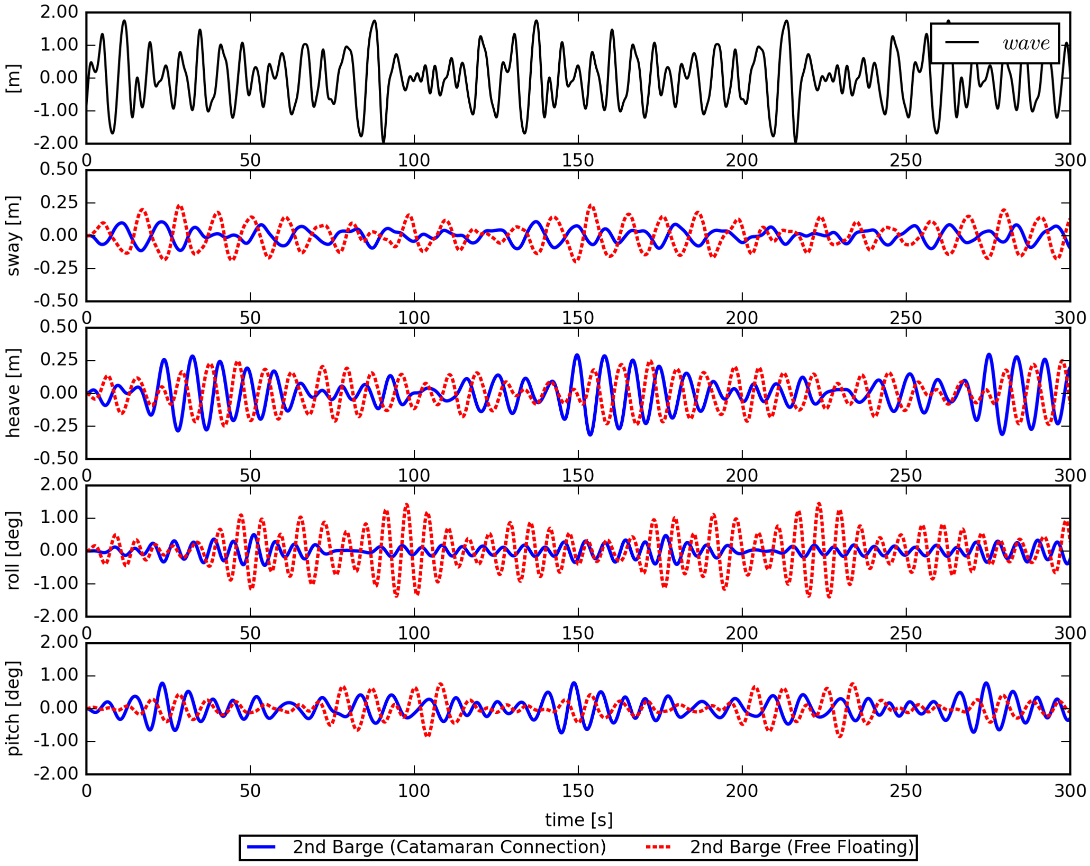

Figure D.12: *Comparison of the 2nd Barge Motions for Two Systems (Irregular Head Wave)*

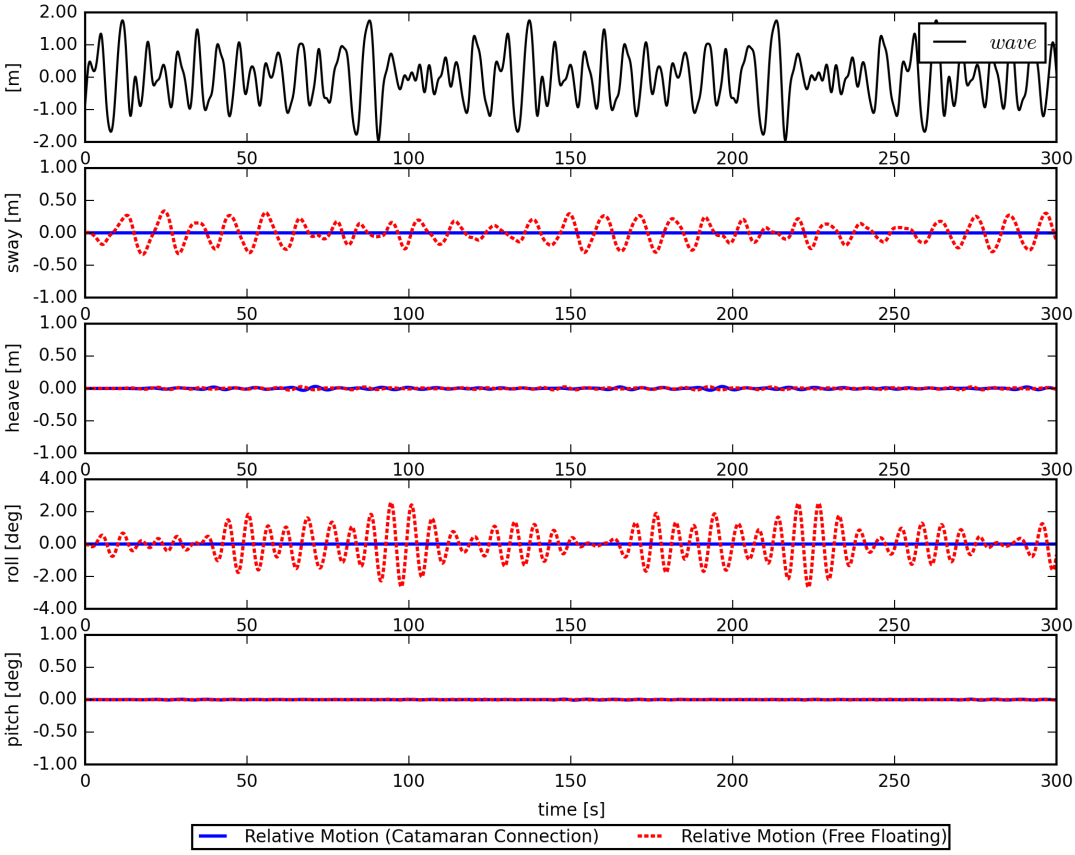

Figure D.13: *Comparison of the Relative Motions for Two Systems (Irregular Head Wave)*

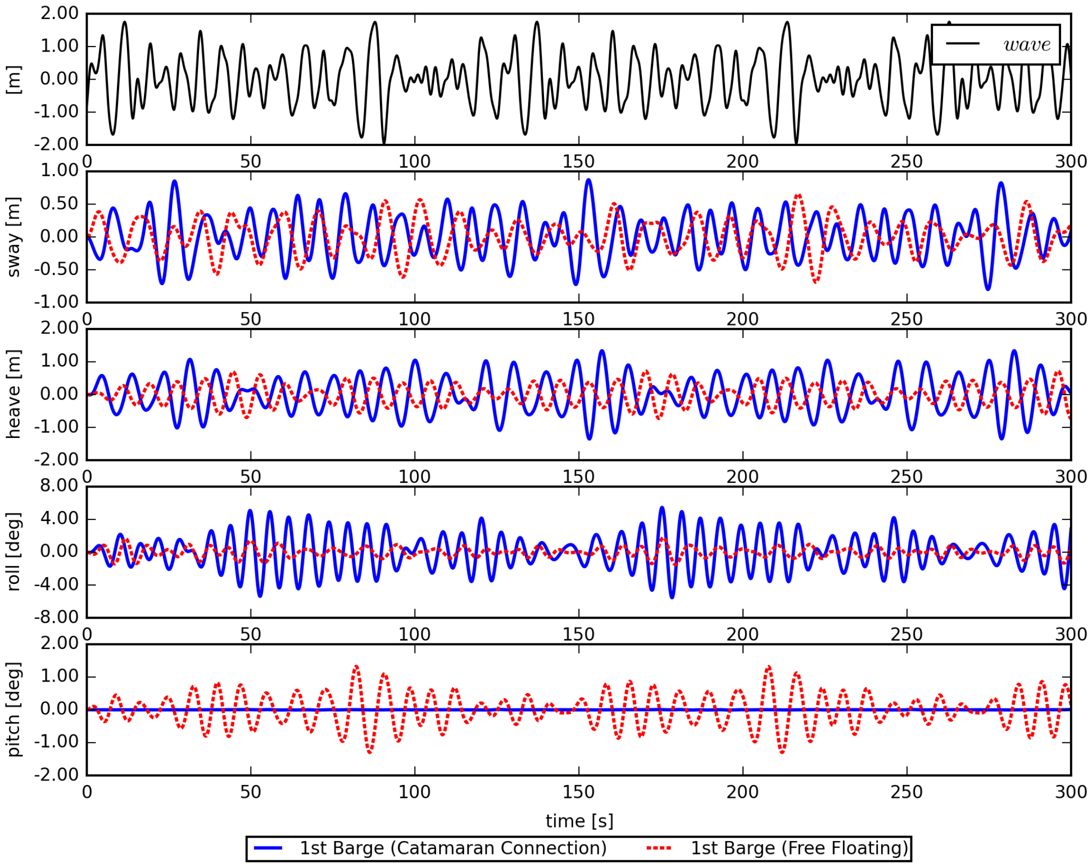

Figure D.14: *Comparison of the 1st Barge Motions for Two Systems (Irregular Quartering Wave)*

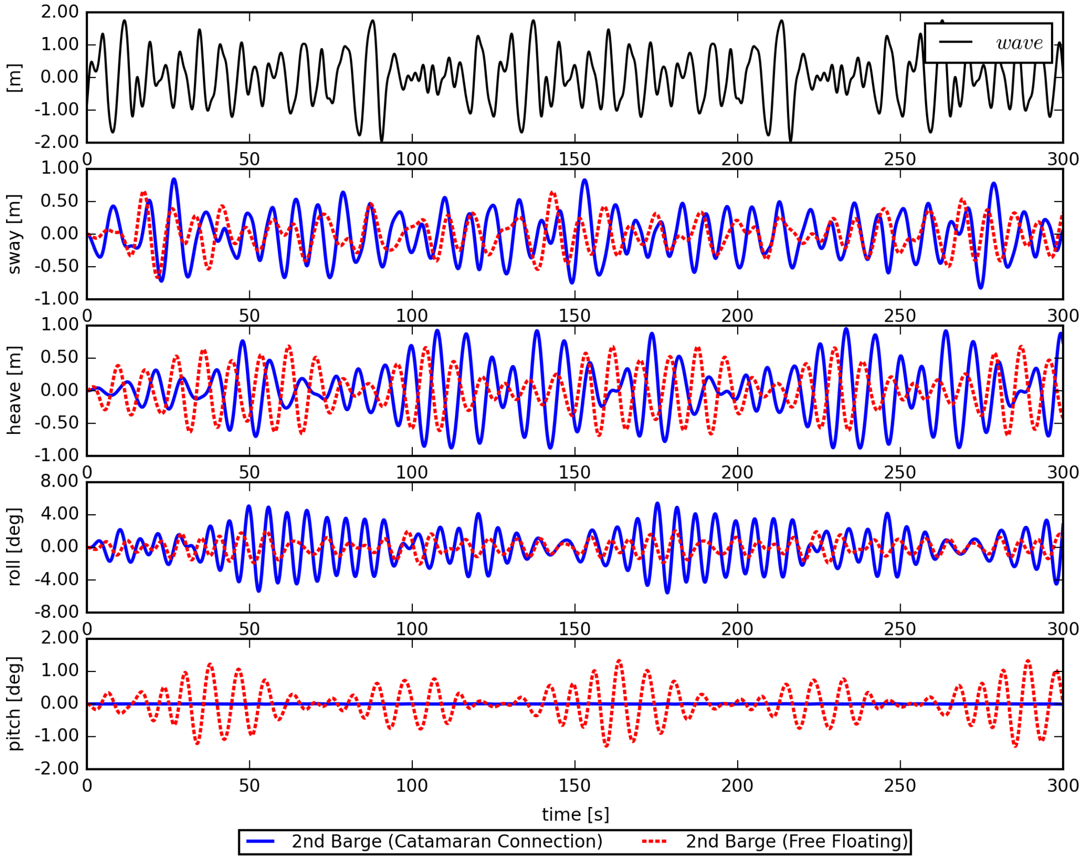

Figure D.15: *Comparison of the 2nd Barge Motions for Two Systems (Irregular Quartering Wave)*

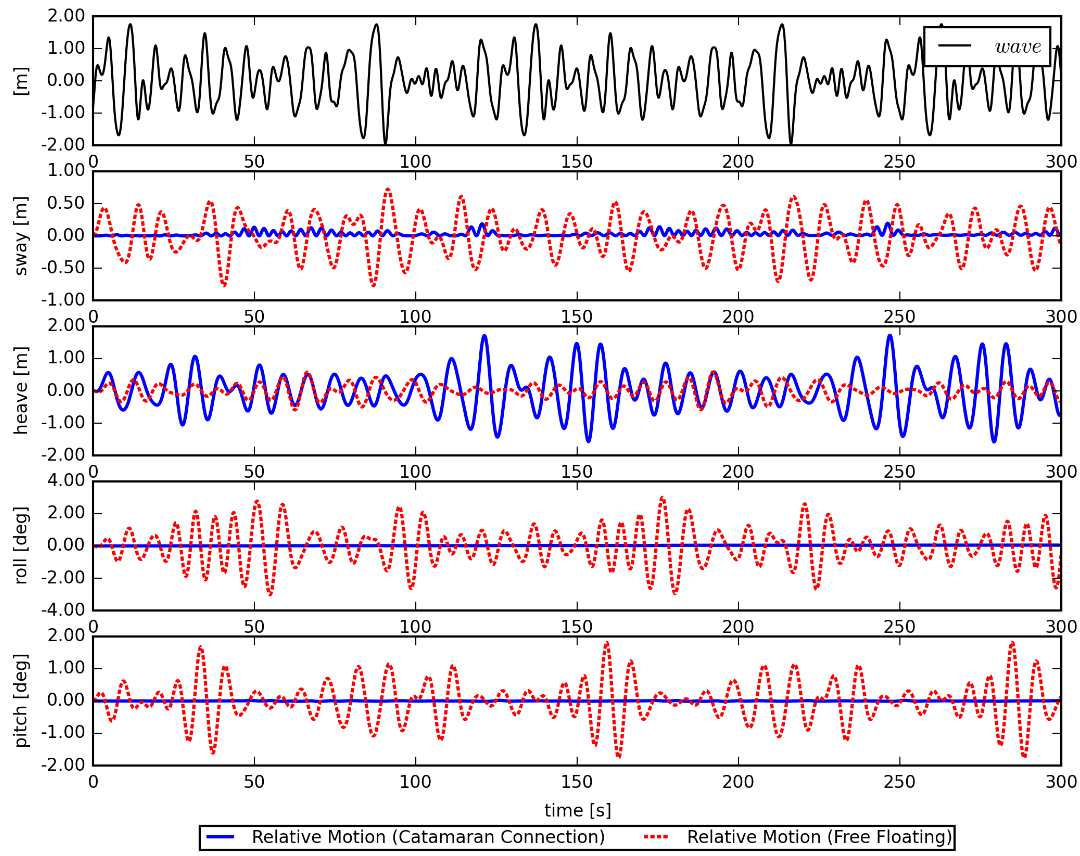

Figure D.16: *Comparison of the Relative Motions for Two Systems (Irregular Quartering Wave)*

Appendix E

Runge-Kutta Methods

Runge-Kutta methods are a class of numerical methods for computing numerical solutions to the initial value problem (IVP) consisting of the ordinary differential equation (ODE):

$$\dot{U} = F(t, U(t))$$

and the initial conditions

$$U(t_0) = U_o$$

where $U \in \mathbb{R}^M$, $F : \mathbb{R} \times \mathbb{R}^M \to \mathbb{R}^M$ and $t \in [t_0,\ t_f] \subset \mathbb{R}$. By taking $h = \triangle t$ with $t_n = t_0 + nh$, the simplest Runge-Kutta method, Euler's method, can be computed as:

$$U_{n+1} = U_n + hF(t_n, U_n)$$

Even though Euler's method is simple to understand and easy to implement, the global error is proportional to h. Then, highly accurate numerical solutions can be calculated using a s-stage quadrature formula:

$$U_{n+1} = U_n + h \sum_{j=1}^{s} b_j F(t_n + c_j h, \bar{U}_j)$$

where $\bar{U}_j$ is an estimation for U at the node point c_j. Explicit Runge-Kutta methods build these stage estimates recursively using:

$$\begin{aligned}
\bar{U}_1 &= U_n \\
\bar{U}_2 &= U_n + ha_{21}F(t_n, \bar{U}_1) \\
&\vdots \\
\bar{U}_s &= U_n + h\sum_{k=1} a_{sk}F(t_n + c_k h, \bar{U}_k)
\end{aligned}$$

where a_{jk} are the stage weight for $\bar{U}_j$ and $\sum_{k=1}^{j-1} a_{jk} = c_k$. An alternative formulation which lends itself well to implementation:

$$\begin{aligned}
K_1 &= F(t_n, U_n) \\
K_2 &= F(t_n + c_2 h, U_n + ha_{21}K_1) \\
&\vdots \\
K_s &= F(t_n + c_s h, U_n + h(a_{s1}K_1 + \cdots + a_{s,s-1}K_{s-1})) \\
U_{n+1} &= U_n + h(b_1 K_1 + \cdots + b_s K_s)
\end{aligned}$$

This formulation also makes it obvious that a general s-stage Runge-Kutta scheme will require s temporary vectors for the K_s.